A Quasi-Passive Biarticular Prosthesis and Novel Musculoskeletal Model for Transtibial Amputees

Andrea Willson

A thesis

submitted in partial fulfillment of the

requirements for the degree of

Master of Science in Mechanical Engineering

University of Washington

2017

Committee:

Patrick Aubin

Katherine Steele

Eric Seibel

Program Authorized to Offer Degree:

Mechanical Engineering

University of Washington

Abstract

A Quasi-Passive Biarticular Prosthesis and Novel Musculoskeletal Model for Transtibial Amputees

Andrea Willson

Chair of the Supervisory Committee:
Patrick Aubin, Ph.D.
Affiliate Assistant Professor
Mechanical Engineering

Transtibial amputees alter their gait pattern to compensate for prosthetic feet with limited functionality. The lack of biarticular actuation is one prominent example of the differences between commercially available prosthetic feet and the intact human lower limb. A novel biarticular prosthesis (BP) with a quasi-passive clutched spring mechanism to improve transtibial amputee gait was designed and evaluated. An open-sourced amputee musculoskeletal model was developed, validated, and utilized to evaluate how the BP affected gait. Seven transtibial amputee subjects walked on a treadmill using their prescribed prosthesis and then wearing the BP under different spring configurations and with biofeedback. Motion capture and ground reaction force data were collected, processed, and then OpenSim was used to perform inverse kinematics, inverse dynamics,

and static muscle force optimization. Mechanically the BP performed as expected with the biarticular spring replicating the function of the gastrocnemius, albeit at torque levels much lower than biological. The BP had no significant effect on gait symmetry nor total muscle force. The developed open sourced musculoskeletal model is a valuable community resource that will aid future studies of amputee gait.

TABLE OF CONTENTS

LIST OF FIGURES

LIST OF TABLES

ACKNOWLEDGEMENTS

This work was completed with invaluable support from members of the VA Center for Limb Loss and Mobility, and was partially funded by RR&D grants from the Department of Veterans Affairs.

Chapter 1. INTRODUCTION

1.1 AMPUTEE POPULATION

Lower limb amputation is a growing problem in the United States, particularly as a result of dysvascular disease and diabetes mellitus [1]. A study estimating the prevalence of limb loss found that the amputee population in the United States is approximately 2 million [1]. Over 33% of these amputees have major lower limb amputations [1]. The size of the amputee population is expected to surpass 3.6 million by 2050 [1]. Currently about 45% of amputees are above the age of 65, but by 2050 over 60% will be [1]. Prosthesis technology needs to be able to enhance the mobility of aging amputees, and current devices fall somewhat short. Amputees experience secondary conditions such as lower back pain, or knee osteoarthritis and knee pain [2]. Additionally, amputees tend to walk slower, have a higher metabolic cost of walking, and have bilateral asymmetries [3]. Asymmetries in amputee gait have been measured in kinematics, kinetics, muscle forces, metabolic cost, and work transfer. These effects are caused by walking compensations the amputees employ. A reduction in gait asymmetries may improve amputee gait and quality of life.

1.2 AMPUTEE GAIT COMPENSATIONS & ASYMMETRIES

Amputees exhibit several asymmetries and compensations when walking. First, there are kinematic and kinetic differences in amputee gait compared to unaffected limbs. A comparison of amputee and non-amputee gait found important differences in both the affected and contralateral limbs compared to non-amputees [4]. They showed that amputees

have elevated hip extension, knee flexion, and ankle dorsiflexion angles in the intact limb, and increased hip and knee flexion on the affected side [4]. Significant differences have been found between the net knee moment in the affected limb and the contralateral limb or non-amputee limb. Ferris et al. found that that the knee flexor moment peak was substantially reduced [5], Sanderson & Martin found that amputees walked with a flexor moment throughout the entire stance phase [6], and Bateni et al. described an elevated knee extensor peak in early stance [4]. All three papers found similar ankle and hip moments. The anterior-posterior ground reaction force in the affected limb is reduced compared to non-amputees, and loading and propulsive force production on the contralateral limb are elevated [7]. The many demonstrated differences in kinematic symmetry and joint kinetics between amputees and non-amputees have become important outcome measures for studying amputee gait.

The residual limb muscle activity is also altered from non-amputee walking. An electromyography (EMG) study by Fey et al. found that the rectus femoris, biceps femoris long head, and vastus lateralis were more active on the residual limb than the contralateral limb [8]. These findings were expected, as a consequence of the amputees' missing ankle plantar flexor muscles [8]–[10]. The lack of ankle plantar flexors has also been linked to increased iliopsoas muscle force [3]. Muscle activity is relatively easy to measure, and can give insight into analyses of prototype prostheses as well as the performance of muscle-based simulation results. Within this thesis, we EMG is utilized to qualitatively measure muscle activity and to validate our musculoskeletal model.

Amputees have a lower self-selected walking speed than non-amputees [3], which by itself results in different gait patterns and muscle activations [11]. Healthy transtibial amputees walk about 85% as fast as non-amputees, and individuals who had an amputation

as a result of dysvascular disease walk only 40-65% as fast as non-amputees [12]. Temporal asymmetries, such as reduced residual limb stance phase time, are also prevalent at slower speeds [13]. Loading asymmetries, such as increased intact limb vertical ground reaction force, are more substantial during faster walking [13]. With increasing walking speed, residual limb hip joint power and work increase, potentially as a result of increased biarticular hamstring activity [14].

Finally, amputees experience a higher metabolic cost of walking than non-amputees, for any given ambulation speed [15]. One study by Genin et al. found that transtibial amputees have up to a 15% higher metabolic cost than non-amputees, and transfemoral amputees are 30-60% higher [16]. Total muscle force is an outcome measure that is associated with metabolic cost and serves as a good indicator of effort [17], [18]. This study will use simulated total muscle force as an indicator of metabolic cost. As shown, amputees have many gait deficiencies compared to non-amputees. To ameliorate these gait compensations and secondary disorders, improved lower limb prostheses are needed that can better replicate the function of the intact foot and ankle.

1.3 CURRENT DEVICES

1.3.1 *Passive Devices*

Most amputees currently wear passive, composite prosthetic feet (Figure 1-1). These have elastic storage and return (ESR) properties, which can help support the trunk in late stance [3]. ESR, however, cannot fully compensate for the role of the missing ankle plantar flexors, and various muscle groups on both the residual and intact limb have elevated activation [3]. Similar passive orthoses have been shown in simulation to replicate

uniarticular soleus (SOL) function, but not gastrocnemius (GAS) function [19]. Different devices have different stiffness properties, which result in very different muscle compensations [20]. Passive devices also tend to weigh about 35% less than the intact limb [21], though there is some disagreement on the effect of mass on the energetic cost of amputee walking [21], [22].

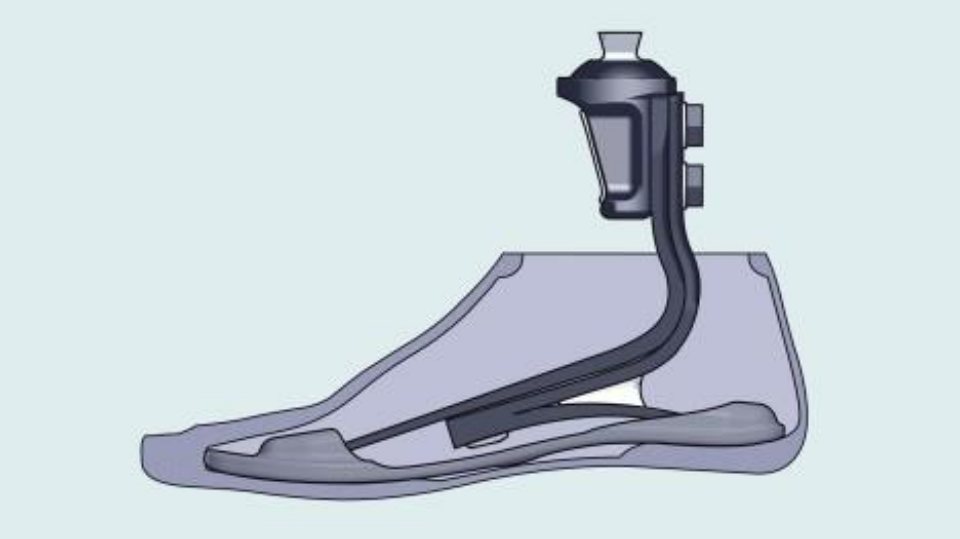

Figure 1-1. Example ESR foot inside cosmesis. (Ottobock USA, Minneapolis MN).

1.3.2 *Powered Devices*

Powered devices aim to address some amputee gait impairments. The BiOM (BionX Medical Technologies, Bedford, USA), for example, uses kinetic and kinematic sensing to determine gait cycle phase and add power at the ankle during push-off [23]. Despite the weight of the BiOM (Figure 1-2), it was shown to decrease the metabolic cost of amputee walking on even ground [24], [25]. However, many gait compensations are still present in amputees walking with the BiOM. Ankle range of motion (ROM) is still below intact limbs, and proximal compensations, such as at the hip, are further elevated with the powered device [5]. Vanderbilt University's Center for Intelligent Mechatronics is also developing a

powered ankle prosthesis that can adapt to walking, standing, and variable terrain [26]. Both the BiOM and the Vanderbilt device actuate just the ankle, which can only replicate soleus muscle function, not the gastrocnemius (See Section 1.4).

Figure 1-2. BiOM powered ankle-foot prosthesis (BionX Medical Technologies, Boston MA)

1.4 GASTROCNEMIUS AND SOLEUS ROLES IN HEALTHY WALKING

The gastrocnemius (GAS) and soleus (SOL) are the primary ankle plantar flexors. GAS is the largest ankle plantar flexor, and has a distinct and important role in healthy gait. The GAS is biarticular, and spans both the knee and ankle joints to cause ankle plantar flexion and knee flexion when it contracts. Lower-limb amputees lack the function of the GAS and other distal leg muscles in healthy walking; GAS accelerates the leg into swing during late stance phase, while the SOL accelerates the trunk forward [27]. The lack of plantar flexor muscles has been linked to increased rectus femoris, biceps femoris, vastus lateralis, and iliopsoas muscle force [3], [8]–[10]. The biarticular nature of the GAS also allows for work transfer between the knee and ankle [28], [29]. Several studies have investigated work transfer of biarticular muscles, but these were done with non-gait tasks like cycling or

jumping, and focused primarily on biarticular muscles between the hip and knee [28], [29]. Further analysis of the work transfer can yield important insight into biarticular GAS function during gait.

Additionally, van der Krogt et al. have shown that human gait is sensitive to GAS and SOL weakness [30]. In their simulations of healthy gait, they found that GAS weakness caused increased muscle activation in biceps femoris, semimembranosus, semitendinosus, iliopsoas, gluteus medius, gluteus maximus, sartorius, and SOL [30]. Also of note in their studies, van der Krogt et al. found that 80% weakness of both plantar flexors (GAS and SOL) resulted in a total muscle stress increase of over 200%. These findings indicate the importance of the ankle plantar flexors in overall gait energetics.

Research into the musculotendon morphology of GAS during gait shows that GAS is nearly isometric in mid to late stance phase, and the force production is primarily from tendon stretch during this time [31]. Tendons are a passive elastic element in series with the muscle, and as such act as simple springs in muscle models [32]. Collins et al. showed that a passive clutched spring in parallel with the ankle plantar flexors could reduce SOL activation by 22% and the metabolic cost of walking by up to 7%, which indicates that quasi-passive spring design solutions may also have the potential to reduce the effort of amputee gait [33].

1.5 Amputee Gait Simulation

Computational musculoskeletal models of walking are useful tools to evaluate neuromuscular coordination of gait. These models simulate walking with rigid bodies linked together with joints that are actuated by dynamic force producing muscles. Many researchers are using OpenSim [34] to perform simulations of amputee gait, but there is no

amputee musculoskeletal model that has been validated and made available to other research groups. Some groups simply use the existing full-body models with muscles deactivated. Joshi et al., for example, used the existing musculoskeletal model, but removed the GAS and allowed the tibialis anterior (TA) and SOL to serve as the prosthesis ESR components. Amputees and prostheses have very different mass properties at the distal limb, and these differences are unaccounted for with this approach [21], [35]. It would be more appropriate to use either an idealized torque actuator or other actuators/springs that are more representative of passive prosthetic elasticity than TA and SOL. Other studies have neglected muscles altogether, opting to limit their focus to joint kinematics and kinetics [36]. This work, by LaPre et al. states that "Tibia mass and inertial properties were modified appropriately," but does not elaborate on these modifications [36]. Additionally, there are many muscle and metabolic cost measures (Section 1.2) that are not available with this limited analysis. In addition to the need for amputee-specific models, there is also research that shows that prosthesis-specific models may be needed for improved ankle accuracy in amputee running [37]. Overall, there is a demonstrated need for an amputee specific musculoskeletal model for use in muscle-based simulations of amputee gait. One of the primary contributions of this thesis will be the development and open-source release of a transtibial amputee OpenSim musculoskeletal model that is qualitatively validated [38].

1.6 Other Related Studies

To date, no other prostheses with biarticular knee-ankle coupling have been built or tested. In some preliminary work at MIT, Endo et al. added a clutched spring mechanism to the knee of a powered ankle transtibial prosthesis [39] and one subject wore it with

moderate success. They showed a decrease in overall metabolic cost while wearing the device compared to a passive device, though the hamstring muscle activation was elevated. This design however, actually uses a uniarticular spring at the knee to represent the biarticular GAS, neglects the ankle in its optimization analysis, and was only tested on one subject [39]. Herr, a co-author on this work, does have a patent pertaining to biarticular spring related devices [40]. Unal et al. have also presented a biarticular prosthesis design for transfemoral amputees with simulated results [41] and demonstrated the mechanical function with a non-amputee [42]. We are most interested in transtibial amputees because they represent a much larger population, and this thesis outlines the development and testing of a quasi-passive prototype biarticular prosthesis for transtibial amputees.

1.7 PROJECT INTRODUCTION

The goal of this research is to develop a quasi-passive biarticular prosthesis (BP) for transtibial amputees, using a clutched-spring mechanism that spans both the knee and ankle joints. To aid in this study and in future analyses, another aim is to develop and validate a generic amputee model for use in OpenSim simulations of amputee gait. To best contribute to this body of work, we have chosen outcome measures in kinematic symmetry, kinetics, individual muscle forces, work transfer, and total muscle force as an indicator of metabolic cost. The principal contributions of this thesis work are:

1. A prototype quasi-passive biarticular prosthesis for transtibial amputees
2. A novel musculoskeletal model for simulations of amputee gait
3. Analysis of the impacts of a biarticular prosthesis on amputee gait

Chapter 2. DEVICE DEVELOPMENT

In this section, a series of early simulations and preliminary studies are described. This work led to the final prototype version of the BP device, an amputee-specific musculoskeletal model, and understanding that led to the development of hypotheses and study procedures. The takeaways of this pilot work were:

1. Proof-of-concept that a biarticular clutched spring can produce similar force to GAS and reduce compensatory muscle activations.
2. An understanding of how attachment point, spring stiffness, and clutch timing can affect device function, as well as sensitivity to each parameter.
3. Development of a final prototype BP that is safe for amputees to wear and mechanically functions as intended.

2.1 Toward a Biarticular Prosthesis: Simulations of Healthy Walking with a Prosthetic GAS Spring

2.1.1 *Introduction*

As a preliminary test of concept, the potential to replicate GAS function using a spring mechanism was explored using available healthy walking data in OpenSim [34]. The purpose of this preliminary study was to determine if a passive clutched spring could generate forces resembling the magnitude and timing of a healthy GAS muscle and better understand what spring properties were necessary to achieve this. Healthy walking kinematics and kinetics were simulated under five conditions, outlined in Table 2-1.

Table 2-1. Test conditions for preliminary simulation

Test condition	Description
1	Normal GAS muscle (control)
2	GAS muscle removed (no-GAS)
3	Replace GAS with a clutched biarticular spring of stiffness 50 N/mm
4	Replace GAS with a clutched biarticular spring of stiffness 100 N/mm
5	Replace GAS with a clutched biarticular spring of stiffness 150 N/mm

The aim of this work was to demonstrate the use of a biarticular spring in place of GAS, and better understand the spring properties necessary to best replicate GAS force generation. Evidence suggests that GAS weakness results in elevated iliopsoas muscle force [3], so it was hypothesized that iliopsoas muscle force would increase without the GAS muscle, but improve toward healthy with the addition of the clutched spring. Additionally, it was hypothesized that total muscle stress, as an indicator of metabolic cost, would improve with the addition of the clutched spring.

2.1.2 *Methods*

All simulations were performed in OpenSim using a musculoskeletal model with 54 muscles and 19 degrees of freedom. The kinematic and ground reaction force (GRF) data used were from a healthy male walking at 1.2 m/s and provided in the OpenSim package [34]. The model was scaled using a static trial, and then inverse kinematics was run on the single gait cycle. The Residual Reduction Analysis (RRA) tool was then used to improve dynamic consistency and reduce the residual forces, and Computed Muscle Control (CMC) simulations were run for each test condition. The healthy condition was simulated with all 54 muscles active and no additional force elements added. The second condition, no-GAS, used the same model, but the right GAS muscle was removed. In conditions 3-5 (spring), the

right GAS was removed, and a clutched biarticular spring was added with proximal and distal attachments points matching the anatomical GAS. GAS stiffness is estimated to be 100 N/mm [31], so simulations with spring stiffness values of 50 N/mm, 100 N/mm, and 150 N/mm were performed. The timing of the clutch for the spring element was based on knee angle (Figure 2-1). The spring was engaged at peak stance phase knee flexion, at approximately 15% of the gait cycle, and disengaged when the knee again reached this same flexion angle, just before toe off (approximately 55% gait cycle).

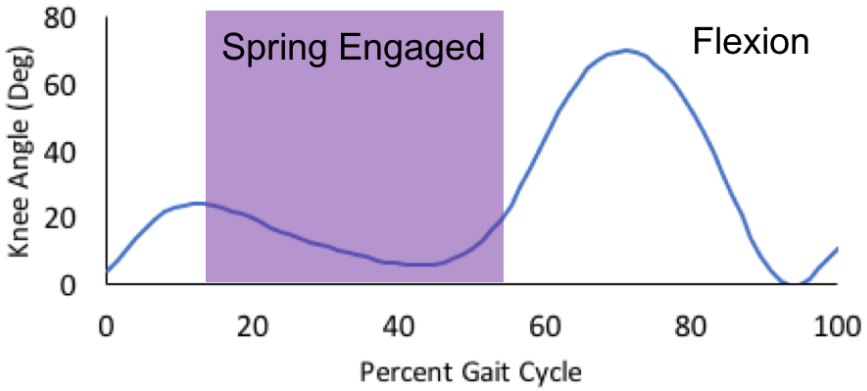

Figure 2-1. Knee angle across one gait cycle. The shaded region indicates when the clutch is engaged such that the spring can produce force.

2.1.3 *Results and Discussion*

Figure 2-2 shows the GAS or spring forces for each condition. In general, the springs were all able to replicate the general shape of the GAS force curve, but varied in peak force production. It is clear that the clutch spring mechanism disengaged too early in the gait cycle because the spring force drops to zero near 55% of the gait cycle, while GAS remained active until toe-off at about 60% (Figure 2-2). The 100 N/mm spring produced peak force nearest to the healthy GAS (1666 N vs. 2225 N), but it is likely that a stiffness between 100 and 150 N/mm would be closer (Figure 2-2). Compared to the control condition, the no-GAS

condition showed greatly increased peak iliopsoas force (2552 N vs. 946 N) during stance phase (Figure 2-3). Of the spring stiffness values, k=100 N/mm showed iliopsoas muscle forces most similar to the healthy control condition (Figure 2-3). The k=100 N/mm yielded a peak iliopsoas force of 1235 N, much lower than the no-GAS condition, though still higher than healthy (946 N). Of note is that the 150 N/mm spring resulted in a similar peak iliopsoas force to the 100 N/mm spring, but had less iliopsoas force than the healthy condition during much of the gait cycle (Figure 2-3).

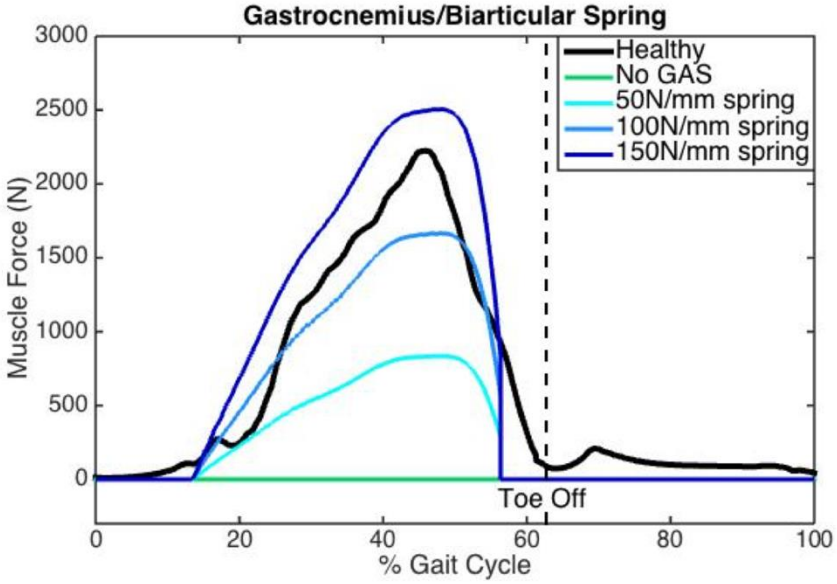

Figure 2-2. Healthy GAS muscle force compared to spring forces for different spring stiffness values.

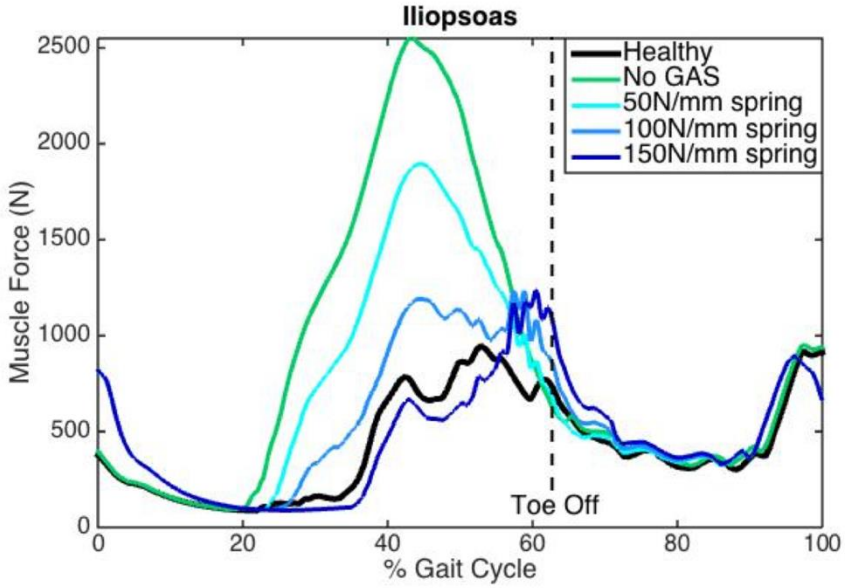

Figure 2-3. Iliopsoas muscle force over gait cycle for all experimental conditions: healthy (control), no-GAS, 50N/mm spring, 100N/mm spring, and 150 N/mm spring.

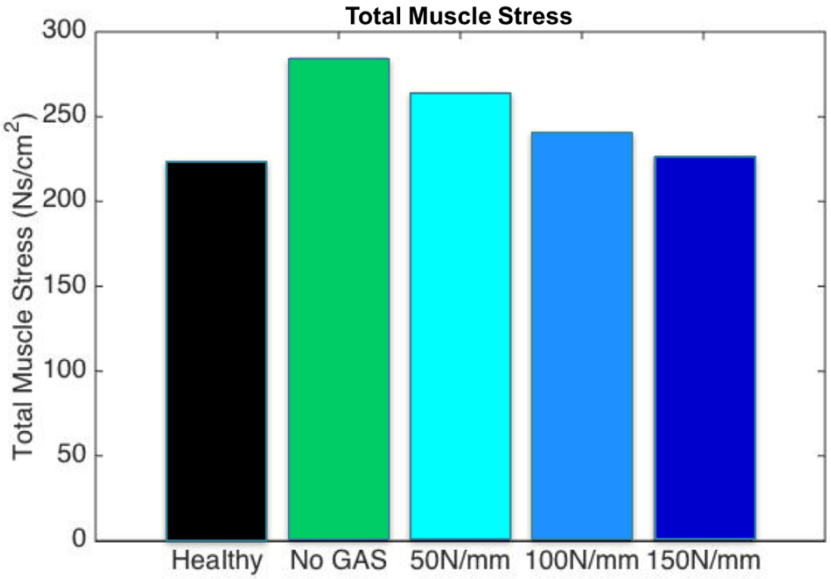

Figure 2-4. Total muscle stress calculated for each condition.

Using the CMC results, total muscle stress was also calculated for each of the test conditions, and the results are shown in Figure 2-4. The no-GAS condition had the highest total muscle stress, and the healthy control condition had the lowest. All three spring

stiffnesses improved (lowered) total muscle stress compared to no-GAS, and the 150 N/mm spring stiffness was the closest to healthy (Figure 2-4).

2.1.4 *Conclusions*

This preliminary work supports the hypothesis that the addition of a biarticular clutched spring can help replicate GAS function. GAS produces a force curve similar to that of a passive tension spring for much of stance phase. In amputees, a clutched spring mechanism has the potential to reduce iliopsoas compensation as well as total muscle stress and metabolic cost. A second preliminary study investigated the optimization of biarticular spring design parameters such as spring stiffness, attachment points, and clutch timing (Section 2.2). This work is somewhat limited because the data used is from a non-amputee, and because the kinematics are held constant across conditions. Additional preliminary investigations address this limitation by modifying the model to better represent a transtibial prosthesis and simulate experimentally collected amputee gait data.

2.2 Toward a Biarticular Prosthesis: Sensitivity Analysis of Spring Parameters

2.2.1 *Introduction*

The potential benefit of a clutched biarticular spring to replace lost GAS function was described earlier. As GAS contributes to both the ankle and knee torque generation, joint torque was a measure of interest to compare the biarticular spring to the biological GAS. The aim of this study was to analyze the sensitivity of ankle and knee joint moment contributions to various spring parameters. We hypothesized that a biarticular spring element could

replicate GAS contributions to knee and ankle joint moments, and that parameters such as attachment point, clutch timing, and stiffness would have a significant effect on device function.

2.2.2 *Methods*

A generic unilateral transtibial amputee model was developed in OpenSim [34] such that the residual shank and prosthesis match average mass properties from literature [43], [44]. These properties and calculations are described in detail in Section 3.3 but other features described in Chapter 3 were not present in this early iteration. The model has 21 degrees of freedom and 50 muscles. The prosthetic ankle is driven exclusively by a reserve actuator. A passive biarticular spring was added to the model, and the kinematic and ground reaction force (GRF) data were from a healthy male walking at 1.2 m/s, provided in the OpenSim package [34]. The baseline (BL) spring had the same attachment points as GAS in the healthy model and a stiffness of 100 N/mm, which is an estimate of the physiological GAS stiffness [31]. The length of GAS at 20% of the gait cycle (when GAS begins producing force) was used as spring rest length. Each parameter (proximal attachment, clutch timing, and stiffness) was varied individually to measure the effect on knee and ankle joint moment contributions. The knee attachment was moved in the posterior-superior direction by 1cm and then 2.5cm from the GAS anatomical attachment point. New clutch engagement times were chosen to be 18% and 22% of the gait cycle, which resulted in a -1.4 mm and +1.4 mm change in rest length from BL respectively. A static optimization simulation was carried out for each set of biarticular spring parameters. The biarticular spring force, and the biarticular spring's contribution to knee and ankle joint torque were calculated.

2.2.3 *Results and Discussion*

Table 2-2. Peak values of knee moment, ankle moment, and spring force; and a comparison to anatomical GAS moments and forces (%).

	Physiological GAS	Baseline Trial		Attachment Point (+1cm)		Clutch Timing (18%)		Stiffness (150N/mm)	
	Peak Value	Peak	% of GAS	Peak	% of GAS	Peak	% of GAS	Peak	% of GAS
Knee moment Contribution (N/m)	-52.19	-30.97	59.34	-39.79	76.24	-34.67	66.43	-46.46	89.02
Ankle moment Contribution (N/m)	-98.44	-57.28	58.19	-64.13	65.15	-64.1	65.12	-85.92	87.28
Force (N)	2094.8	1223.6	58.41	1357.2	64.79	1368.8	65.34	1835.3	87.61

The BL trial did not match GAS force or contributions to knee and ankle moment (Table 2-2). Moving the knee attachment 1 cm posteriorly and superiorly more closely replicated GAS function, generating 76% of GAS knee moment contribution, and 65% of the ankle moment contribution (Table 2-2,

Figure 2-5). Knee attachment +2.5cm away from BL resulted in peak knee moment contribution 6% greater than physiological GAS.

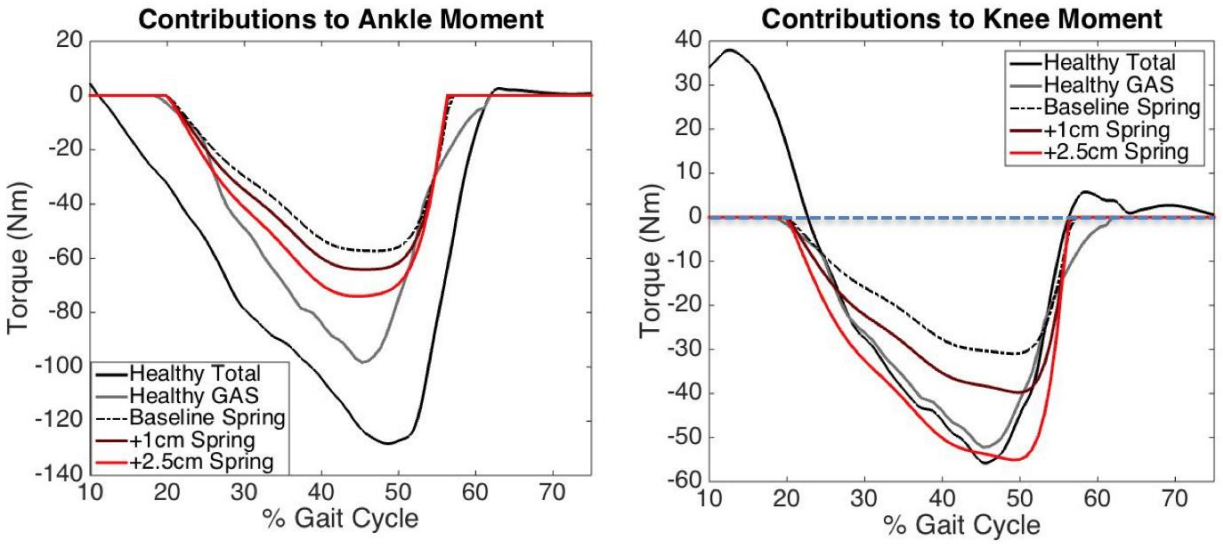

Figure 2-5. Contributions to ankle and knee joint moments with varied proximal attachment points. Healthy Total (Solid black line) represents the net joint torque. The blue dashed line indicates the zero knee torque contribution from current transtibial prostheses.

Engaging the clutch 2% of the gait cycle early (or about 25 milliseconds) increased both knee and ankle moment contribution 7% (Figure 2-6). This large change in moment contribution with a small change in timing indicates that the device function is highly sensitive to clutch timing. Knee and ankle moment contributions varied directly with changes in spring stiffness (Figure 2-7).

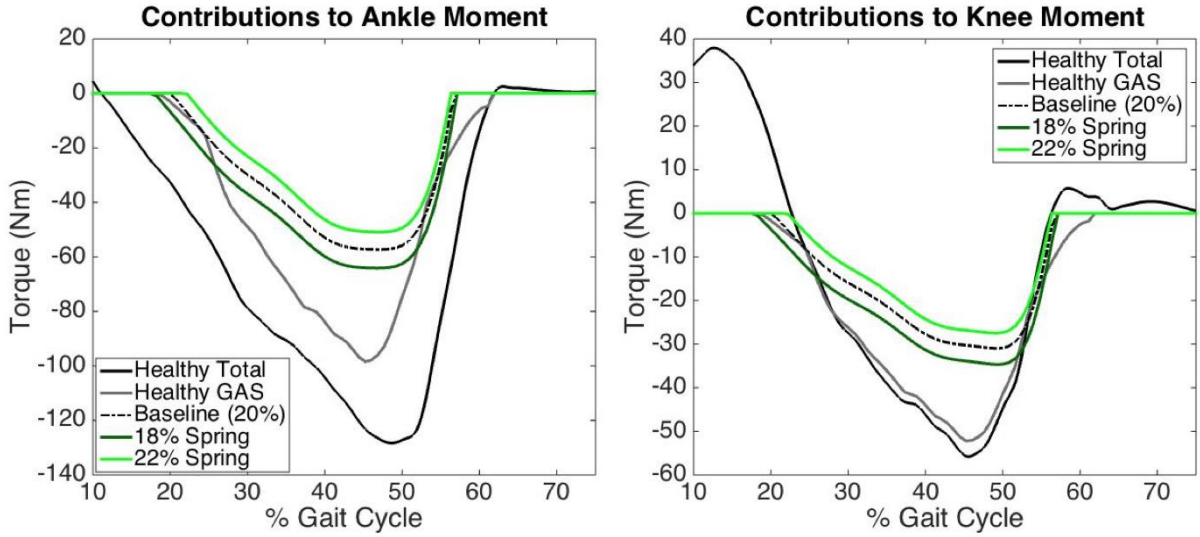

Figure 2-6. Contributions to ankle and knee joint moments with varied clutch timing. Healthy Total (Solid black line) represents the net joint torque.

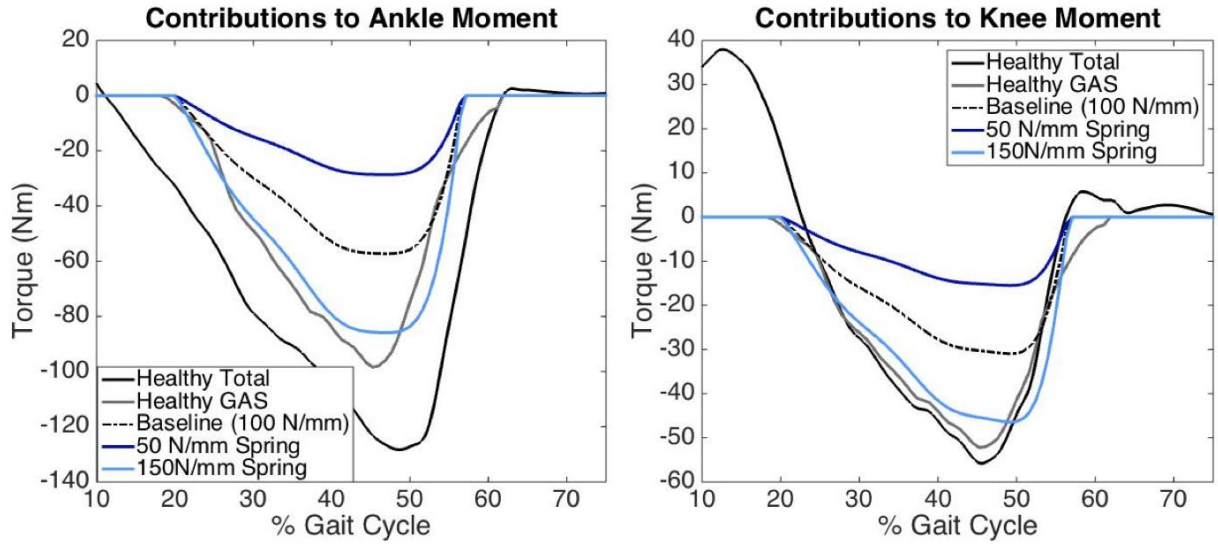

Figure 2-7. Contributions to ankle and knee joint moments with varied spring stiffnesses. Healthy Total (Solid black line) represents the net joint torque.

2.2.4 *Conclusion*

To summarize, increasing the moment arms of the biarticular spring by small amounts can increase the spring's contribution to knee and ankle moments. Earlier clutch timing and higher spring stiffness also have comparable effects. Moving the proximal attachment point can alter the joint moment contribution without requiring an increase in spring force, thus altering the attachment point (and thereby the moment arm) may provide significant design advantages in reducing the spring stiffness necessary to match GAS function. 100 N/mm is very stiff for commercially available springs of a reasonable size. Using less force to achieve the same torque outcome may also improve comfort at the proximal attachment by reducing skin shear. These simulations neglect soft tissue compliance at the proximal attachment point, which may be an important factor in the design of the device. We plan to use this simulation framework to carry out simulation-based design optimization for the proposed biarticular prosthesis. Future work will focus on determining optimal spring parameters given engineering design constraints. Subject specific simulation and optimization could also potentially be used to design patient specific biarticular prostheses. Restoring GAS function may improve mobility and the quality of life for those with lower limb loss. Additionally, these simulations are based on healthy (non-amputee) kinetics and kinematics. The next study addressed these limitations.

2.3 Evaluation of the Mechanical Function of a Novel Lower-Limb Biarticular Prosthesis

2.3.1 *Introduction*

We have previously shown in simulation that a stiff (100 N/mm) clutched spring element can replicate GAS function, and that similar timing to healthy GAS activation is desired (Sections 2.1 & 2.2). In the physical device however, the biarticular element interfaces with mid-thigh soft tissue of an unknown stiffness, which limits the effective stiffness of the biarticular spring. The purpose of this study was to evaluate the mechanical function of our first iteration biarticular prosthesis (BP) compared to a healthy GAS and earlier BP simulations. We also aimed to measure the effective stiffness of the biarticular spring during gait and make qualitative observations about the timing of the clutch-spring system.

2.3.2 *Methods*

An initial BP prototype was built (Figure 2-8), which features a clutched spring that attaches below the ankle to an ESR foot, and above the knee to a rigid thigh cuff. A force sensitive resistor in the heel detects heel strike. A microcontroller with software specified engagement and disengagement timing parameters controls an electromechanical clutch that engages the biarticular spring. A load cell is attached in series to the spring to measure spring force. One transtibial amputee subject walked on an instrumented treadmill while wearing the BP. 3D motion capture data 120Hz as well as ground reaction forces, spring on/off signal, and spring force data (1200 Hz) were collected.

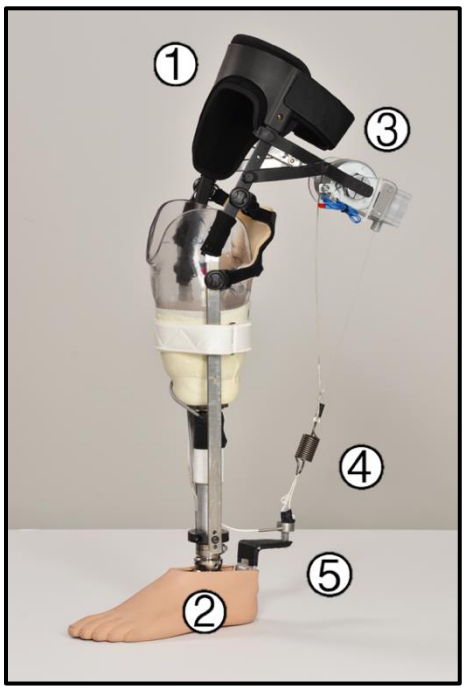

Figure 2-8. Early iteration BP prototype. 1: Rigid thigh cuff proximal attachment. 2: Sensor in heel to detect heel strike. 3: Electromechanical clutch to engage spring. 4: Biarticular spring. 5: Load cell in series with biarticular spring.

OpenSim [34] was used to compute joint kinematics, moment arm, and spring length. A generic unilateral transtibial amputee model was developed in OpenSim such that the residual shank and prosthesis match average mass properties from literature (Section 2.2). The model has 21 degrees of freedom and 72 muscles of the lower body. Inverse kinematics was performed to determine joint angles, muscle moment arms, and biarticular spring length. Matlab was then used to estimate the effective spring stiffness of the BP and to calculate power and peak energy stored in the spring. Effective BP stiffness was determined by performing a linear fit to the force (measured from the load cell) vs. displacement (measured from marker distances). Elastic energy stored in the spring was determined by the estimated stiffness value (k) and the peak force (F) over the gait cycle, using $U = \frac{1}{2}\, k(x_{max})^2$. Finally, the BP's contribution to knee and ankle power was determined by the

force, F, and moment arm measurements, $r(t)$, multiplied by the derivative of the joint angles, $P = Fr(t)\frac{d\theta}{dt}$. Power was then integrated to calculate work.

2.3.3 *Results and Discussion*

The average effective BP spring stiffness was 3.7 N/mm, which resulted in a peak force of 217.5 N ± 15 N over the course of each gait cycle. The peak elastic energy stored in the spring during a gait cycle was 6.7 J on average. The total work done by the BP on the knee and ankle was -9.11 and -3.37 J, respectively. Negative work values indicate that the joints did net work on the spring, i.e., more energy was transferred from the knee and ankle into the biarticular spring than was returned from the spring to the knee or ankle joints.

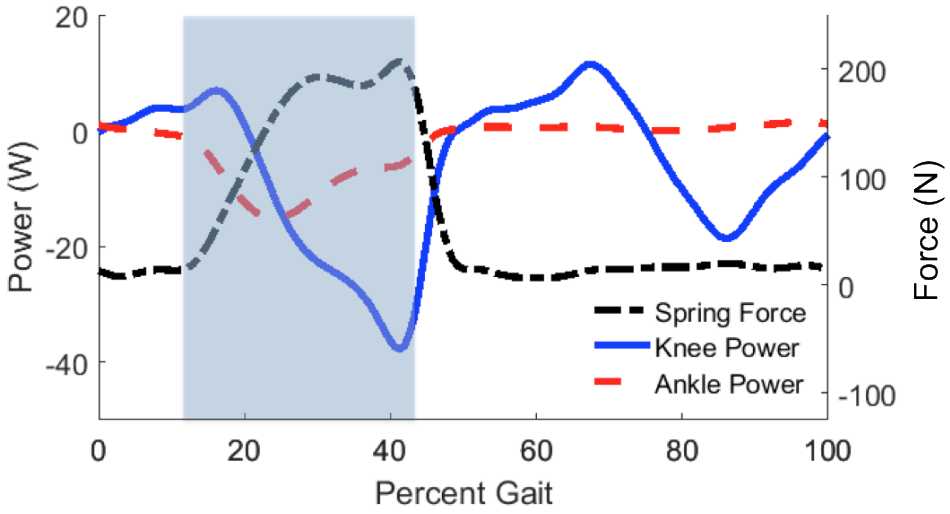

Figure 2-9. BP Spring force and its contribution to knee and ankle power over one gait cycle. The blue shaded region represents the window for which the clutch was engaged.

A cornerstone of the BP is its ability to allow the knee to transfer power to the ankle, so as to increase plantar flexor power during push-off. While a reasonable amount of energy was stored in the spring during this pilot data collection, the clutch disengaged too early in the gait cycle (Figure 2-9, blue region), thereby preventing the BP from returning the power

to the ankle joint. This timing error also created a steep drop in force that was very uncomfortable for the wearer. This work led to additional device modifications, which are described in the following sections.

2.4 Final Device Modifications and Mechanical Testing

2.4.1 *Device Description*

A final version of the BP prototype was built (Figure 2-11). There is still a clutched spring that attaches below the ankle and above the knee. The clutch is now ratcheted so that, when engaged, the string connecting the spring can shorten but not lengthen (Figure 2-10).

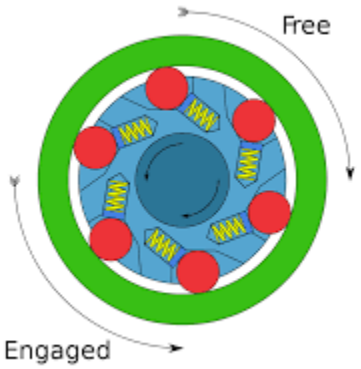

Figure 2-10. Graphic showing one-way function of the ratcheted clutch.

This one-way motion ensures that the spring begins producing force when the knee-to-ankle distance is at its minimum during stance, which is known to be near 20% of the gait cycle. Heel strike was detected with an instrumented pylon. Depending on equipment availability, this is either a pylon with the iPecs (RTC electronics Inc., Dexter MI) in series, or a pylon instrumented with a strain gauge. A load cell is attached in series to the spring to measure spring force. The microcontroller engages the clutch after heel strike occurs, and disengages the clutch once both the BP spring force and the vertical ground reaction force

fall below their respective threshold. A small recoil spring ensures that the string connecting the spring does not slack when the clutch is disengaged. The addition of the ratcheted clutch ensures that BP force production begins just after minimum string length, regardless of variations in gait and sensing. The iPecs/instrumented pylon to detect heel strike provides more consistent ground reaction force data than the heel sensor. The BP uses a College Park Venture foot (Figure 2-12) that has a known axis of plantar-dorsiflexion at the ankle to aid in precise marker placement. Exploded views of the clutch mechanism are shown in Figure 2-13.

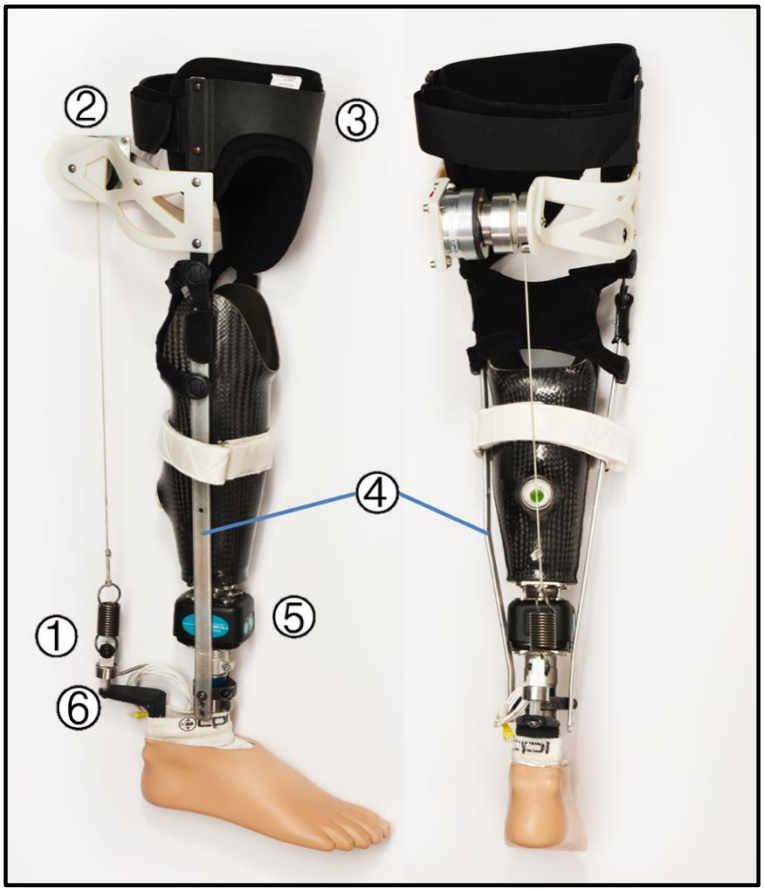

Figure 2-11. Finalized BP design. 1: Biarticular spring that actuates the ankle and knee when stretched. 2: Ratcheted (one-way) clutch that engages the spring when a minimum knee-to-ankle distance is reached. 3: Rigid thigh cuff that enables proximal attachment. 4: Uprights that support the thigh cuff and maintain knee alignment. 5: iPecs 6 DoF load cell to detect heel strike. 6: Load cell to measure spring force.

Figure 2-12. College Park Venture foot used in BP prototype.

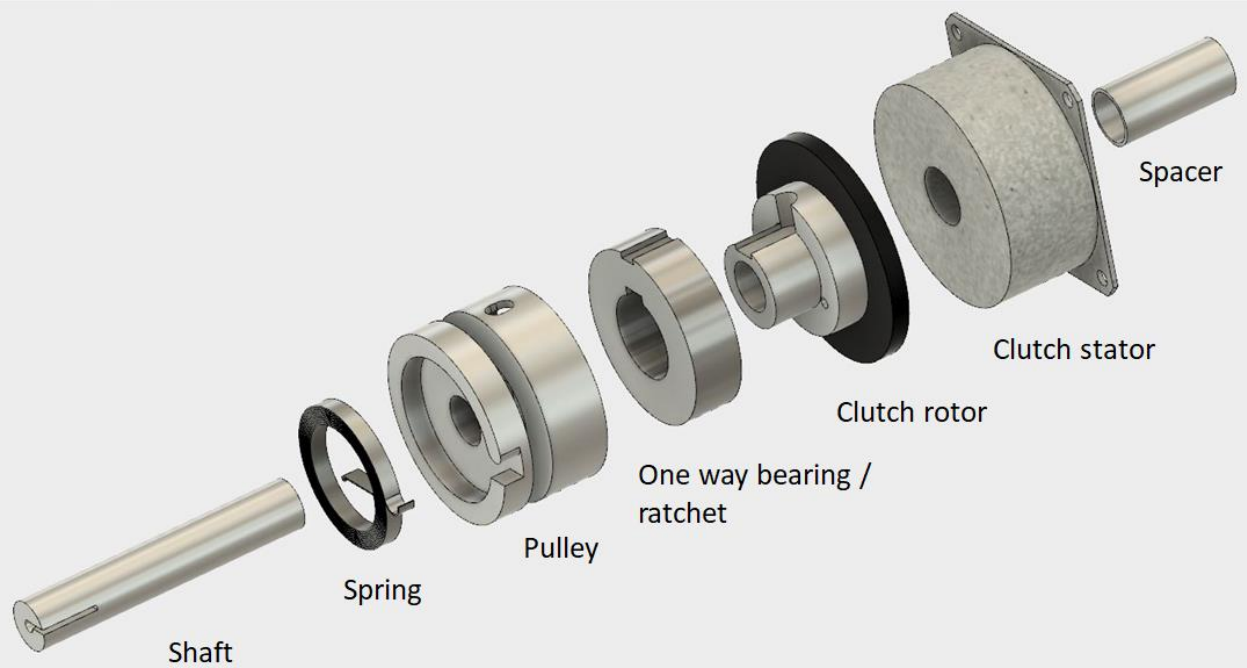

Figure 2-13. Exploded view of clutch components. From left to right: shaft, torsional recoil spring, recoil spring housing & string pulley, ratchet (one-way) bearing, EM clutch rotor, EM clutch stator.

2.4.2 *Mechanical Testing*

To verify the mechanical function of the BP, one amputee subject walked while wearing the BP. The strain-gauge pylon was used. Full 3D motion capture and ground

reaction force data were collected, in addition to several device measurements that were compared for timing and consistency. A string potentiometer was connected in parallel to the BP spring to measure knee-to-ankle distance as the subject walked. The sequence of mechanical events and state diagram of the BP is shown in Figure 2-14.

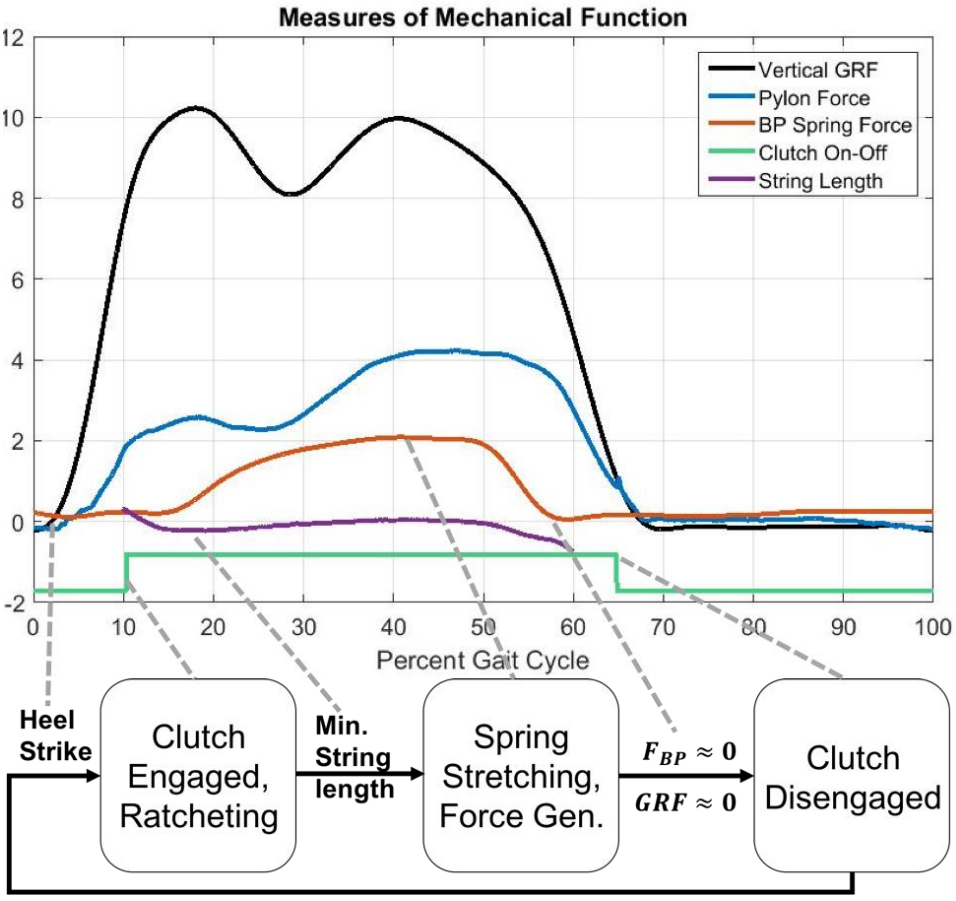

Figure 2-14. Comparison of analog data traces to observe BP mechanical function and timing. Gray dashed lines connect data traces to BP states and events.

The BP functioned as expected and was demonstrably ready to be worn by additional amputees for further testing. The clutch engaged shortly after heel strike, around 10% of the gait cycle. Device function is relatively insensitive to this timing because the BP spring will not start producing force until the minimum knee-to-ankle distance is reached, which occurs near 20% of the gait cycle. From there, the BP spring is stretched and produces force as the

knee-to-ankle distance is increased with typical gait kinematics. This force naturally falls to zero before toe off. It is important that the clutch does not disengage when the spring is still loaded, because it would result in a rapid step down in force and could be unsafe to wearers. Both BP force and the force detected by the pylon must drop below threshold before the clutch is disengaged. This ensures that the spring is no longer loaded, and that the clutch is disengaged for swing phase. This testing also gave insights into study protocol improvements for future subjects, described in Chapter 4.

Chapter 3. MODEL DEVELOPMENT

3.1 RAJAGOPAL MODEL DESCRIPTION

One goal of this study was to develop and validate an OpenSim musculoskeletal model of transtibial amputees. To this end, we started with the most state-of-the-art full body model, developed by Rajagopal et al. [45]. This model has 37 degrees of freedom (20 in the lower body), 80 Hill-type muscles in the lower body, and 17 ideal torque actuators to drive the upper body. The muscle properties were based on 21 cadavers and MRI images of 24 young healthy subjects. The model represents a 75kg, 170cm tall male but can be scaled to match subject specific measurements (Section 4.5.1).

The geometry consists of 22 rigid body segments, each defined with a local coordinate system and its joints. Each degree of freedom is represented with its own coordinate. For example, each hip joint has *hip_abduction*, *hip_rotation*, and *hip_flexion* coordinates. Of note is that the torso and head together are modeled as one rigid body, so torso movement other than at the base of the spine, such as neck motion, cannot be accurately modeled.

Each muscle is modeled as a massless linear actuator with wrapping and path points to most accurately define the line of action for each muscle [45]. For muscles that fan out anatomically and don't have a precise line of action, like gluteus maximus, multiple massless linear actuators were used. Muscle parameters, such as maximum isometric force, optimal fiber length, and pennation angle were defined using experimentally determined values. Additional musculotendon parameters were defined based on cadaver and MRI imaging studies.

This model was tested in simulation for both walking and running [45]. To validate the model's muscle outputs, Rajagopal et al. performed a qualitative comparison of the model's muscle force outputs and experimentally measured EMG signals. Many of the major features of the EMG signals were represented in the simulated muscle force estimates, and the OpenSim force outputs also matched well with Perry [46].

3.2 Body Geometry and Joint Definitions

To create a transtibial amputee OpenSim, model changes were made to the lower leg. SolidWorks CAD models of a generic socket, pylon, and foot were built. Though the socket and pylon are typically rigidly connected, these were modeled as separate bodies to generalize the model. These files were built to match the size of the full body model, and the socket and pylon were given equal height as if the amputation occurred at exactly half of the tibia length. The foot is a size 27cm, which is a common foot size for amputees but can also be scaled to individual subjects like any other body. The geometry files for the tibia and fibula were modified to resemble a mid-tibia amputation.

To accommodate as many future research interests as possible, the joint between the socket and the residual tibia was given two degrees of freedom: socket internal-external rotation with respect to the tibia and socket pistoning (superior-inferior translation). Both of these degrees of freedom were locked for this study, but other researchers looking at transverse socket torque [47], [48] and socket pistoning [49], [50] may use these coordinates. The pylon is connected to the socket with a single degree of freedom joint that allows the pylon to rotate about the vertical axis with respect to the socket (internal-external rotation). For our study the socket-pylon joint was locked. Finally, the ankle was defined with three degrees of freedom: plantar flexion-dorsiflexion, internal-external rotation, and inversion-eversion. During level walking, prosthesis motion is mostly plantar flexion-dorsiflexion, but these other degrees of freedom have been included for their potential to help answer other research questions [51]. Additionally, foot external rotation is an important setting for prosthetists to fit devices to amputees [52]. This degree of freedom should generally remain locked, but it can be locked to a subject-specific external rotation angle. These steps were repeated on a new full body model using the other limb, such that a generic left amputee model and a generic right amputee model were both created.

3.3 MASS PROPERTIES

The mass properties of the bodies at the distal leg are substantially different for amputated limbs than intact limbs. Prostheses are lighter weight than intact limbs, and some studies into prosthesis mass distribution have found that adding weight to the distal limb, even to match the intact side have adverse effects [21], [22], [53]. As such, it is important to have a model that represents the average mass properties of current prostheses as best as

possible. To best estimate generic residual limb and prosthesis mass properties, a literature search was conducted that resulted in five conclusions, described in Table 3-1. These conclusions are averages and are generally true for the transtibial amputee population, but likely vary for individuals.

Table 3-1. Conclusions from literature regarding amputee lower-limb mass properties.

Conclusion	Description	References
A	The center of mass (COM) for the entire below-knee segment is roughly 30% closer to the knee joint than intact limbs	[21], [22], [35], [44]
B	The COM for the residual limb is about 25% of the knee-to-ankle distance below the knee	[43]
C	The mass of the residual limb is 50% of the original tibia segment mass	[43]
D	The total mass for the entire below-knee segment is about 65% that of non-amputees	[43]
E	The moment of inertia (MOI) about the transverse axis through the knee joint is roughly 55% of a non-amputee's MOI	[21], [22], [35], [44]

A series of calculations were performed in Matlab to make sure mass properties were calculated correctly. This code is provided in Appendix A. In OpenSim, each body has its own COM defined in its own local coordinate frame, and the intact model contains more bodies than the prosthesis model. (Figure 3-1).

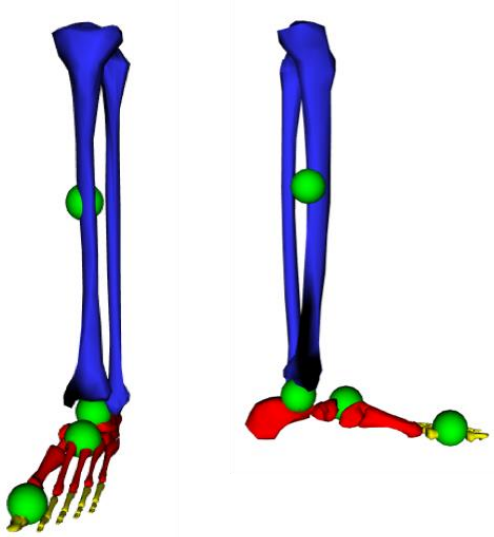

Figure 3-1. Bodies and centers of mass defined as in [45] for the intact lower limb. Blue is the body, *calcn* (heel and mid-foot bones) is in red, and the *toes* body is in yellow. Not visible is *talus*, which articulates with the tibia and the calcaneus. Green spheres show the center of mass for each body.

The following procedures were carried out to create the mass distribution for the amputee leg model. All COMs below the knee were translated into the same reference frame—with the knee at the origin. Once all COM values were in a global reference frame, COMs for all below-knee bodies were combined to obtain the total intact below-knee COM. This location was then moved 30% closer to the knee joint (Conclusion A). Then, the residual limb mass was set to be half that of the intact tibia body mass (Conclusion C), and the residual limb COM was set to 25% of the model's knee-to-ankle distance (Conclusion B). The masses and COMs of the socket and pylon were estimated based on the SolidWorks models and known material properties. With all these factors accounted for, the mass of the foot segment was solved.

With the new masses and COMs calculated for the amputee model, the moments of inertia were re-computed to match using the follow method. First, the intact MOIs, reported

about the center of mass, were translated to moments of inertia about the knee joint center, using the Parallel Axis Theorem:

$$I_{knee} = I_{COM} + M * d^2$$

In the above equation, I_{COM} is the given MOI about the COM, M is the body mass, and d is the distance from the COM to the knee. I_{knee} is the MOI about the knee joint. These MOIs were then reduced by 45% (Conclusion E). Finally, the Parallel Axis Theorem was used in the reverse direction to resolve for the MOI about the center of mass, using the calculated masses and COMs for the amputated limb:

$$I_{COM,amputee} = (0.55 * I_{knee}) - M_{amputee} * {d_{amputee}}^2$$

These body masses, centers of mass, and moments of inertia were input into the generic amputee OpenSim model files so that the mass properties of the model's residual limb and prosthesis match best possible estimates of amputee mass properties (Figure 3-2).

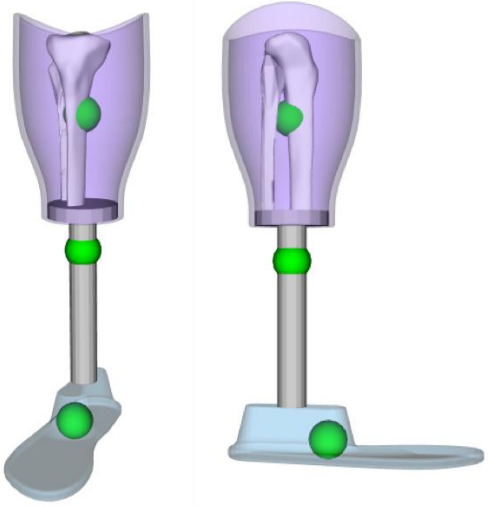

Figure 3-2. Bodies and centers of mass as defined for the prosthesis. Purple is the socket, gray is the pylon, and light blue is the foot. Green spheres show the center of mass for each body. Residual tibia and fibula are also shown.

3.4 MUSCLE PROPERTIES

Amputees experience a number of muscle imbalances compared to non-amputees, but these differences vary greatly across subjects. A study by Nolan et al. looked at the hip flexor and hip extensor strength in active and sedentary amputees [54]. They found that active amputees were 8-14% stronger in their residual limb than their intact, but that sedentary amputees were up to 49% weaker in the residual limb compared to the intact limb. Another strength study in transtibial amputees found that the residual limb quadriceps were 35-51% weaker than contralateral, and hamstrings were 42-60% weaker [55]. They also found no significant differences in strength asymmetries compared across time since amputation. Ryser et al. found a 27% reduction in strength of the residual limb hip abductors of transfemoral amputees, compared to both the intact limb and matched non-amputee subjects [56].

These different results make it difficult to settle on a scheme of muscle imbalance for a generic amputee model. Because there is too much variability in muscle strength across amputees, the default muscle strengths from Rajagopal's model [45] were left unchanged. Simulations of muscle weakness have concluded that human gait is most sensitive to weakness in plantar flexors, hip abductors, and hip flexors [30]. Because transtibial amputees generally lack the plantar flexor muscles, only the hip abductors and hip flexors are of concern. Van der Krogt et al. found that hip abductor weakness (glutes medius), was compensated for by increased gluteus minimus (GMIN), gluteus maximus (GMAX), semimembranosus (SMM), and decreased iliopsoas (IP) activity [30]. Hip flexor (iliopsoas) weakness was compensated for by increases in rectus femoris (RF), adductor longus (ADL), biceps femoris short head (BFSH), and GAS. With these compensations delineated in

simulation, it may become more clear to researchers of amputee gait if their results are indicative of muscle weakness in particular muscles, so that they can adjust the model accordingly. Simulation work studying cerebral palsy (CP) and crouch gait also found particular sensitivity to plantar flexor muscle weakness [57]. Additional work is ongoing to improve muscle simulation with heterogeneous populations like CP patients, using MRI, muscle synergies, and continuum descriptions of muscle [58], [59].

At the point of amputation, there are also a variety of differences in muscle reattachments. The level of amputation as well as other complications in amputation surgeries affect where and how the residual limb muscles can be reattached. Despite reattachment difficulties in amputation, most below-knee muscles are rendered ineffective in creating joint torque or motion, but this can impact EMG signals. We were interested in including the gastrocnemius muscle in the model, because its biarticular nature means it could flex the knee if reattached. However, not enough was known about the residual muscle specifics of the amputee population or our subject population, so all below-knee muscles were excluded from the amputee model. The amputee model includes 72 Hill-type muscles. To help answer this question in future work, this study measures EMG of the residual GAS and tibialis anterior (TA).

The full musculoskeletal amputee model is shown in Figure 3-4.

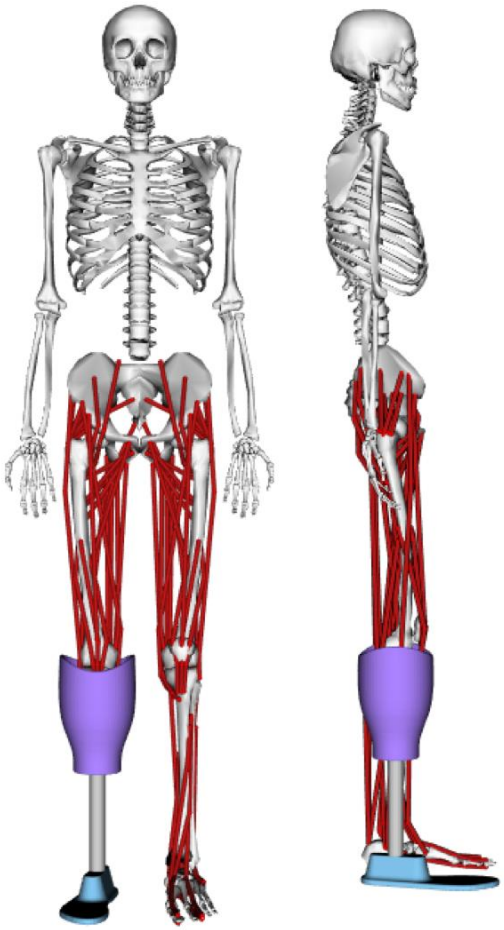

Figure 3-3. Final amputee musculoskeletal model for use in OpenSim.

3.5 Recommendations for Use of the Generic Amputee Model in OpenSim

This model is available open-sourced through OpenSim's project website (https://simtk.org/projects/biartprosthesis), and it was built with other potential research applications in mind. To that end, in this section I hope to highlight a few features and possibilities of the new generic amputee model to aid other researchers. First, because the pylon and socket are included as separate bodies, it is possible to scale them separately. By positioning a marker at the base of the socket, where it meets the pylon, separate scaling factors can be assigned to the residual limb and the pylon (Section 4.5.1). This will allow the

scaled model to match the specific subject and level of amputation and make the scaled mass properties more accurate. An example of this marker placement is shown in Figure 3-4 below.

Figure 3-4. Static trial images showing the placement of the pylon marker. This marker is later used in scaling to separately scale the residual limb and pylon segments.

It is also possible to set a subject specific ankle external rotation angle using this model. To do this, the external rotation could be measured during data collection, or this degree of freedom could be unlocked during the scaling process only. Unlocking this degree of freedom during scaling would allow the foot to externally rotate during the least-squares fitting that determines the static trial pose. This would allow OpenSim to estimate the external rotation angle based on the marker positions for the static trial. From there, the ankle external rotation should be locked at the static pose angle for analysis of the dynamic trials, as this degree of freedom is typically set by the prosthetist and then locked.

Finally, there are some limitations to the functionality of this model. As described above, the model's muscle parameters were unaltered from healthy estimates, but amputees exhibit muscle weakness heterogeneously in a variety of muscle groups. Additionally, this

generic amputee model was not analyzed using any running-style prosthetic feet, such as the Flex-Foot Cheetah (Össur Americas, Inc., California USA). Furthermore, some research has shown that modeling prosthetic ankles as pin joints can be inaccurate and sensitive to marker placement [20], [37]. The biarticular prosthesis uses a College Park Venture foot (Figure 2-12) that does have a known plantar-dorsiflexion axis of rotation, but other feet are more subject to this limitation. Other researchers will need to consider how the model's ankle pin joint could affect their results, and potentially alter the model for their specific purposes.

Chapter 4. METHODS

4.1 HYPOTHESES

We developed six measures of interest to understand the function of the BP, and designed experimental and simulation protocols to test several hypotheses associated with these measures. The following outcome measures were analyzed across test conditions for each subject:

Aim 1. Determine the impact of the biarticular prosthesis on kinematic symmetry of the ankle, knee, and hip joints. Symmetry will be measured by the R^2 correlation between the left and right side joints.

H1.1-H1.3: Kinematic symmetry at the ankle, knee and hip will be greater than the prescribed prosthesis when wearing the BP with the small (H1.1), medium (H1.2) and large (H1.3) spring.

H1.4-H1.6: Kinematic symmetry at the ankle, knee and hip will be greater than the BP baseline (recoil only) when wearing the BP with the small (H1.4), medium (H1.5) and large (H1.6) spring.

H1.7: The biofeedback condition will have greater kinematic symmetry at the ankle, knee, and hip than the same spring without biofeedback.

Aim 2. Determine the BP spring's contribution to net torque at the knee and ankle joint for different biarticular spring stiffnesses. The peak torque generated by the biarticular spring will be measured as a percentage of the net peak joint torque.

H2.1 – H2.3: The peak torque generated by the BP spring at the knee and ankle will be greater than zero for the small (H2.1), medium (H2.2), and large (H2.3) spring.

H2.4 – H2.5: The peak torque generated by the BP spring at the knee and ankle will increase with increasing spring stiffness, e.g. small spring torque is less than medium spring torque (H2.4) which is less than the large spring torque (H2.5).

H2.6: The peak torque generated by the BP spring used during the biofeedback condition will be larger than that same spring during the non-biofeedback condition.

Aim 3. Compare BP torque to contralateral GAS torque at the knee and ankle. The comparison measure will be the mean absolute error (MAE) between the BP torque and prescribed condition GAS torque over the gait cycle.

H3.1-H3.3: MAE between the BP and GAS torque contributions will be lower than the prescribed prosthesis when wearing the BP with the small (H3.1), medium (H3.2) and large (H3.3) spring.

H3.4-H3.6: MAE between the BP and GAS torque contributions will be lower than the BP baseline (recoil only) when wearing the BP with the small (H3.4), medium (H3.5) and large (H3.6) spring.

H3.7: The biofeedback condition will have less MAE between the BP and GAS torques than the same spring without biofeedback, at both the ankle and knee.

Aim 4. Determine the impact of the BP on total muscle force, as an indicator of metabolic cost. Total muscle force is calculated as the sum of all muscle forces in the model over the entire gait cycle.

H4.1: Total muscle force for the BP baseline condition will be higher than that of the prescribed condition, because of the increase in device weight.

H4.2 – H4.3: Total muscle force will decrease as spring stiffness increases such that the small spring has a higher total muscle force than the medium spring (H4.2), which has a higher total muscle force than the large spring (H4.3).

H4.2-H4.4: Total muscle force will be less than the prescribed prosthesis when wearing the BP with the small (H4.2), medium (H4.3) and large (H4.4) springs.

H4.5-H4.7: Total muscle force will be less than the BP baseline (recoil only) when wearing the BP with the small (H4.5), medium (H4.6) and large (H4.7) springs.

Aim 5. Determine BP work at the knee and ankle, as a measure of work transfer between joints. This is calculated as the BP torque times the change in joint angle, summed only over the gait cycle period where the BP spring is active.

H5.1-H5.2: BP work at the knee and ankle will be larger in magnitude with increasing spring stiffness, e.g. the small spring with do less work than the medium spring (H5.1), and the medium does less work than the large spring (H5.2).

H5.3-H5.5: BP work at the knee and ankle be greater in magnitude than the prescribed prosthesis (zero) when wearing the BP with the small (H5.3), medium (H5.4) and large (H5.5) springs.

H5.6-H5.8: BP work at the knee and ankle will be greater in magnitude than the BP baseline (recoil only) when wearing the BP with the small (H5.6), medium (H5.7) and large (H5.8) springs.

H5.9: The BP will transfer work from the knee to the ankle, which would be shown by a negative knee work value, and a positive ankle work value.

Aim 6. Qualitatively compare the EMG and Static Optimization muscle force outputs, to validate the generic amputee model.

The following sections describe in detail the data collection, processing, and analysis procedures, from subject recruitment and data collection to OpenSim simulations.

4.2 SUBJECT DEMOGRAPHICS

Gait data for seven transtibial amputee subjects (n = 7) was collected. Full demographic data for the subjects is summarized in Table 4-1. Six subjects were male and one was female. The average age was 51±12.3, the average height was 1.78m ± 0.06, and the average weight was 91.5kg ± 15.3. Participants chose their comfortable treadmill walking speed (held constant across conditions), and the mean self-selected walking speed was 0.84m/s ± 0.22.

Table 4-1. Demographic data for study participants

Subject	Sex	Age	Height (m)	Weight (kg)	Walking Speed (m/s)	Prescribed Prosthesis
1	M	45	1.75	111.6	1	College Park Soleus
2	F	55	1.77	89.4	0.5	not recorded
4	M	63	1.75	87.1	0.9	Ossur Variflex
5	M	59	1.83	105.9	0.8	Ossur Variflex
6	M	63	1.69	74.0	0.6	College Park Velocity
7	M	31	1.87	100.7	1	Ossur Proflec XC
8	M	41	1.81	71.9	1.1	Ossur Re-flex

4.3 DATA COLLECTION

With VA Puget Sound Health Care System and University of Washington IRB approval, 8 transtibial amputee subjects were recruited through VA Puget Sound Healthcare System. Researchers posted flyers and called a directory of amputees who had indicated potential willingness to participate in VA Center for Limb Loss and Mobility (CLIMB) gait studies. One subject (Subject 3) could not participate in the study because his prescribed prosthesis socket was not compatible with the BP. Each subject came to the lab for two visits: once for a fitting and again for the full data collection.

The purpose of the fitting session was to meet and consent subjects, as well as to take detailed leg measurements to custom fit components of the BP to each individual subject. The uprights (Figure 2-11) need to be customized to each subject's leg length so that the knee hinge aligns with the anatomical knee joint, and the thigh needs to be sized for the thigh cuff. A detailed protocol for the fitting session is provided in Appendix B. First, researchers would explain the study consent forms, and have willing subjects sign. Once consented, the subject's height and weight were recorded. Photographs of the subject from the waist down were recorded to aid in later device fit customization. Then additional measurements of the subject's affected limb were taken, such as thigh circumference, the height of the tibial

plateau above the ground, and knee width. If possible, the BP was installed on the subject's socket and worn briefly to assess clearance, sizing, and other comfort considerations. Finally, if time permitted, subjects would walk on the lab treadmill in their prescribed prosthesis to help acclimate to the difference in treadmill walking.

On the day of the data collection, subjects were limited to a session of four hours. A summary of data collection methods is shown in Figure 4-1. Motion capture data was collected using a 12 camera Vicon system (Oxford Metrics, Oxford UK) and an instrumented treadmill (Bertec Corp., Columbus, OH). Prosthesis forces and torques were measured using an iPecs 6 DoF load cell (RTC Electronics, Inc., Dexter, MI), and BP spring forces were measured using a single axis load cell in series with the BP spring. The test conditions are described in Table 4-2 below.

Table 4-2. Description of walking test conditions

Condition	Description
C1	Walking at self-selected speed, wearing prescribed foot
C2	Walking at self-selected speed, wearing BP completely disconnected
C3	Walking at self-selected speed, wearing BP with just the recoil spring attached
C4	Walking at self-selected speed, wearing BP with SMALL spring
C5	Walking at self-selected speed, wearing BP with MEDIUM spring
C6	Walking at self-selected speed, wearing BP with LARGE spring
C7	Walking at self-selected speed, wearing BP and preferred spring. Given a trace of BP force and instructed to try to maximize it

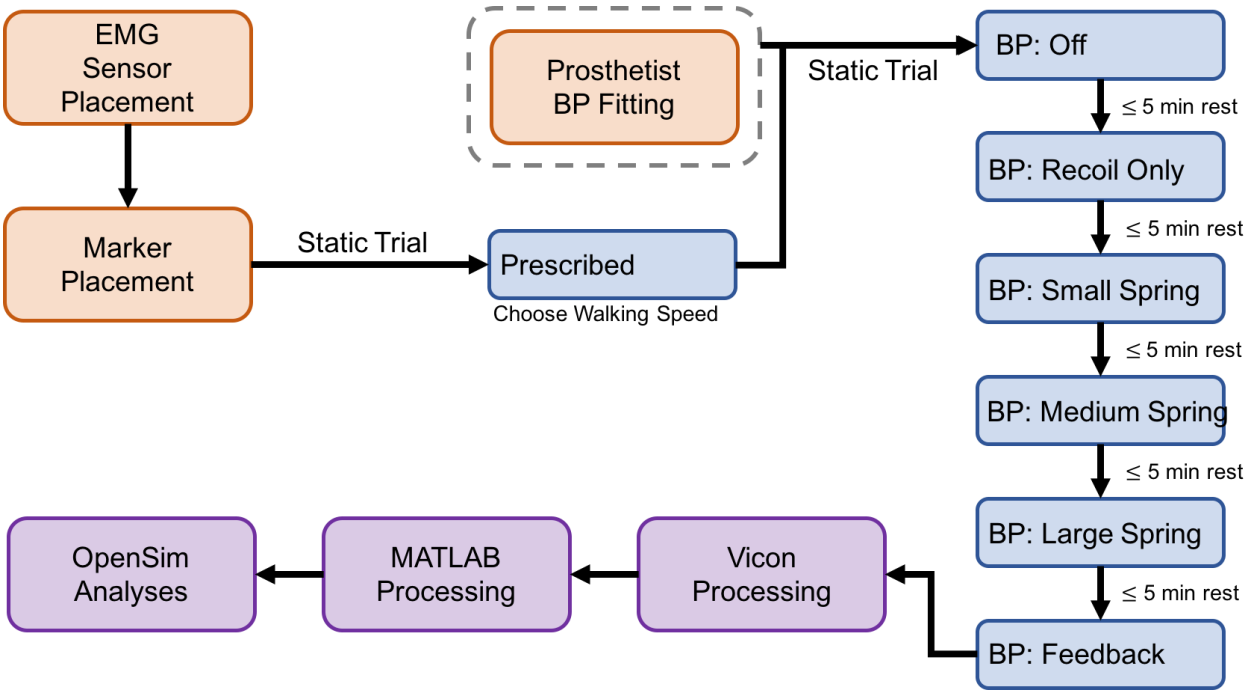

Figure 4-1. Flow chart of data collection and processing procedures.

First, subjects changed into tight fitting clothing and appropriate footwear and then height and weight were recorded. Fifteen wireless EMG sensors (Noraxon USA, Inc., Scottsdale, AZ) were then placed on the lower limbs to record activity of major muscles. A graphic of the placement locations, as well as a list of the muscles measured is shown in Figure 4-2 and Table 4-3. Subjects would perform an isometric exercise specific to each muscle (http://www.seniam.org/) so that the muscle belly could be found. Then the placement area would be shaved and cleaned with alcohol. The EMG electrode and ground would be placed and then taped down. In cases where the exact muscle belly could not be determined through a contraction exercise, anatomical landmarks were used to approximate the muscle location. This was most common when placing the gluteus maximus sensors and sensors at the distal affected limb. Low-profile electrodes were used for muscles inside the socket (GAS and TA), as well as rectus femoris on the affected limb to avoid discomfort when

wearing the prostheses (Figure 4-3). Most EMG sensors were placed with subjects prone and supine on a table with their prosthesis removed, and then subjects stood while wearing their prescribed device to attach the pairs of gluteus maximus and gluteus medius sensors. Because the muscle reattachments in amputation surgery and the level of amputation on the tibia were not consistent between subjects, soleus on the affected limb was not measured. Location of the medial gastrocnemius and tibialis anterior varied more on the residual limb than the intact limb. Additional documentation on the EMG placement exercises and locations is provided in Appendix C. As the EMG sensors were placed, voluntary contraction exercises were performed to check the signal to noise ratios of the signals.

Table 4-3. EMG Placement Locations

Sensor Number	Limb	Muscle
1	Residual	Gluteus maximus (GMAX)
2	Residual	Gluteus medius (GMED)
3	Residual	Biceps femoris long head
4	Residual	Rectus femoris (RF)
5	Residual	Vastus medialis origin (VMO)
6	Residual	Tibialis anterior (TA)
7	Residual	Medial gastrocnemius (GAS)
9	Intact	Gluteus maximus (GMAX)
10	Intact	Gluteus medius (GMED)
11	Intact	Biceps femoris long head
12	Intact	Rectus femoris (RF)
13	Intact	Vastus medialis origin (VMO)
14	Intact	Tibialis anterior (TA)
15	Intact	Medial gastrocnemius (GAS)
16	Intact	Soleus (SOL)

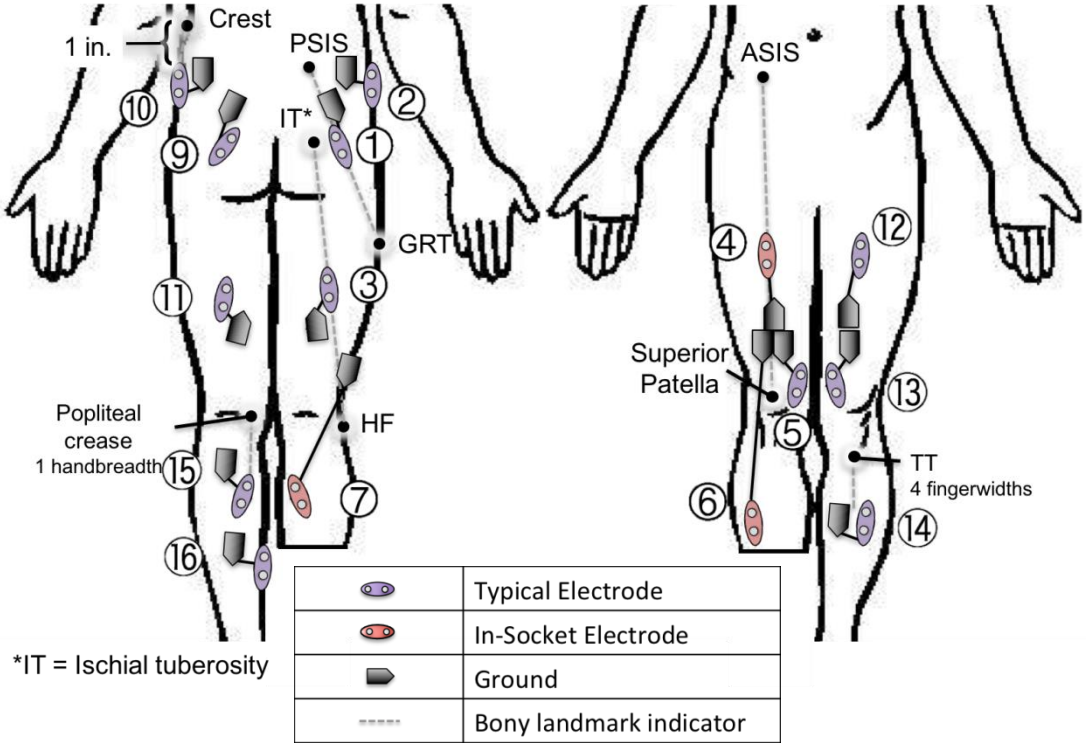

Figure 4-2. EMG sensor placement diagram.

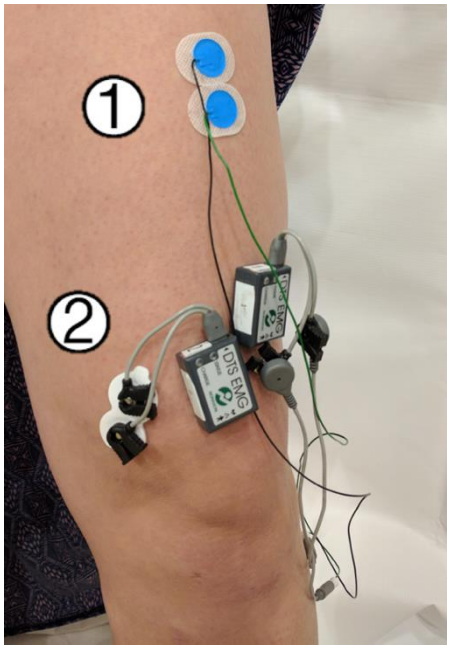

Figure 4-3. EMG electrode types used. 1: In-socket electrode, 2: Typical electrode.

Once EMG placement was completed, subjects donned a safety harness, that would later be attached to a rope to prevent falling while walking on the treadmill. After the harness, 74 reflective markers were placed on the subject. About half of these markers were placed on anatomical bony landmarks, while the rest were placed in rigidly attached clusters on the thighs, shanks, and upper arms. An additional 3 markers were placed on the BP to define the line of action of the clutched spring. A diagram of these marker locations is shown Figure 4-4.

Anthropometric measurements of the shoulder, elbow, wrist, knee, and ankle width, as well as leg length (ASIS to medial malleolus of the tibia) were measured and recorded. We then collected a static motion capture trial by having the participant stand straight up while looking forward, with their arms slightly abducted at the shoulder and their palms facing forward in the middle of the data collection volume (Figure 4-5). This static trial was used to help label the motion capture markers, as well as to scale OpenSim models to match each specific subject for future analyses.

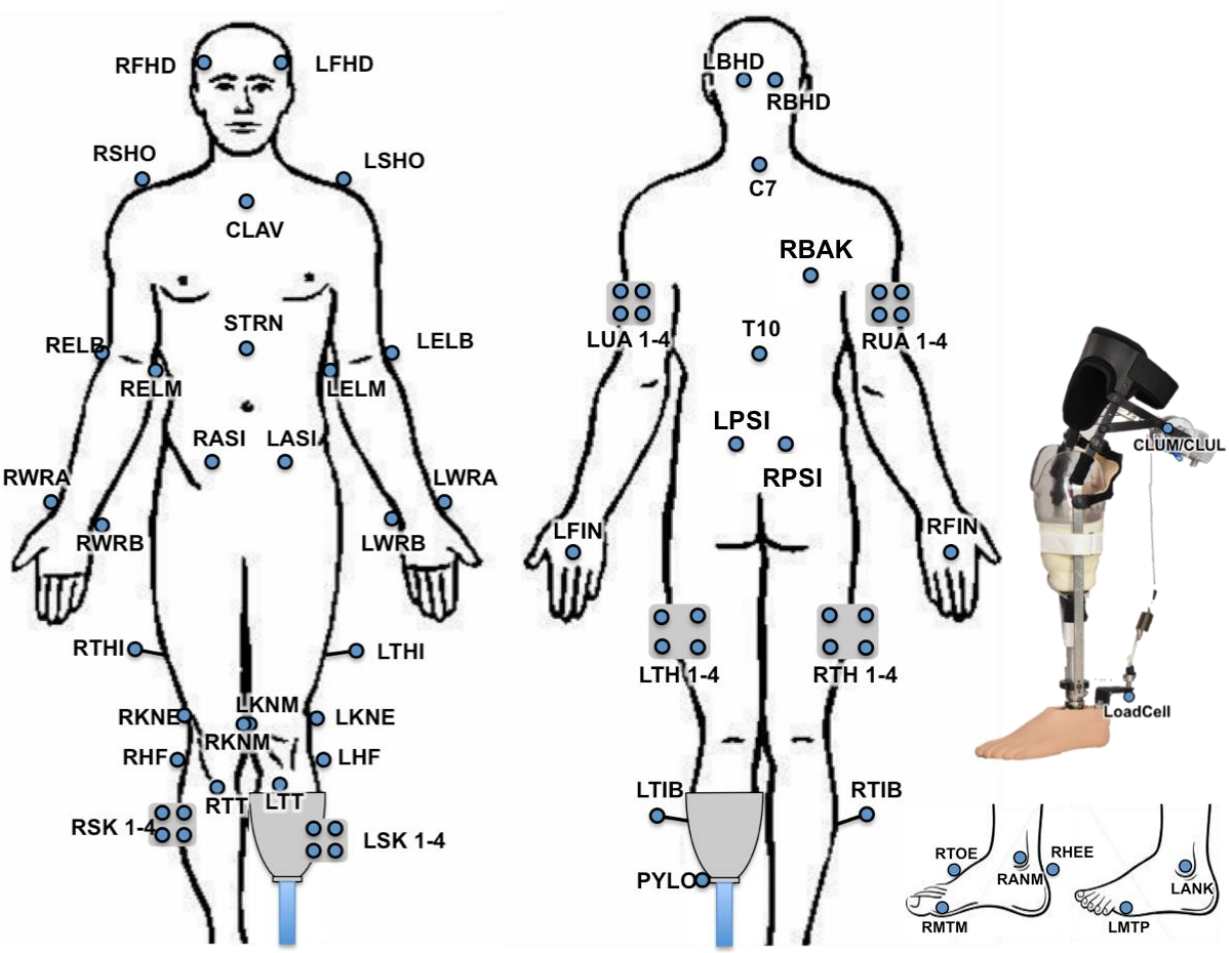

Figure 4-4. Marker placement locations. Full descriptions of each marker's placement are detailed in Appendix D.

Figure 4-5. Image of static pose during a prescribed foot static trial.

Once the static trial was recorded, the walking trials could begin. We first had subjects walk on the treadmill with their prescribed prosthesis at a slow speed (0.5 m/s) and then increased or decreased speed in increments of 0.1 m/s at the subject's request. This was their self-selected treadmill walking speed that was used for all walking trials. Given that the BP likely feels very different from their prescribed prosthesis, if subjects were unsure when choosing between two speed increments, we encouraged them to choose the slower of the two.

After determining their self-selected treadmill walking speed, subjects continued to walk while wearing their prescribed prosthesis. We collected data until we had five 10-second trials where subjects appeared to be walking in steady-state and were centered on the treadmill such that each foot only contacted one force plate. This usually took 3-5 minutes. These prescribed prosthesis trials were the first condition (C1). Before subjects walked with the BP, a prosthetist would ensure the best possible fit and alignment of the BP. Due to scheduling conflicts, this happened at varying points during or after EMG placement, marker placement, and the prescribed walking trials. Transitioning into the BP from the prescribed leg involved removing and replacing many of the markers on that leg, and occasionally required repositioning of EMG sensors. Measurements of the affected limb (knee width, ankle width, and leg length) were retaken, as well as subject weight. We collected a new static trial with the subject in the same position, and then they began walking at the same speed for the rest of the test conditions (Table 4-2, Figure 4-1).

The second walking condition (C2) was with the BP unpowered and its string disconnected, as a baseline measure. Subjects could sit and rest between all test conditions as desired. Next, the string and recoil spring (Figure 2-11) were connected. The recoil spring

applies a small force (20-30N) throughout the gait cycle to ensure the string does not get slack, and the effect of this design choice was tested in condition three (C3). Condition four (C4) was the first condition with the fully functional BP, connected to the smallest spring (k = 1.85 N/mm). Condition five (C5) had the medium spring stiffness (k = 3.7 N/mm), and condition six (C6) had the largest spring (k = 10.5 N/mm).

Finally, subjects were asked throughout which spring size they preferred to walk with, and their preferred spring was used again in Condition 7 (C7), which also included feedback to the wearer. For C7, we placed a monitor in front of the treadmill at a convenient height for the subject to see. We fed the output from the spring load cell as a real-time running graph plotted through LabView (Figure 4-6). The program also kept track of the maximum value reached (volts, corresponding to Newtons of force in the spring), and plotted this max value as well. Subjects were instructed to try to maximize the traces on the graph, which would mean increasing the force going through the BP spring. No kinematic methods were suggested, but subjects tried various kinematic changes to try to achieve a higher force. Measuring these changes, as well as the increase in force generation was the aim of C7.

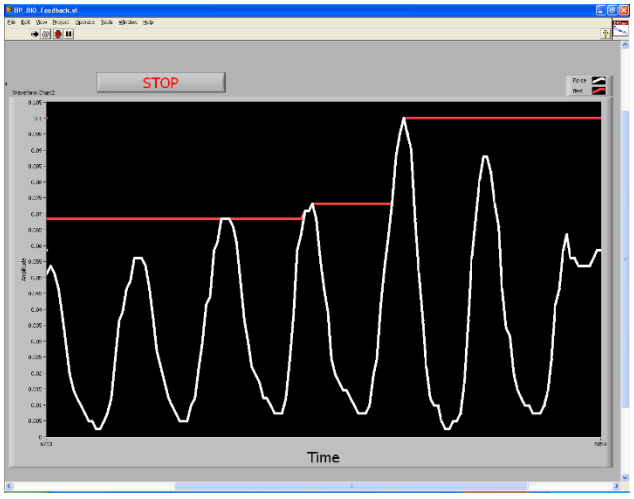

Figure 4-6. Screen shot of Biofeedback LabView program. The white trace shows the BP spring force amplitude in real time, while the red trace shows the all-time maximum.

Once five good 10-second trials of each of the seven conditions were collected, we ended the session by removing all the markers and EMG sensors, and putting the subject's prescribed foot back on. One subject deviated from this strict protocol. Subject 2 altered their preferred walking speed after the initial prescribed trials, so after C7 they changed back into their prescribed prosthesis and collected additional C1 trials at the new, slower speed before removing the sensors and markers.

4.4 Data Processing

Once gait data was collected in the lab, the motion capture data and force data was processed and exported from Vicon Nexus. First, all the marker trajectories for the dynamic trials were auto-labelled based on the static trial. This procedure uses the Vicon Plugin Gait model and the anthropometric measurements collected during marker placement. The success of the auto-label was checked (the wrist markers are often reversed), and then small gaps in the marker trajectories were filled using splines and surrounding marker trajectories. The marker data was batch exported as TRC files for each trial, and the ground reaction force, EMG, and BP signal outputs for a given trial were exported in a CSV file.

Custom Matlab codes were written to further process the exported data and prepare input files for OpenSim analyses. A block diagram of the Matlab processing is shown in Figure 4-7.

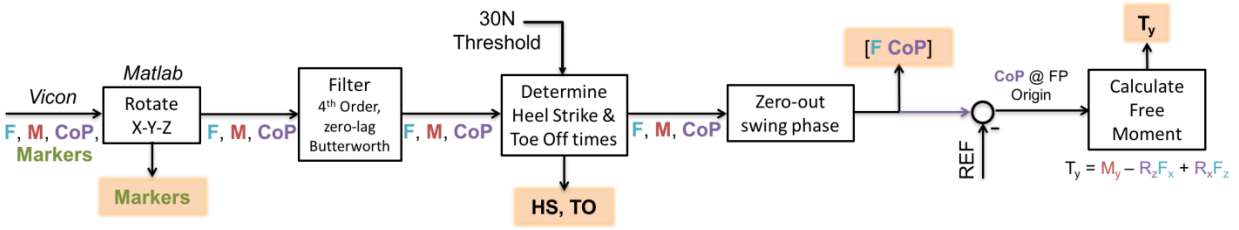

Figure 4-7. Matlab processing block diagram. The outputs are rotated marker trajectories, indexed heel strike and toe off times for both feet, as well as the MOT files of the ground reaction forces for use in OpenSim.

The various data streams exported from Vicon (marker trajectories, GRFs, and spring data) require different levels of processing to prepare for use in OpenSim. The marker trajectories were generally the simplest to prepare: the coordinate data only needed to be rotated to match the OpenSim reference frame.

Vicon	OpenSim
X – Y – Z	Z – X – Y

For some trials, however, markers fell off or weren't picked up by the cameras. Generally, these markers were just ignored in the OpenSim analyses, but markers such as CLUM and LoadCell were needed for spring force calculations. When these markers went missing, their trajectory was estimated using surrounding markers and their known relative position from the static trial. For the LoadCell marker, the knee marker, medial and lateral ankle markers, as well as the medial/lateral metatarsophalangeal markers were used to track a local reference frame at the ankle, and then with a rigid-body assumption the

LoadCell marker position could be estimated. Similarly, the CLUM marker trajectory could be estimated based on the CLUL marker and the thigh cluster markers. This method was tested on data where the marker was not missing, and the maximum error was consistently below 1.5 cm. For additional information, the Matlab function used for these calculations is provided in Appendix E.

Ground reaction forces were also transformed into the OpenSim reference frame. In OpenSim, X is the anterior direction, Y is the vertical direction, and Z is the mediolateral direction. This convention is used from here forward. The BP spring force and the ground reaction forces and moments are filtered at 20 Hz using a zero lag fourth order Butterworth filter. The centers of pressure were filtered at 5 Hz, also with a zero lag fourth order Butterworth filter. Heel strike times were determined based on a threshold value of 30 N applied to the vertical ground reaction force; a vertical GRF below 30 N was considered swing phase. To eliminate swing-phase noise from the treadmill, the centers of pressure (CoP), Forces, and Moments were all set to zero during swing. The free moment about the vertical axis (y-axis) was then determined using the equation:

$$T_y = M_y - R_z F_x + R_x F_z$$

where *M* is the moment reported from the treadmill force plate, *R* is the vector of the distance from the center of pressure to the force plate origin, and F is the filtered force data. The CoP is reported from Vicon at the global origin, not the force plate origin. To determine the R-vector with respect to the force plate origin, a reference value, REF is subtracted.

The BP spring forces were also applied as external loads to the OpenSim model where applicable, so another MOT file was generated that also contained the spring force and CoPs. Since the spring is in tension between its attachments to the femur and the foot, the force measured from the spring was applied to both the femur and the foot in an equal and opposite manner (Figure 4-8).

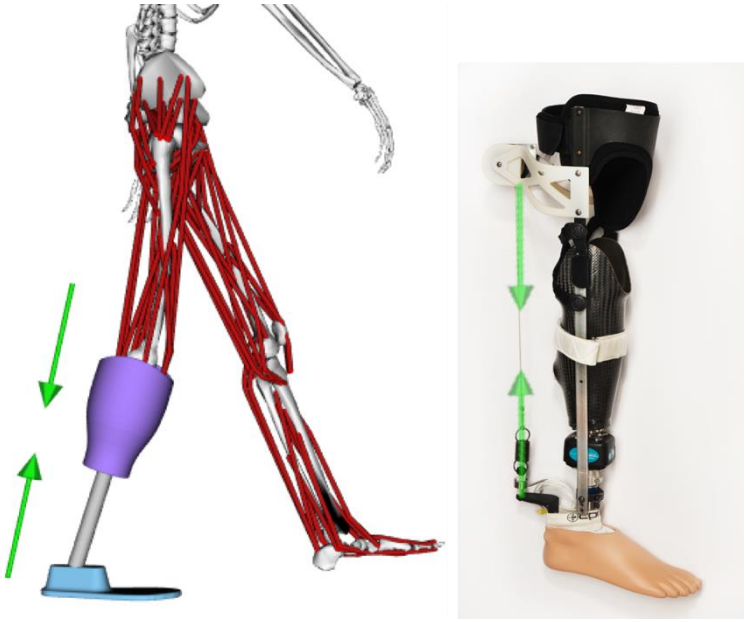

Figure 4-8. OpenSim Model with the BP spring force applied, and an image of the BP showing the direction of force application. The proximal force is applied to the femur, and the equal and opposite force is applied to the foot, along the line of action of the spring.

A block diagram of the BP force calculations is shown in Figure 4-9. The voltage recorded from the load cell in series with the BP spring is first converted to Newtons (1V = 100N), and then filtered at 20 Hz using a 4th order, zero-lag Butterworth filter. The proximal and distal points of force application (CoP) were calculated based on the three markers that were placed on the BP during data collection: CLUM, CLUL, and LoadCell (Figure 4-4).

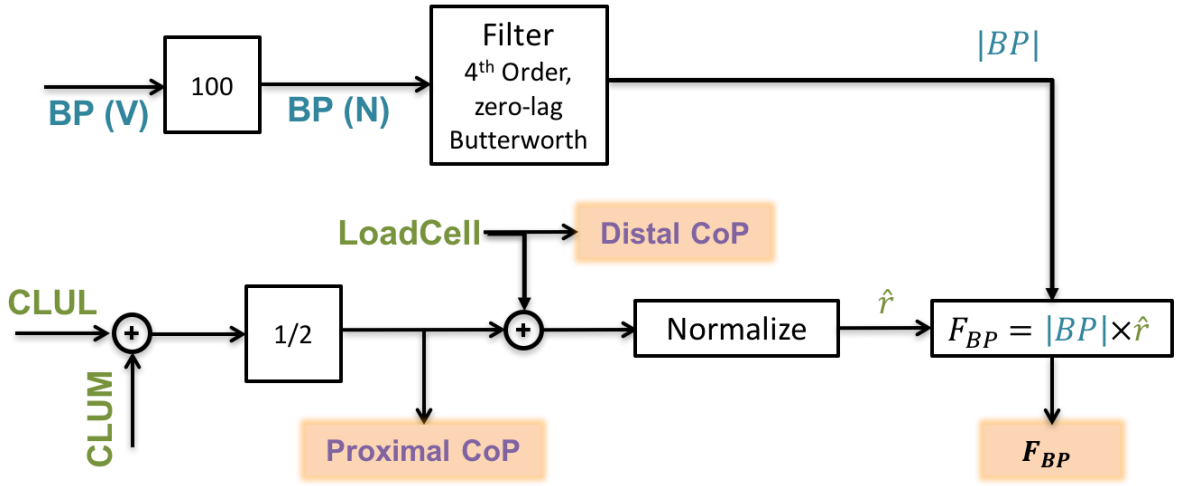

Figure 4-9. Block diagram of Matlab calculations for BP spring force applied to the model.

CLUL and CLUM are the lateral and medial markers on the clutch, and their average is taken as the proximal CoP. The LoadCell marker location itself is used as the CoP for the distal spring force. The vector representing the line of action of the spring is calculated by subtracting the distal CoP from the proximal. This vector is normalized so it has unit magnitude, and then multiplied by the BP force magnitude.

4.5 OpenSim Analyses

After processing the data in Vicon and preparing files for OpenSim, the amputee musculoskeletal model described in Chapter 3 was used to analyze each subject's gait data in OpenSim with the following processes: Scaling the model, inverse kinematics, inverse dynamics, static optimization, and muscle analysis. The inputs and outputs to each process are summarized in Table 4-4.

Table 4-4. Summary of inputs and outputs to each OpenSim process

OpenSim Process	Inputs	Outputs/Results
Scaling	Static trial marker trajectories, Subject weight, Generic amputee model	Subject-specific model
Inverse Kinematics	Subject-specific model, Dynamic trial marker trajectories	Joint angles
Inverse Dynamics	Subject-specific model, Inverse Kinematics joint angles, Ground reaction forces, BP spring force	Joint torques
Static Optimization	Subject-specific model, Inverse Kinematics joint angles, Ground reaction forces, BP spring force	Muscle forces
Muscle Analysis	Subject-specific model, Inverse Kinematics joint angles, Ground reaction forces, BP spring force	Muscle moment arms at ankle and knee

4.5.1 *Scaling*

Two models were scaled for each subject, one for the prescribed foot trials (C1), and one for all BP trials. This was necessary because the markers had to be adjusted, and the weight of the BP is larger than that of subjects' prescribed prostheses. OpenSim scales models by allowing the user to define pairs of markers, the difference of which is used in the scaling factor for the associated bodies. The generic (unscaled) model has attached markers in locations that match the experimental marker set, and the scaling factor is determined by comparing the distance of the marker pair on the model and the distance between the experimental marker pair in the static trial. It is more accurate to scale bodies in the X, Y, and Z directions separately where possible [60]. If a body is roughly cylindrical such as the femur, a scale factor defined along the bone (Y) can be used while scaling X and Z together [60]. OpenSim is limited to using the absolute distance between the marker pairs, and these markers can rarely be aligned perfectly along an axis. Therefore, to help with scaling, any

anatomical markers were projected onto planes so that direct X, Y, and Z scaling factors could be determined. These virtual markers are described in Table 4-5.

When scaling, OpenSim scales each body by the defined scale factors. In many cases, multiple pairs of markers were used and then averaged to determine the overall scale factor for a body. Additionally, some directions on some bodies did not have a good marker pair to define the scale factor. In these cases, such as torso_x (anterior-posterior torso scale factor), the pairs from the other two directions were averaged to get the third. Note that the definition of the model and the inclusion of the PYLO marker to define the boundary between socket and pylon allows for individual scaling of the residual shank and the pylon. Scaling these separately will keep the estimated mass properties as accurate as possible, allowing for any level of below-knee amputation.

Table 4-5. Description of virtual markers used for scaling

Virtual Marker	Associated Scale Factors	Description
LKJC, RKJC	Residual_y, shank_y, thigh_y	Left and Right knee joint centers. The average of medial and lateral knee markers.
LHEv, RHEv	foot_x	Heel markers, projected onto the floor.
LTOv, RTOv	foot_x	Toe markers, projected onto the floor.
LMPv, RMPv	foot_z	MTP markers, projected onto the floor.
LMTv, RMTv	foot_z	MTM markers, projected onto the floor.
LNKv, RNKv	shank_xz	Ankle marker (lateral), projected onto the floor.
LNMv, RNMv	shank_xz	Ankle marker (medial), projected onto the floor.
ASIm	pelvis_x	Mean of the ASIS markers.
PSIm	pelvis_x	Mean of the PSIS markers
LPm	torso_x, torso_y, thigh_y	Mean of left side pelvis markers (LPSI and LASI).
RPm	torso_x, torso_y, thigh_y	Mean of right side pelvis markers (RPSI and RASI).
LAJC, RAJC	shank_y, pylon_y	Ankle joint centers. Average of medial and lateral ankle markers.
LEJC, REJC	forearm_y, upperam_y	Elbow joint centers. Average of medial and lateral ankle markers.
LWJC, RWJC	forearm_y	Wrist joint centers. Average of medial and lateral ankle markers.
LSHv	torso_x, torso_z	Left shoulder marker, projected vertical to LPm.
RSHv	torso_x, torso_z	Right shoulder marker, projected vertical to RPm.

An example of the full setup of the OpenSim scaling tool is provided in Appendix F. Because many of the markers used were not marking anatomical locations, the high variability in placement could affect the static position the scaling tool determines, and therefore where the final marker positions are fixed relative to each body. To correct for this, these markers were not included in the least-squares fit to determine static posture. The model markers and weights were adjusted as needed to best match placement for a given subject.

4.5.2 *Inverse Kinematics*

Once the models were scaled, the joint angles were calculated using OpenSim's Inverse Kinematics tool. This tool uses a weighted least-squares fit on all the markers to position the model at each time step, using the following equation [34].

$$\min_{\mathbf{q}} \left[\sum_{i \in \text{markers}} w_i \left\| \mathbf{x}_i^{\text{exp}} - \mathbf{x}_i(\mathbf{q}) \right\|^2 + \sum_{j \in \text{unprescribed coords}} \omega_j \left(q_j^{\text{exp}} - q_j \right)^2 \right]$$
$$q_j = q_j^{\text{exp}} \text{ for all prescribed coordinates } j$$

In the above equation, q is the vector of angles being solved for, x_i are the experimental marker positions, and w_i are the weights given to each marker. In this analysis, the only inputs were experimental markers, not experimentally determined coordinates, so ω_j and q_j are not used.

Matlab was used to batch process the inverse kinematics trials for each subject. The code for this is based on the sample code that is included in the OpenSim installation, with only minor modifications. A sample inverse kinematics setup file is provided in Appendix G.

4.5.3 *Inverse Dynamics*

Once the inverse kinematics results were obtained, the Inverse Dynamics (ID) tool in OpenSim was used. This tool uses the calculated motion of the model (joint angles, velocities, and accelerations), as well as the external forces (ground reaction forces) to solve for the unknown joint torques in the model. This is an application of the classical equations of motion using generalized coordinates. For the prescribed trials (C1), ID was run once for each trial, applying the ground reaction forces and the inverse kinematics results motion (filtered at 6 Hz) to the model. The unknown torque that is solved for is attributed to the muscle forces acting at the joint.

$$\tau_{unknown} = I\alpha - \tau_{GRF} - \tau_{other}$$

$$\tau_{unknown} = \tau_{muscle}$$

Here, $I\alpha$ is the known motion from the inverse kinematics results, τ_{GRF} is the torque from the applied ground reaction forces, and τ_{other} are other torques accounted for, such as Coriolis and centrifugal forces. In this application, $\tau_{unknown}$ is the torque that can be attributed to the muscles. However, for BP trials, this setup was manipulated to further delineate the results using the spring force. When the BP spring is applying force to the model, the torque effect is not completely clear because the exact moment arms with respect to the knee and ankle are not known. To easily solve for BP spring torque, inverse dynamics was run twice for each BP trial: once with the spring forces neglected, and once with the spring forces applied as external loads like the ground reaction forces. In the first run, with spring forces neglected, both muscle torques and the BP spring torque fall into the $\tau_{unknown}$ variable.

$$\tau_{unknown} = I\alpha - \tau_{GRF} - \tau_{other}$$

$$\tau_{unknown} = \tau_{muscle} + \tau_{BP}$$

When the spring forces are applied in the second ID run, the muscles and the BP torque can be separated because only the muscle torque is unknown:

$$\tau_{muscle} = I\alpha - \tau_{GRF} - \tau_{other} - \tau_{BP}$$

Thus, the specific torque applied from the BP spring can be calculated by subtracting the results of the two ID runs.

$$\tau_{BP} = \tau_{unknown} - \tau_{muscle}$$

Sample setup files for the two ID runs are provided in Appendix H. These ID analyses were also run using a Matlab batch process derived from the example code provided in OpenSim.

4.5.4 *Static Optimization*

Static Optimization (SO) was performed on each trial, which solves for the individual muscle forces in the model. The inputs to SO are the ground reaction forces and inverse kinematics results (filtered at 6Hz). For the BP trials, SO was only run once, applying the BP spring force to the model as an external load with the GRF, so that the simulation only solved for muscle forces. First, SO determines the overall joint torque attributed to the muscles, similar to ID. Then it applies force-length-velocity muscle characteristics to the activation of each muscle, and solves using a cost function of activation squared. In other words, it applies known activation-to-force relationships to the muscles, and minimizes activation to theoretically distribute the force generation between muscles most efficiently. A sample setup file for Static Optimization is provided in Appendix I. Static Optimization was run in

batch processes in Matlab similar to previous OpenSim analyses. In some cases, Static Optimizations could not find a solution with the given number of iterations for a given time step. Gait cycles that included failed time points were ignored, but neighboring data was unaffected because each time step is analyzed individually under the static optimization algorithm.

4.5.5 *Muscle Analysis*

A muscle analysis was performed using the Analyze tool in OpenSim to determine the moment arms of a single specific muscle (GAS) at the ankle and knee. The muscle analysis uses the same input filtered IK results and external forces (ground reaction forces and BP spring forces) to resolve the geometry of the muscles at the specified joints. The outputs are contained in a file with a column for each specified muscle, and the value in meters of the perpendicular moment arm at each time step. Torque from an individual muscle can therefore be calculated by $\tau = F * r$, where F is the muscle force output from SO, and r is the moment arm output from the muscle analysis. These muscle analyses were also performed as a batch process in Matlab, using the exact same code as Static Optimization, but a different setup file specifying the muscles and joints of interest.

4.6 Outcome Measure Calculations

4.6.1 *Kinematic Symmetry*

For each gait cycle, the left and right joint angles were plotted against each other, as in Figure 4-10. Using Matlab's *fitlm* function, a linear fit of the amputated vs. intact limb was created. The R^2 value of this linear fit was reported for each individual gait cycle.

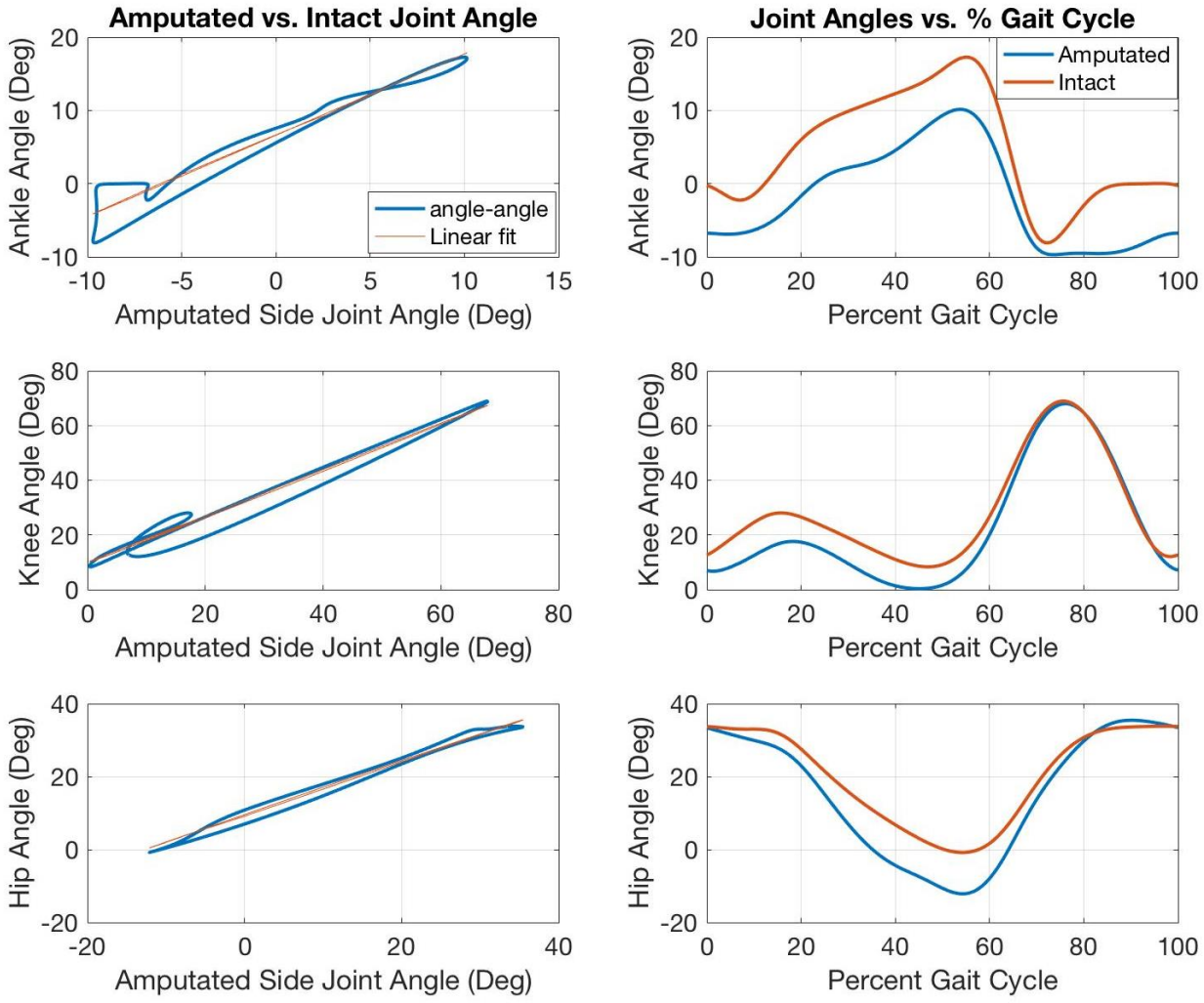

Figure 4-10. Sample kinematic symmetry plots from Subject 1, showing average of all C1 (prescribed) trials. Left: Angle-Angle plots shown with linear fit line. Right: Amputated and intact side joint angles plotted over the gait cycle.

4.6.2 *BP Torque Contribution*

The ankle and knee joint torque contributions of the biarticular spring were calculated from the inverse dynamics results. The ID results from when spring forces were applied were subtracted from the ID results from when the spring forces were not applied (Section 4.5.3). The peak BP torque at the ankle and the knee for each gait cycle was found (ankle plantar flexion and knee flexion), and reported as a percentage of the peak net torque at the joint for each gait cycle. Sample ankle and knee net and BP torques are shown below in Figure 4-11 and Figure 4-12.

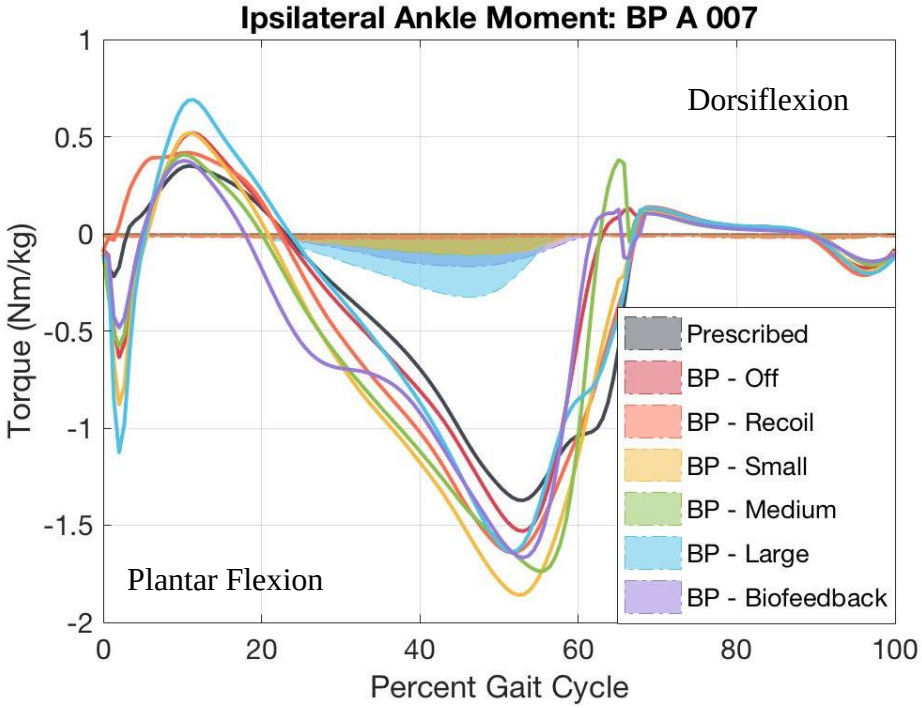

Figure 4-11. Sample average ankle torque plot from Subject 7. Solid lines are the net ankle torque for each condition, and shaded regions are the BP torque contribution.

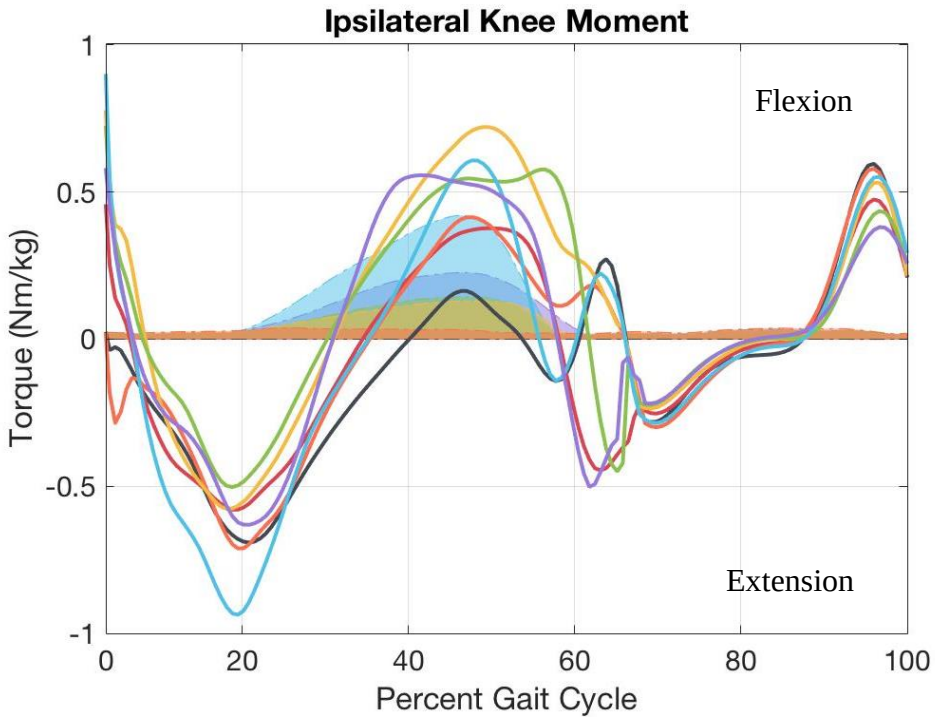

Figure 4-12. Sample average knee torque plot from Subject 7. Solid lines are the net knee torque for each condition, and shaded regions are the BP torque contribution.

4.6.3 *BP vs. Contralateral GAS Torque (MAE)*

BP joint torque was calculated using the dual ID results as described earlier. BP torque vs. C1 GAS torque is shown at the ankle in Figure 4-13 and at the knee in Figure 4-14. For the prescribed condition (C1), GAS torque at the ankle and knee was determined using the muscle output from Static Optimization (Section 4.5.4) multiplied by the moment arm output from the Muscle Analysis (Section 4.5.5). To compare the similarity of the BP torque and GAS torque, the Mean Absolute Error (MAE) between the GAS and each BP curve was calculated for each gait cycle. MAE is calculated as the summed magnitude of the difference at each time step, divided by the total number of time steps.

$$MAE = \sum_{i=1}^{n} \frac{\left|\tau_{BP,i} - \tau_{GAS,i}\right|}{n}$$

Since the BP torque is zero by definition in C1 (prescribed), the MAE for C1 represents the difference between the GAS torque curve and a line at zero.

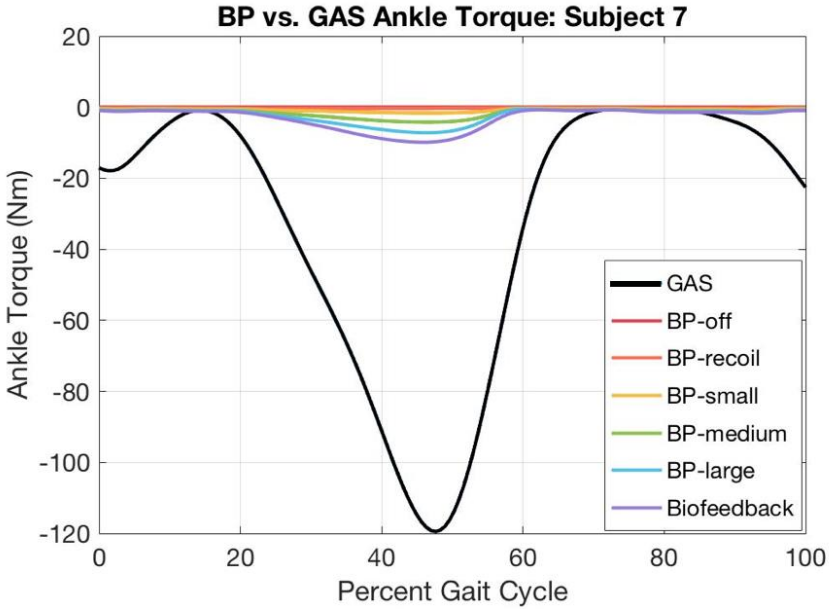

Figure 4-13. BP spring and contralateral GAS torque generated at the ankle, averages from one representative no-handrail subject (Subject 7). Only GAS from C1 is shown, compared to each BP condition.

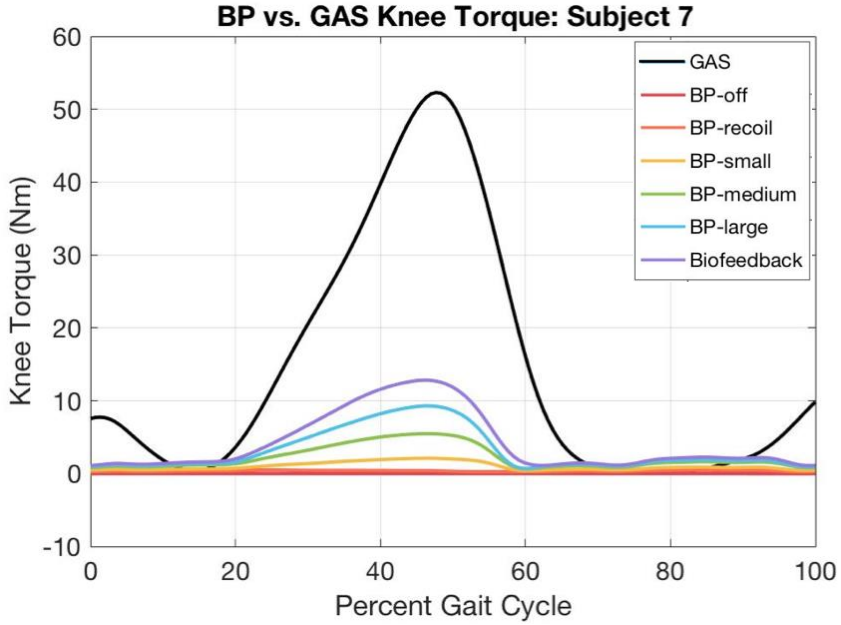

Figure 4-14. BP spring and contralateral GAS torque generated at the knee, averages from one representative no-handrail subject (Subject 7). Only GAS from C1 is shown, compared to each BP condition.

4.6.4 *Total Muscle Force*

Total muscle force was calculated over each gait cycle based on the Static Optimization results. There are 72 muscles included in the model, and the output from each was summed together, and then summed across all time points to get one total force, in Newtons, for each gait cycle analyzed.

4.6.5 *BP Knee and Ankle Work*

The work that the BP spring did on the knee and ankle was calculated as the sum of the BP spring torque times the change in angle for each time step.

$$W = \sum_{i=n1}^{n2-1} \tau_{BP,i} * (\theta_{i+1} - \theta_i)$$

Because the BP spring was only active for a fraction of the gait cycle, BP work calculations were limited to the active time window for each subject, which $n1$ and $n2$ describe in the equation above. Example plots that represent this calculation can be found in Figure 4-15.

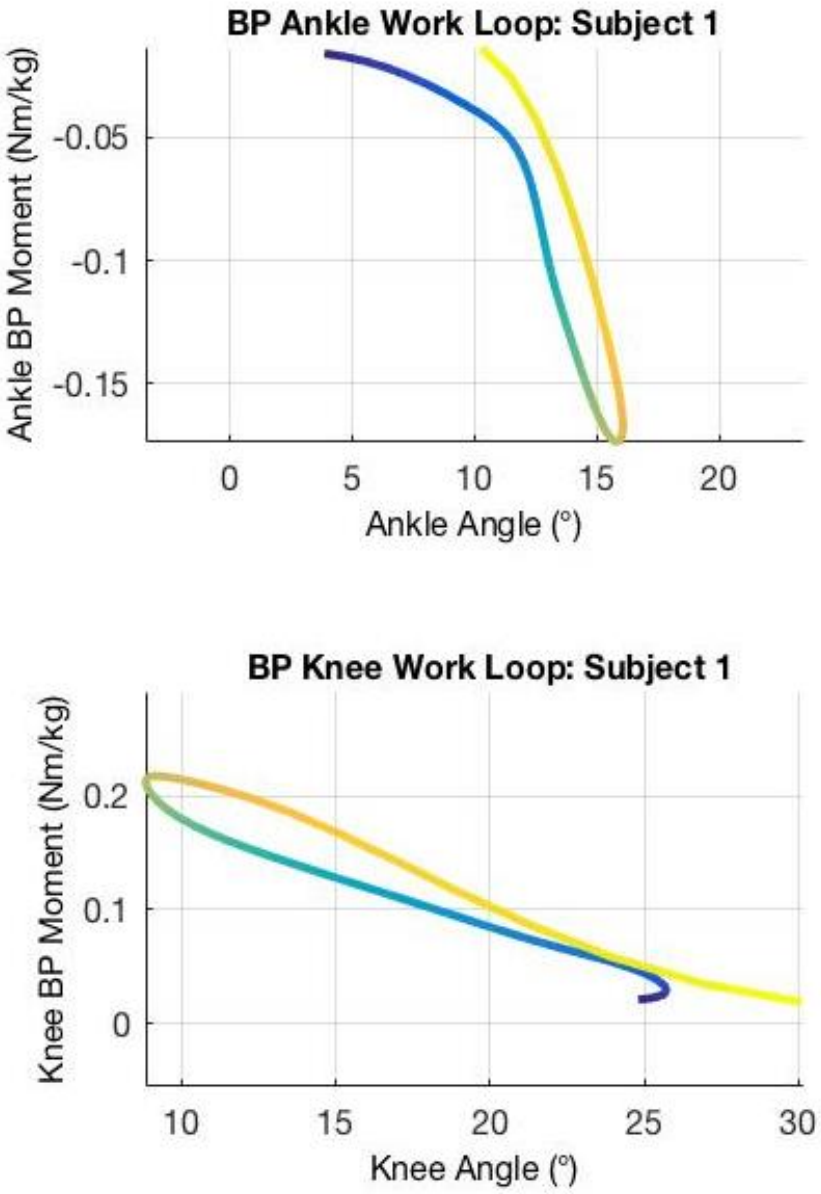

Figure 4-15. BP ankle and knee work loops. Time is represented with the blue (start) to yellow (end) shading, and represents the gait cycle window for which the BP spring is active. The integral of this curve is BP work.

4.7 Statistical Methods

For each of the qualitative outcome measures (Aim 1 – Aim 5), linear mixed effects regression was used to determine the association between outcome (the dependent variable) and condition (the independent fixed effect, modeled as a set of 6 dummy

variables). Study subject and study subject by condition interaction were modeled as random effects. The significance of the association between outcome and condition was tested using a likelihood ratio test. Selected pairwise differences and 95% confidence intervals were estimated and tested simultaneously for significance adjusting for multiple comparisons using the single step method [61]. All analyses were carried out using R 3.4.1 [62], the lme4 package to carry out the linear mixed effects regression [63], and the multcomp package [61] to carry out the simultaneous pairwise comparisons.

Eight pairwise comparisons of interest were carried out, which are summarized in Table 4-7. The small, medium, and large spring conditions (C4, C5, and C6) were each compared to both the prescribed control (C1) and to BP baseline (C3 – recoil only). The biofeedback condition (C7) used each subject's preferred spring, and so was only compared to the small, medium, or large (C4, C5, C6) condition using the same spring. Most subjects preferred the medium spring (C5), and two preferred the large spring (C6). Spring choice by subject is summarized in Table 4-6. For each subject, 15-40 gait cycles were analyzed for each condition.

Table 4-6. Preferred spring stiffness for each subject, used in the biofeedback condition

Subject	Preferred Spring
1	Medium
2	Large
4	Medium
5	Medium
6	Large
7	Medium
8	Medium

Table 4-7. Pair-wise comparisons of interest

Condition Pairs	Description
C1 vs C3	Prescribed (control) vs. BP baseline condition
C1 vs C4	Prescribed (control) vs. BP - Small spring
C1 vs C5	Prescribed (control) vs. BP - Medium spring
C1 vs C6	Prescribed (control) vs. BP - Large spring
C3 vs C4	BP baseline vs. BP - Small spring
C3 vs C5	BP baseline vs. BP - Medium spring
C3 vs C6	BP baseline vs. BP - Large spring
C7 vs C5/C6	Biofeedback condition vs. condition with the same spring stiffness

4.8 EMG Signal Processing

To process the EMG data, raw signals were first high-pass filtered at 40 Hz using a fourth order, zero-lag Butterworth filter. Any DC offset was then removed using Matlab's *detrend* function. The absolute value of the detrended data was taken, and then a low-pass filter (fourth order, zero-lag Butterworth) with a 10 Hz cutoff frequency was applied. Finally, because there was a sensor delay that offset the EMG data from the Vicon GRF and marker recordings, 512 ms was removed from the beginning of each trial. This ensured that the EMG used in analysis aligns with all other experimentally recorded data. For comparison between EMG and Static Optimization results, both data sets were normalized to a 0-1 scale. This comparison is presented in Section 5.6. Post analysis of the processed EMG signal was performed to confirm good signal to noise ratio. Signals that qualitatively look erroneous because of bad contact with the skin or excessive movement artifact where selectively removed from further analysis.

Chapter 5. RESULTS

5.1 KINEMATIC SYMMETRY

Kinematic symmetry of the ankle, knee, and hip were compared using the R^2 calculations described in Section 4.6.1. Average R^2 values for each subject and condition are summarized in Table 5-1. Overall, the omnibus tests showed a significant difference ($p < 0.01$) in ankle R^2 values between conditions, a smaller but significant ($p < 0.05$) difference in knee R^2 values between conditions, and no significant differences in hip R^2.

Across all conditions, the hip had the highest R^2 value (most symmetrical), followed by the knee and then the ankle (Figure 5-1). Only one of the eight pairwise comparisons of interest (Table 4-7) was significantly different; the biofeedback condition (with subjects' preferred spring) had *significantly reduced* symmetry from the BP condition with the same spring (C5 or C6) in both the knee ($p < 0.001$) and hip, though small ($p = 0.0169$). These significant findings pertain to hypothesis H1.7 (Section 4.1). A summary of p-values for all eight pairwise comparisons can be found in Table 5-2.

Table 5-1. Kinematic symmetry R2 values for each subject in each condition. Yellow shows low correlation, green shows strong correlation.

ANKLE							
Condition	Subject 1	Subject 2	Subject 4	Subject 5	Subject 6	Subject 7	Subject 8
C1	0.922	0.924	0.864	0.680	0.653	0.558	0.249
C2	0.815	0.789	0.744	0.827	0.678	0.460	0.194
C3	0.790	0.734	0.757	0.797	0.664	0.491	0.163
C4	0.748	0.710	0.714	0.825	0.659	0.461	0.117
C5	0.827	0.802	0.732	0.814	0.614	0.410	0.209
C6	0.768	0.758	0.716	0.757	0.708	0.375	0.126
C7	0.883	0.795	0.533	0.777	0.465	0.369	0.240
KNEE							
Condition	Subject 1	Subject 2	Subject 4	Subject 5	Subject 6	Subject 7	Subject 8
C1	0.956	0.958	0.888	0.821	0.747	0.965	0.917
C2	0.939	0.909	0.849	0.846	0.865	0.961	0.946
C3	0.923	0.908	0.848	0.882	0.866	0.938	0.943
C4	0.888	0.940	0.839	0.851	0.915	0.939	0.957
C5	0.935	0.930	0.864	0.817	0.850	0.971	0.953
C6	0.888	0.901	0.853	0.797	0.886	0.979	0.941
C7	0.878	0.860	0.777	0.776	0.771	0.884	0.932
HIP							
Condition	Subject 1	Subject 2	Subject 4	Subject 5	Subject 6	Subject 7	Subject 8
C1	0.980	0.973	0.824	0.864	0.942	0.974	0.937
C2	0.974	0.946	0.957	0.946	0.889	0.945	0.934
C3	0.963	0.964	0.948	0.950	0.916	0.960	0.940
C4	0.925	0.974	0.951	0.952	0.941	0.955	0.934
C5	0.964	0.979	0.934	0.943	0.911	0.976	0.932
C6	0.951	0.965	0.916	0.939	0.886	0.979	0.919
C7	0.925	0.779	0.882	0.885	0.836	0.933	0.931

C1 (prescribed), C2 (BP w/o spring), C3 (BP recoil only), C4 (BP small spring), C5 (BP medium spring), C6 (BP large spring), C7 (BP w/ biofeedback)

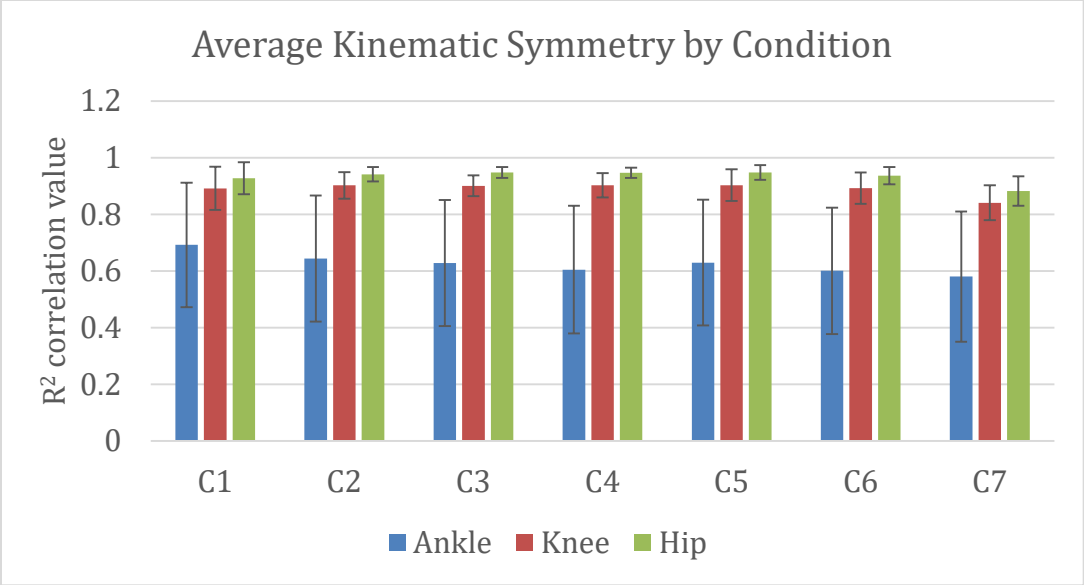

Figure 5-1. Kinematic Symmetry R^2 values for each condition, averaged across all subjects. Error bars indicate the 95% confidence interval.

Table 5-2. P-values for kinematic symmetry at the ankle, knee, and hip. Significance is in bold.

P-values	Ankle	Knee	Hip
C1 vs C3	0.251	1.00	0.891
C1 vs C4	0.184	1.00	0.939
C1 vs C5	0.232	0.978	0.850
C1 vs C6	0.0708	1.00	1.00
C3 vs C4	1.00	1.00	1.00
C3 vs C5	1.00	1.00	1.00
C3 vs C6	0.986	0.988	0.717
C7 vs C5/6	0.178	**0.000274**	**0.0170**

There was a notable trend in knee kinematics across conditions for two subjects (Subjects 2 and 6). As spring stiffness increased, knee extension during late stance decreased, which is a further deviation from healthy walking (Figure 5-2).

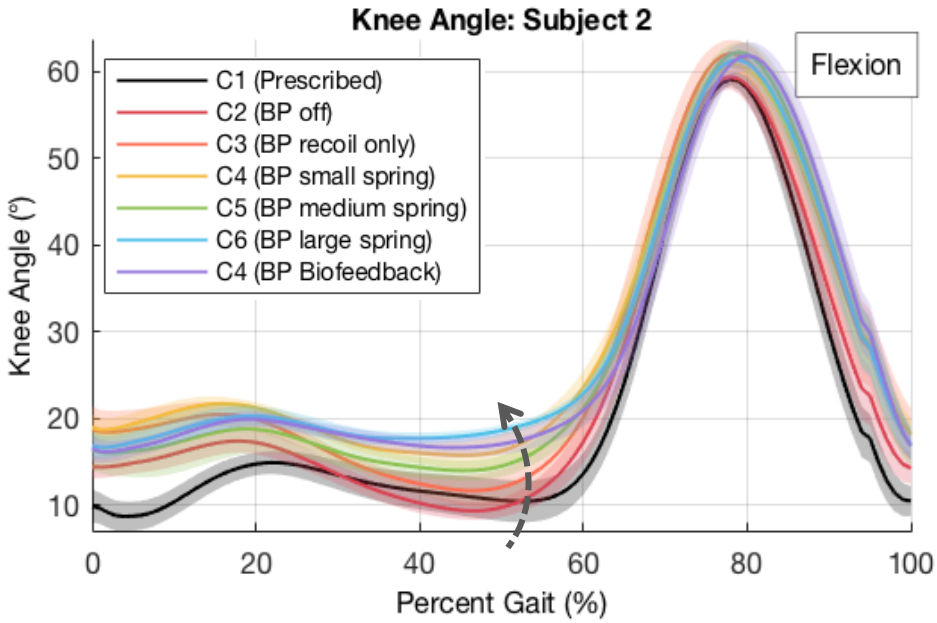

Figure 5-2. Average knee angle over gait cycle for each condition, for Subject 2. Arrow indicates the trend of interest.

5.2 BP Torque Contribution

The BP spring's contributions to ankle and knee joint torque were calculated from the inverse dynamics results (Section 4.6.2). Average BP torque contribution by subject is summarized in Table 5-3. The omnibus tests for both BP torque contribution to knee and ankle torque showed a significant difference across conditions (p-values < 0.001).

Because C1 (prescribed) has a BP torque contribution of 0 percent by definition, the pairwise comparisons including C1 were not performed. Rather, BP condition values are to be considered significantly different from C1 if the 95% confidence interval does not contain zero. The 95% confidence intervals are presented to show significance from C1 in Table 5-4. All pairwise comparisons except C7 vs. C5/C6 were significant at the ankle, and all but C7 vs. C5/C6 and C3 vs. C6 were significant at the knee (Table 5-5)(Hypotheses H2.6 and H2.5). In

general, increasing spring stiffness resulted in increased BP torque contribution, as expected (Figure 5-3).

Table 5-3. BP torque contribution percentage averages by subject and condition. Yellow shows low/zero contribution, green shows large contribution

ANKLE							
Condition	Subject 1	Subject 2	Subject 4	Subject 5	Subject 6	Subject 7	Subject 8
C1	0	0	0	0	0	0	0
C2	0.216	0.273	1.68	0.0870	0.184	0.03	0.120
C3	1.16	2.00	1.75	2.05	2.48	1.69	2.36
C4	9.40	7.39	4.80	11.6	6.38	6.05	7.08
C5	13.5	9.09	6.25	25.8	7.44	7.39	9.67
C6	14.3	13.9	7.23	60.9	9.78	17.2	19.2
C7	18.8	14.5	15.2	33.3	13.3	13.9	11.6
KNEE							
Condition	Subject 1	Subject 2	Subject 4	Subject 5	Subject 6	Subject 7	Subject 8
C1	0	0	0	0	0	0	0
C2	0.376	1.42	5.81	0.204	0.628	0.0530	0.339
C3	2.77	9.50	7.46	6.19	7.97	3.86	5.10
C4	15.7	34.1	19.4	18.7	18.8	10.2	14.9
C5	21.8	54.1	20.8	28.1	22.2	12.2	19.8
C6	31.8	73.8	30.4	45.3	27.3	33.8	33.1
C7	26.7	48.7	50.4	29.1	28.2	24.4	24.1

C1 (prescribed), C2 (BP w/o spring), C3 (BP recoil only), C4 (BP small spring), C5 (BP medium spring), C6 (BP large spring), C7 (BP w/ biofeedback)

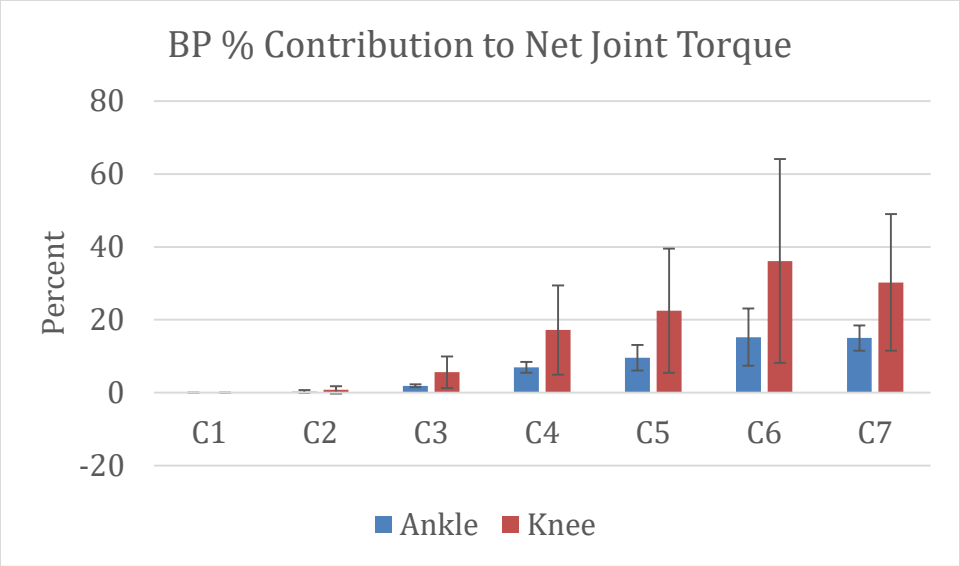

Figure 5-3. All subjects average BP percent contribution to net ankle and knee torque for each condition. Error bars indicate the 95% confidence interval.

Table 5-4. 95% Confidence intervals for BP torque contribution. Conditions that are significantly different form zero (C1) are in bold.

Condition	Ankle CI (lower bound)	Ankle CI (upper bound)	Knee CI (lower bound)	Knee CI (upper bound)
C2	-0.0990	0.692	-0.217	1.81
C3	**1.46**	**2.32**	**1.24**	**9.96**
C4	**5.45**	**8.47**	**4.96**	**29.5**
C5	**6.11**	**13.1**	**5.45**	**39.5**
C6	**7.37**	**23.1**	**8.16**	**64.1**
C7	**11.5**	**18.5**	**11.5**	**49.0**

C1 (prescribed), C2 (BP w/o spring), C3 (BP recoil only), C4 (BP small spring), C5 (BP medium spring), C6 (BP large spring), C7 (BP w/ biofeedback)

Table 5-5. BP Torque Contribution: P-values for pairwise comparisons of interest. Significance is in bold.

P-Values	Ankle	Knee
C3 vs C4	**< 1.00 e-05**	**0.0336**
C3 vs C5	**1.11 e-05**	**< 1.00 e-03**
C3 vs C6	**< 1.00 e-05**	0.177
C7 vs C5/6	0.964	0.390

5.3 BP Torque vs. Contralateral GAS Torque

BP joint torque at the ankle and knee for each condition was compared to the joint torques generated by the contralateral GAS during the prescribed condition (C1). Average MAE at the knee and ankle for each subject and condition are given in Table 5-6. There were two subjects (Subjects 2 and 6) that preferred to hold onto the treadmill handrail even when asked to release if they were able to do so. Handrail use appeared to have a large impact on the contralateral GAS torque generated. Peak GAS torque for these two subjects was roughly 10% that of the other subjects, so for this analysis the handrail subjects were considered separately from the no-handrail subjects. MAE results for each group are presented in Figure 5-4 and Figure 5-5.

Table 5-6. Average MAE between BP and contralateral GAS torques. Subjects that used the handrail are shown in red. Yellow is high MAE (worse), green is low MAE (better).

ANKLE							
Condition	Subject 1	Subject 2	Subject 4	Subject 5	Subject 6	Subject 7	Subject 8
C1	8.60	0.626	12.2	13.7	0.361	29.2	21.2
C2	8.66	0.716	11.4	13.8	0.302	29.2	21.2
C3	8.33	0.870	11.5	13.0	0.515	28.1	20.4
C4	5.79	2.63	10.7	11.3	1.86	26.3	19.0
C5	5.10	3.29	10.3	10.4	2.17	25.9	18.5
C6	5.12	4.97	9.81	14.1	2.95	23.3	17.4
C7	3.93	5.67	7.40	9.60	3.79	23.5	17.9
KNEE							
Condition	Subject 1	Subject 2	Subject 4	Subject 5	Subject 6	Subject 7	Subject 8
C1	4.29	0.339	5.47	6.02	0.199	12.9	8.19
C2	4.36	0.485	4.49	6.09	0.151	12.9	8.17
C3	4.08	1.15	4.60	5.30	0.948	11.6	7.26
C4	2.10	5.19	3.57	3.51	3.11	9.18	5.68
C5	2.94	6.40	2.99	3.17	3.64	8.65	5.02
C6	4.24	9.29	2.63	6.72	4.85	4.99	3.72
C7	5.66	10.4	3.93	4.78	6.15	5.79	4.35

C1 (prescribed), C2 (BP w/o spring), C3 (BP recoil only), C4 (BP small spring), C5 (BP medium spring), C6 (BP large spring), C7 (BP w/ biofeedback)

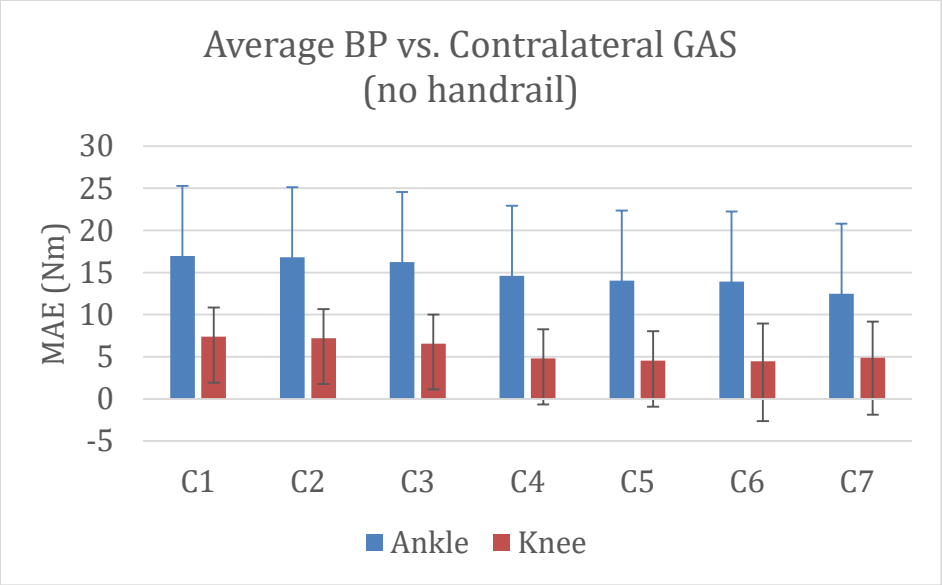

Figure 5-4. Mean Absolute Error (MAE) between the C1 (prescribed)GAS curve and BP spring torque, for subjects that were able to walk without using the handrail.

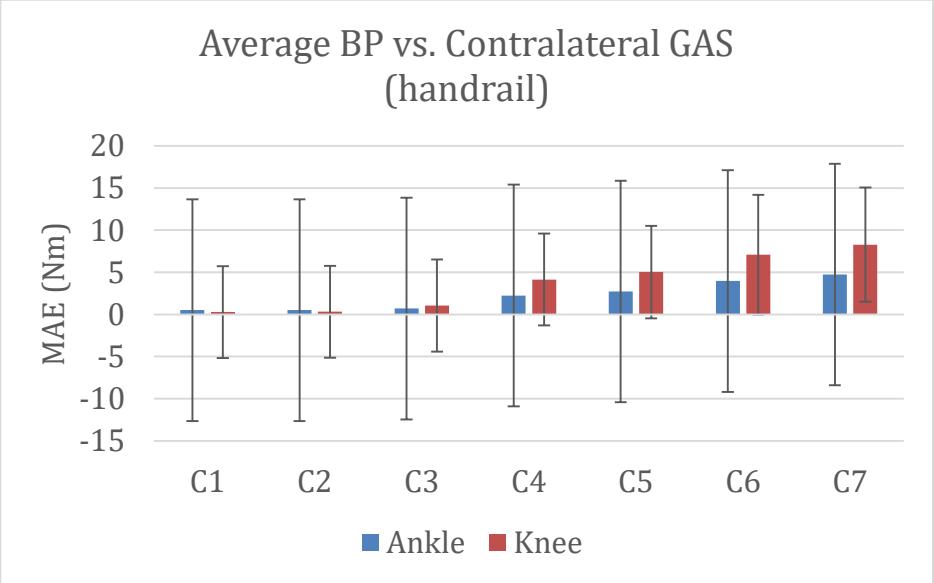

Figure 5-5. Mean Absolute Error (MAE) between the C1 (prescribed) GAS curve and BP spring torque, for subjects that used the handrail while walking.

Table 5-7. BP Torque vs. Contralateral GAS: P-values for pairwise comparisons of interest. Significance is in bold.

P-Values	Ankle (no handrail)	Knee (no handrail)	Ankle (handrail)	Knee (handrail)
C1 vs C3	**0.00730**	**0.0134**	0.926	0.641
C1 vs C4	**0.00210**	**0.00480**	**0.0464**	**0.00640**
C1 vs C5	**0.00130**	**0.0153**	**0.0345**	**0.0119**
C1 vs C6	0.0960	0.378	0.255	0.141
C3 vs C4	**0.0119**	**0.0219**	0.0828	0.0138
C3 vs C5	**0.00530**	**0.0643**	**0.0406**	**0.0278**
C3 vs C6	0.219	0.641	0.295	0.202
C7 vs C5/6	**0.0120**	0.706	0.0669	0.146

C1 (prescribed), C2 (BP w/o spring), C3 (BP recoil only), C4 (BP small spring), C5 (BP medium spring), C6 (BP large spring), C7 (BP w/ biofeedback)

For the no-handrail group, C4 (small spring) and C5 (medium spring) were both significantly different than C1 (prescribed) and C3 (BP-recoil), with p-values all below 0.025 (Table 5-7). These comparisons are associated with hypotheses H3.1, H3.2, H3.4, and H3.5. For the handrail users, many of the same pairwise conditions were statistically significant, but it is difficult to draw conclusions with only two subjects in the group. Additionally, the no-handrail group had significant differences at between C1 and C3 ($p < 0.05$), and between C7 and C5/C6 at the ankle ($p = 0.012$), which supports hypothesis H3.7.

5.4 Total Muscle Force

Total muscle force was calculated by summing the Static Optimization results (4.6.4). There was high variability between subjects, and as such no trends or significant differences were found. Condition averages for each subject are presented in Figure 5-6. P-values for the comparisons of interest (for hypothesis H4.1 – H4.7) are given in Table 5-9. The biofeedback

(C7) comparison (vs. C5/C6) was near significance, ($p = 0.0675$), and the mean for C7 was the higher of the two. Means across all subjects for each condition are presented in Table 5-8.

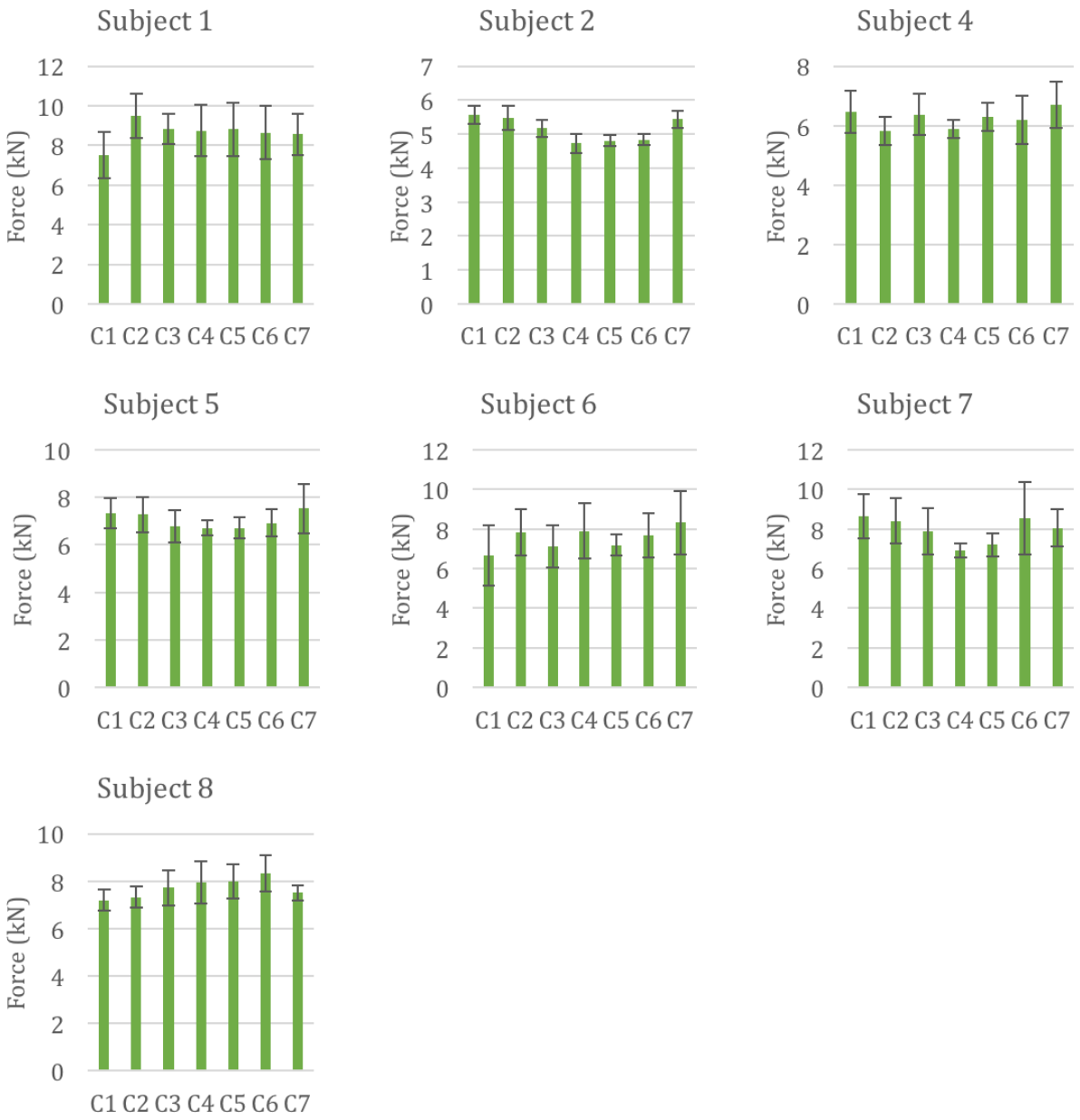

Figure 5-6. Average total muscle force (in Newtons) for each subject under each condition. Error bars show the standard deviation of the averaged gait cycles. C1: prescribed, C2: BP w/o spring, C3: BP recoil only, C4: BP small spring, C5: BP medium spring, C6: BP large spring, C7: BP w/ biofeedback.

Table 5-8. Average total muscle force across all subjects for each condition

Condition	Mean (N)
C1 (prescribed)	7050
C2 (BP – off)	7370
C3 (BP – recoil only)	7130
C4 (BP - Small spring)	6980
C5 (BP – Medium spring)	7000
C6 (BP – Large spring)	7300
C7 (BP – Biofeedback)	7440

Table 5-9. Total Muscle Force: P-values for pairwise comparisons of interest

Comparison	p-value
C1 vs C3	0.996
C1 vs C4	1.00
C1 vs C5	1.00
C1 vs C6	0.820
C3 vs C4	0.997
C3 vs C5	0.997
C3 vs C6	0.983
C7 vs C5/6	0.0675

5.5 BP Knee and Ankle Work

The work that the BP spring did on the knee and ankle was calculated for each gait cycle (Section 4.6.5). Negative work corresponds to the joint losing or transferring energy to the spring, while positive work means the spring does work on the joint. The omnibus tests for both knee and ankle work showed an across - condition significance ($p < 0.01$). Condition averages for each subject are given in Table 5-10. All pairwise comparisons of interest were significant ($p \leq .00129$), except for the biofeedback comparison (C7 vs. C5/C6) of knee work (Table 5-11 & Table 5-12). Hypotheses H5.3 – H5.8 are supported by these

comparisons. Hypotheses H5.1 and H5.2 stated that the knee and ankle BP work would increase in magnitude as spring stiffness increased. This trend is true at the ankle, but the medium spring (C5) yielded the highest knee work value. The biofeedback comparison at the ankle was significant ($p < 0.05$) while the knee was not ($p > 0.1$), which indicates a limited effect of the biofeedback. The ankle in the biofeedback condition was not significantly different from C1 (Table 5-12). BP work at the ankle was negative, while work at the knee was positive, which indicates a transfer of energy from the ankle to the knee. This does not support hypothesis H5.9, which stated that the work transfer would occur form the knee to the ankle. Average BP ankle and knee work values are presented in Figure 5-7.

Table 5-10. Condition averages of BP ankle and knee work for each subject

ANKLE							
Condition	Subject 1	Subject 2	Subject 4	Subject 5	Subject 6	Subject 7	Subject 8
C1	0	0	0	0	0	0	0
C2	0	0	0	0	0	0	0
C3	-13.862	-21.134	-27.709	-25.055	-5.232	-22.429	-17.98
C4	-59.735	-41.79	-50.526	-138.012	-9.842	-75.799	-51.928
C5	-58.383	-59.216	-66.232	-318.834	-10.556	-103.419	-69.165
C6	-63.469	-107.801	-93.187	-761.718	-18.468	-207.623	-123.303
C7	-21.88	-104.883	-131.333	-358.865	-2.804	-157.319	-76.804
KNEE							
Condition	Subject 1	Subject 2	Subject 4	Subject 5	Subject 6	Subject 7	Subject 8
C1	0	0	0	0	0	0	0
C2	0	0	0	0	0	0	0
C3	-4.261	17.397	65.342	62.297	13.424	87.021	69.249
C4	42.311	53.641	84.152	120.96	4.449	86.962	82.158
C5	62.726	63.329	86.893	153.031	37.86	117.309	111.613
C6	27.328	65.443	76.306	146.981	39.216	88.307	39.582
C7	27.645	42.474	80.38	133.305	78.283	119.392	100.753

C1 (prescribed), C2 (BP w/o spring), C3 (BP recoil only), C4 (BP small spring), C5 (BP medium spring), C6 (BP large spring), C7 (BP w/ biofeedback)

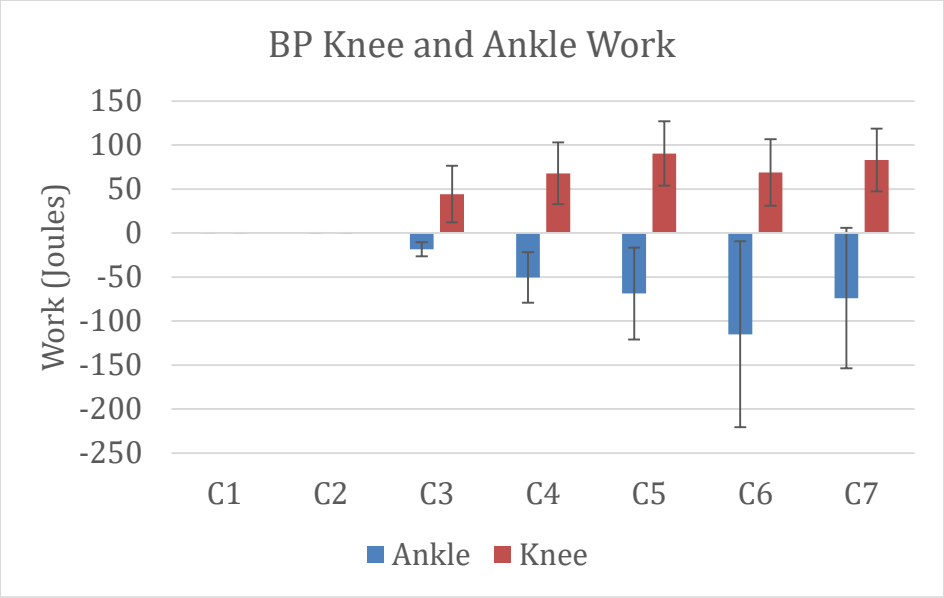

Figure 5-7. BP knee and ankle work averaged across all subjects. Error bars indicate the 95% confidence interval.

Table 5-11. BP Ankle and Knee Work: P-values for pairwise comparisons of interest that do not contain C1. Significance is in bold.

P-Values	Ankle	Knee
C3 vs C4	**< 1.00 e-06**	**0.00129**
C3 vs C5	**< 1.00 e-06**	**< 1.00 e-03**
C3 vs C6	**< 1.00 e-06**	**< 1.00 e-03**
C7 vs C5/6	**0.00134**	0.108

Table 5-12. Confidence intervals to test significance of pair wise comparisons that include C1 (prescribed). Conditions that are significantly different than C1 are in bold.

Condition	Ankle CI (upper bound)	Ankle CI (lower bound)	Knee CI (upper bound)	Knee CI (lower bound)
C3	**-10.3**	**-26.3**	**76.5**	**12.2**
C4	**-21.5**	**-79.1**	**103**	**33.0**
C5	**-16.5**	**-121**	**127**	**53.9**
C6	**-9.31**	**-221**	**107**	**31.2**
C7	5.84	-154	**119**	**47.6**

C1 (prescribed), C2 (BP w/o spring), C3 (BP recoil only), C4 (BP small spring), C5 (BP medium spring), C6 (BP large spring), C7 (BP w/ biofeedback)

5.6 Model Validation: Static Optimization vs. EMG Comparison

A qualitative comparison of the experimentally measured EMG signals and the muscle force outputs from Static Optimization (SO) in OpenSim was performed as a validation measure for the amputee musculoskeletal model. Figure 5-8 shows the average EMG and SO traces over the gait cycle for Subject 1 in the C1 (prescribed) condition. Similar plots for all other subjects are provided in Appendix J.

Since the EMG sensors measure muscle activation, there is a slight delay between EMG activation signals and the SO muscle force output [31]. Overall the Static Optimization results represent most of the large features found in the EMG signals, with this phase delay. Some subjects had low quality EMG signals from muscles such as GMAX or intact GAS and SOL (Appendix J), and thus the comparison for these signals is difficult. There was generally more variability in the EMG measurements than in the SO results (Figure 5-8, Appendix J).

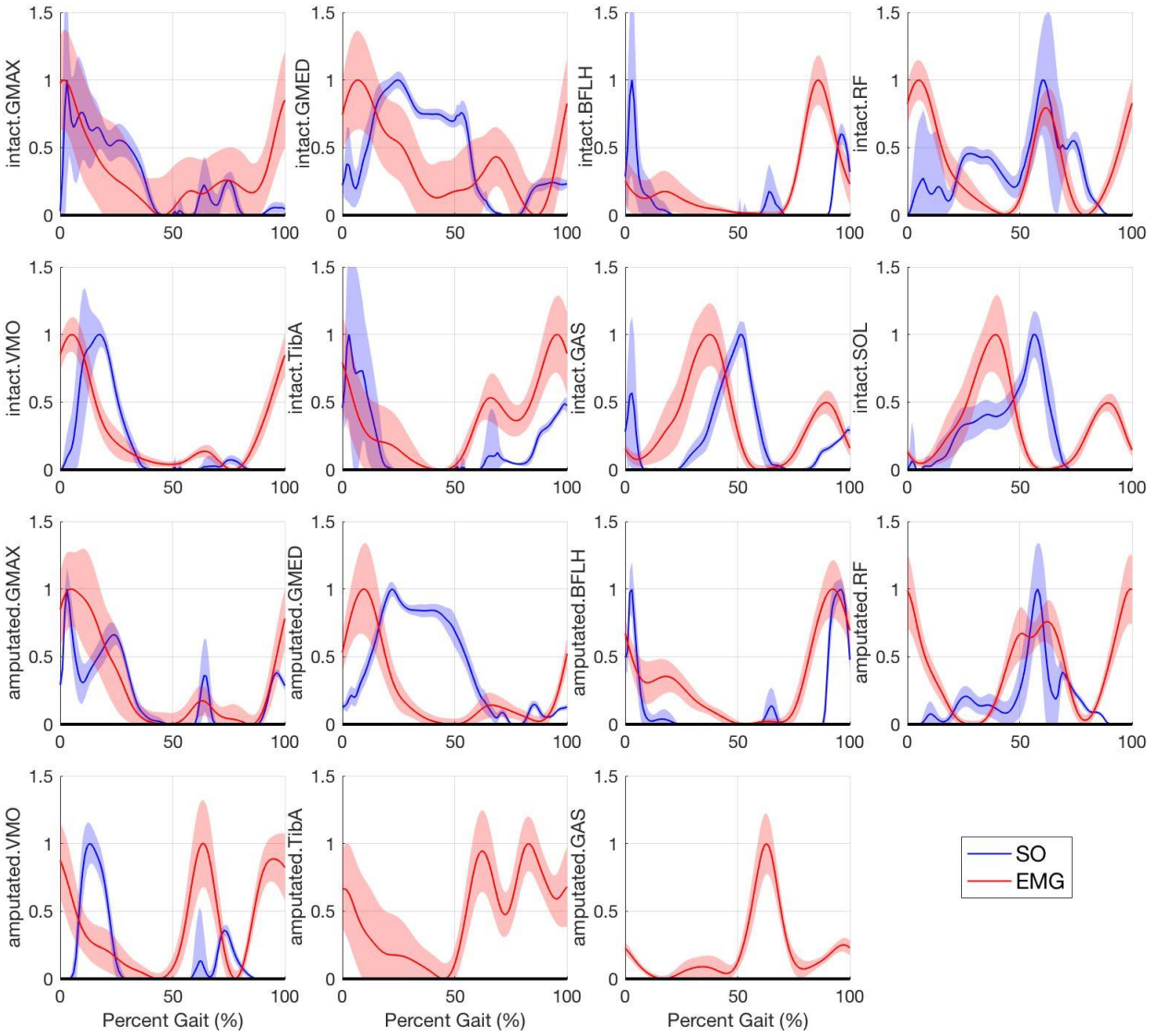

Figure 5-8. Static Optimization (SO) and EMG qualitative comparison for Subject 1. Amputated TibA and GAS were measured experimentally, but were not included in the OpenSim model and have no SO results. Amputated SOL was not measured in EMG or simulated in SO.

Chapter 6. DISCUSSION

The goal of this study was to investigate the effect of biarticular ankle and knee joint actuation on amputee gait. To achieve this, an OpenSim amputee model was developed to analyze seven amputees walking on a prototype BP device. The previous chapter described

a number of outcome measures in this study, and outlined statistically significant findings. Interpretation of these results are discussed in Sections 6.1 – 6.6. The strengths and limitations of this study are presented in 6.7. 6.8 compares the BP to other devices, and future work is considered in Section 6.9.

6.1 KINEMATIC SYMMETRY

The only significant differences found in kinematic symmetry were for the biofeedback comparison (Table 5-2). These results therefore do not support hypotheses H1.1 – H1.6, and there was no significant change in ankle, knee, or hip kinematics between baseline conditions (C1 and C3) and spring conditions (C4, C5, C6). H1.7 stated that the biofeedback condition (C7) would have increased kinematic symmetry over the BP condition that used the same spring. This hypothesis is also not supported by the data, as the significant difference denotes less symmetry in C7 compared to C5/C6.

In all conditions, the ankle was less symmetric than the knee, which was less symmetric than the hip (Figure 5-1). The hip also had the smallest confidence interval of the three joints, which indicates less variability in the data. Between-joint statistical comparisons were not made, but this trend is likely true for most amputees. The ankle is completely artificial in transtibial amputees, and passive prosthetic feet do not have the plantar flexion abilities an intact foot exhibits during push off and swing, which could account for the discrepancy in symmetry. The knee, as the next closest joint, is most likely to compensate for the lack of ankle function and therefore differs from the intact limb more than the hip. In summary, the BP did not statistically change kinematic symmetry, and as one

would expect for transtibial amputees, we found the hip joints to be most symmetrical, followed by the knee and then ankle joints.

For two subjects (Subjects 2 and 6), a substantial reduction in stance phase knee extension was noted (Figure 5-2). These two subjects were the least confident walkers; they chose the slowest self-selected walking speeds (0.5 and 0.6 m/s, respectively), and they held onto the treadmill handrails for the entire data collection. No formal analyses were performed for this measure, but these results indicate that the BP may have more adverse kinematic effects on less proficient walkers.

6.2 BP TORQUE CONTRIBUTION

There were significant differences between conditions for the BP contribution to joint torque at both the knee and the ankle. The BP spring walking conditions—small (C4), medium (C5), and large springs (C6) were all significantly different from zero (Table 5-4), so the data supports hypotheses H2.1 – H2.3. The average BP torque contribution across all subjects was highest in C6 (large spring), followed by C5 (medium spring) and then C4 (small spring). No statistical pairwise comparisons were performed between these test conditions, but these trends support H2.4 and H2.5. This experimental data supports simulation results (Sections 2.1 & 2.2), and gives evidence that a higher spring stiffness will produce more torque at both the knee and ankle joints, despite confounding factors like kinematic changes. There is some evidence that the torque produced by stiffer springs is proportionally less than the change in stiffness, indicating that as spring stiffness increases kinematics are altered, which creates an upper bound on the torques the BP can generate at the knee and ankle. This

effect may be driven by device comfort, and therefore different embodiments of the BP may be able to achieve different peak joint torques.

Though the mean BP torque contribution was higher in the biofeedback condition (C7), no significant differences were found between the C7 and the corresponding spring condition (C5/C6). This is likely due to the large variability in C7, so hypothesis H2.6 is unsupported. Since many subjects experimented greatly during C7, it is possible that reviewing data from individual steps may yield more information about BP function.

The BP torque contribution percentage at the knee was consistently larger than at the ankle. This may suggest that the device's moment arm ratio between the knee and ankle is too heavily weighted towards the knee. Additionally, a rough estimate of contralateral GAS torque contribution to the net ankle moment (based on Subject 7's prescribed foot trials) is 85% on the contralateral ankle. This merits further analysis, but suggests that the BP torque production at the ankle was substantially lower than the contralateral GAS. Comparison to non-amputee GAS torque contribution may be further illuminating.

Most subjects preferred the medium spring, while two preferred the large (Table 4-6). There is a substantial difference in stiffness between these two (3.7 N/mm vs. 10.5 N/mm), and it is possible that an optimal spring stiffness rests somewhere in between these values. Further testing of spring stiffness is necessary.

6.3 BP VS. CONTRALATERAL GAS

For both the handrail and no-handrail groups, significant differences were found between control conditions (C1 - prescribed and C3 – recoil only) and the small and medium spring conditions (C4 and C5). For the no-handrail group, MAE was smaller in C4 and C5 than

in controls C1 and C3, which supports hypotheses H3.1, H3.2, H3.4, and H3.5. This indicates that the BP spring's function is similar to the contralateral GAS. However, no significant differences were found for the C6 (large spring) comparisons to C1 (prescribed) or C3(recoil only), and hypotheses H3.3 and H3.6 are unsupported. This is likely due to the high variability of the C6 data. The large spring was very stiff and presented a bit of a walking challenge to a number of subjects. This apparent increase in effort may have caused greater than average step-to-step variation. Additionally, since the BP torque contribution was generally less than that of the contralateral GAS, it seems that a stiffer BP spring may be required to more closely match the anatomical GAS, yet such a stiff spring would likely cause kinematic changes that greatly limit the spring's torque producing capability. The main challenge therefore may be to design a BP device that is stiff enough to develop large joint torques yet is comfortable to not induce kinematic changes to gait.

For the handrail group, MAE was larger in C4 (small spring) and C5 (medium spring) than in C1 (prescribed) and C3 (recoil only). This is simply a function of the very low GAS torque observed in these simulations. The timing was still similar between GAS and the BP springs, but the BP generated larger and larger torques from C4 to C6 and surpassed the GAS torque, which increased MAE. The low GAS force in these two subjects can be attributed to their handrail use for one or two reasons. First, it is possible that by holding the handrail (located at the front of the treadmill) subjects were able to maintain their anterior/posterior position on the treadmill and perhaps needed less propulsive force in the lower limbs to walk. Second, the handrail is not instrumented and so we were unable to measure the forces exerted by these subjects' hands. This introduced error into our simulations and may have caused unrealistic results.

While the general timing of BP spring force production appears to align with GAS force production of the contralateral limb, these results show that the spring force may return to zero too quickly. BP spring force drops to zero around 55% of the gait cycle, but the contralateral GAS is active until roughly 65% (Figure 4-13 & Figure 4-14). Both the on and off timing is determined by the early-stance minimum distance between the spring origin at the thigh and its insertion at the heel. The knee and ankle moment arms of the BP, along with the subject's kinematics dictate how this biarticular length changes over the gait cycle. A BP with different moment arms or a different clutching mechanism might better match GAS by maintaining the on-time and extending the off-time. For example, a second clutch could be implemented to allow the knee to contribute energy to the BP, but prevent the knee from drawing energy. Additionally, it is possible that adjusting the moment arms as recommended in 6.2 could extend the off timing by reducing the influence of the large knee flexion just before toe off.

The biofeedback condition (C7) did have a smaller MAE than C5/C6 which would indicate that the BP torque produced is more similar to GAS. However, the comparison between C7and the C5/C6 spring conditions was only significant at the ankle and not at the knee for the no-handrail group. C7 and C6 also had a high variability both between and within subjects, so more data is necessary to draw conclusions on hypothesis H3.7.

6.4 Total Muscle Force

As stated in Section 5.4, there were no statistically significant findings for total muscle force. Hypotheses H4.1 – H4.7 are therefore unsupported. This may indicate that the model's default muscles are not an accurate representation of some subjects' individual muscle

forces. As described in Section 3.4, amputees exhibit a variety of muscle weaknesses and the model did not account for these differences. Some previous amputee strength studies found up to 60% weakness in certain muscle groups [54]–[56], which could have a large effect on the Static Optimization procedure used to obtain these results. To improve this analysis in future work, subject-specific muscle strengths should be used, perhaps determined by strength testing during the data collections.

It is also worth noting that this outcome results from the farthest step in the analysis pipeline (Static Optimization in OpenSim). As such, noise and errors in data collection, musculoskeletal model parameters, or processing, get compounded and propagated forward into the total muscle force analysis.

Total muscle force is a less direct measure of metabolic cost. Future work may measure metabolic cost during the experimental data collection using indirect calorimetry on subjects. Additionally, toolboxes in OpenSim to estimate metabolic cost are in development [64]–[66], and may provide a better measure in the future.

6.5 BP Knee and Ankle Work

Hypotheses regarding ankle work were nearly all supported. H5.3 – H5.8 showed that the BP springs do significant work at both joints when compared to zero (C1 – prescribed) and the baseline BP condition (C3 – recoil only). At the ankle, the BP spring work increased in magnitude with spring stiffness, as expected (H3.1 & H3.2). However, the medium spring yielded the highest work value at the knee, which does not support hypothesis H3.2. This suggests that there may be an optimum spring between the medium and large spring stiffnesses. Hypothesis H3.9 stated that the work transfer would be from the knee to the

ankle, and these results show that work was transferred from the ankle to the knee. The BP therefore did not function as intended with this measure, and this is valuable information for future iterations. The spring force dropped to zero just before toe off and was therefore unable to supply energy at the ankle when needed. Further investigation is needed, but it is possible that this timing difference, in conjunction with the large knee moment arm, caused the reverse work transfer to occur. A moment arm that varies with joint angle may be required, or possibly an extra clutch to limit knee energy extraction.

6.6 Model Validation

The comparison of experimental EMG measurements to Static Optimization results show that the model adequately simulates many of the large features of the measured EMG signals. The higher variation in EMG signal is expected, and can be attributed to measurement noise with the surface EMG electrodes. While the force magnitudes of individual muscles may not properly match each subject (Section 6.4), these plots indicate similar timing between the simulated results and experimentally measured data. A previous EMG study found that residual limb plantar flexors are generally inactive in mid-terminal stance, which is different than non-amputees [67]. This is true for in-socket EMG measurements of the medial GAS in many of our subjects (Figure 5-8, Appendix J). Residual SOL was not measured in this study.

6.7 Study Strengths and Limitations

This study presents a novel BP that has the potential to benefit many amputees. However, the current BP prototype iteration is large, heavy, and somewhat uncomfortable to wear. This could have negatively impacted our results by altering kinematics and causing

amputees to walk in an uncomfortable gait. However, initial qualitative user feedback was often positive, indicating a general amputee interest in continuing development of the Biarticular Prosthesis.

The amputee musculoskeletal model provides a valuable tool for analysis of amputee gait. The amputee-specific mass properties and joint definitions should improve accuracy in future simulations of amputee gait. The model muscle outputs are relatively similar to experimentally measured EMG, but total muscle force results indicate that more work is necessary to provide individualized muscle strength parameters to the model.

Many of our measures provide unique insight into device functionality and will help us to improve future device designs. The BP work calculations, for example, indicate that the intended work transfer from the ankle to the knee did not occur, but rather the ankle transferred work to the knee. This measure can be included in future biarticular studies as a valuable measure of device function.

Some measures in this study are limited in what they provide. Total muscle force is only an indirect calculation of metabolic cost, and may be too far down the simulation chain to provide accurate results. Rather, many studies in this field have measured metabolic cost through indirect calorimetry. Our results regarding metabolic cost are inconclusive, and methodological improvements to our approach are necessary for future estimates of metabolic cost. Experimentally measured indirect calorimetry, or improved simulations are necessary to adequately characterize the metabolic cost of walking with the BP.

Additionally, the BP torque comparison to contralateral GAS may not be the most desirable comparison. It is unclear how GAS torque in amputee intact limbs compares to GAS torque in non-amputees. The timing appears similar to non-amputee gait simulations

(Section 2.1), but may be elevated due to increased propulsive forces necessary for amputee gait. If possible, future comparisons of BP torque to non-amputee GAS torque would provide insight on the BP's potential contribution to healthy walking.

6.8 Comparison to Other Devices

Other prosthetic devices were described in Sections 1.3 and 1.6. Endo and Herr developed a transfemoral prosthesis with a powered ankle and a uniarticular spring at the knee to represent GAS [39]. With one bilateral amputee subject, they showed a decrease in metabolic cost of 6% [39]. Our analysis used total muscle force as an indirect indicator of metabolic cost, but a reduction of total muscle force from the BP was not supported. As described earlier, there are possible inaccuracies in the model's muscle parameters with respect to an individual subject, which obscures the results. Subjects 2, 5, and 7 did show a decrease in total muscle force with the biarticular spring element (Figure 5-6), but these findings were not statistically significant. Future work may use indirect calorimetry to experimentally measure metabolic cost, and employ model improvements to increase the accuracy of OpenSim force calculations.

Unal et al. have also developed a transfemoral biarticular prosthesis in simulation, and tested the device on one non-amputee [41], [42]. They showed in simulation that energy could be stored and then delivered at push-off. The BP did effectively store and return energy, but did not operate completely as intended. The spring force dropped to zero before push-off, so energy was returned to the joints too early. Additionally, our results show that the BP transferred energy from the ankle to the knee, which is the reverse of the intended direction. Rather than provide energy to the ankle at push-off, the BP was providing energy

to the knee just before push-off. Future device iterations will address this work transfer for improved function. Unal et al. have not yet tested their device on amputees, and many questions remain about the control system and its ability to adapt to speed changes [42]. The BP's mechanical design easily allows for changes in walking speed because the ratcheted clutch ensures that timing is based on gait cycle events (heel strike and minimum spring attachment distance).

Malcom et al. built and tested a powered lower-limb exoskeleton with ankle plantar flexion actuation [68]. Researchers found that the device had the ability to reduce the metabolic cost of walking (in non-amputees), and was most effective when the device was set to match the medial GAS eccentric and concentric properties, rather than SOL or only concentric GAS [68]. This device provides evidence that quasi-passive actuation such as the BP can reduce the metabolic cost of walking, though the present study showed no significant differences in total muscle force (as an indicator of metabolic cost). The Malcolm et al. device reduced metabolic cost most when the GAS was engaged at 43% of the gait cycle [68], which is a substantially later time than the BP (roughly 20% gait cycle). However, their device was powered so engaging at 43% of the gait cycle means that energy input at the ankle begins then, and the device could contribute to ankle push off. Because the current BP design passively produces force, an earlier engagement time is necessary so that the spring can first be loaded, before returning that energy later in the gait cycle. Peak BP spring force occurs at roughly 45% of gait (Figure 4-14), which denotes the beginning of energy return from the spring. Malcolm et al.'s device provided force through toe off [68], while the BP spring force dropped to zero earlier, as previously discussed.

6.9 FUTURE WORK

Future work will include BP device redesign as well as model improvements. Many questions remain unanswered about ideal BP parameters, such as moment arm ratios and optimal spring stiffness. These results indicate that most subjects prefer stiffness near the medium spring (3.7 N/mm), but additional stiffness values should be tested. Additionally, clutch mechanism improvements can be made to ensure that the spring transfers work from the knee to the ankle for push-off, and to allow larger torques to be applied at the joints without causing discomfort to the wearer.

To better understand the amputee musculoskeletal model's limitations, a muscle weakness sensitivity analysis should be performed. It is likely that the model is sensitive to weaknesses in specific muscle groups, and quantifying these will improve understanding of future simulations with the model. Additionally, there may be minimal strength testing that can characterize specific muscle weaknesses in a subject that can then be incorporated into the subject-specific model. These methods, as well as mathematical models and MRI measurements [58], [59] should be explored in relation to the amputee population.

Chapter 7. CONCLUSION

To improve amputee gait, a quasi-passive clutched spring BP was developed and tested. An OpenSim amputee musculoskeletal model was developed, validated, and used in the analysis of how the BP effects amputee gait. Seven amputee subjects walked on a treadmill using their prescribed prosthesis and then the BP with various spring configurations while 3D motion capture, ground reaction force, and BP analog data were

collected. No significant differences were found in kinematic symmetry or total muscle force. The BP generally applied more torque to the knee and ankle joints as spring stiffness increased, and higher stiffness values compare more favorably to the contralateral GAS. The BP spring transferred work from the ankle to the knee.

In conclusion, this initial study into the benefit of a quasi-passive clutched spring biarticular mechanism has provided many insights for future work and prosthesis design. One of the major factors in future biarticular device designs will be to achieve large levels of knee and ankle torque application without causing discomfort to the wearer. Additionally, more effective mechanisms can be implemented to ensure that work is transferred from the knee to the ankle, as the biological GAS does during gait. These results indicate that slower, less proficient walkers may have trouble adjusting to a device such as the BP, so a deeper exploration of which amputee populations can benefit from a device like the BP is needed. Finally, this study contributes an amputee musculoskeletal model for use in OpenSim simulations of gait. While the mass properties and muscle timings appear to adequately represent experimentally measured motion, the magnitudes of muscle force outputs need to be examined in further detail. In the future more individual-specific muscle parameters need to be included.

REFERENCES

[1] K. Ziegler-Graham, E. J. MacKenzie, P. L. Ephraim, T. G. Travison, and R. Brookmeyer, "Estimating the Prevalence of Limb Loss in the United States: 2005 to 2050," *Arch. Phys. Med. Rehabil.*, vol. 89, no. 3, pp. 422–429, 2008.

[2] D. C. Norvell, J. M. Czerniecki, G. E. Reiber, C. Maynard, J. A. Pecoraro, and N. S. Weiss, "The prevalence of knee pain and symptomatic knee osteoarthritis among veteran traumatic amputees and nonamputees," *Arch. Phys. Med. Rehabil.*, vol. 86, no. 3, pp. 487–493, Mar. 2005.

[3] R. J. Zmitrewicz, R. R. Neptune, and K. Sasaki, "Mechanical energetic contributions from individual muscles and elastic prosthetic feet during symmetric unilateral transtibial amputee walking: A theoretical study," *J. Biomech.*, vol. 40, no. 8, pp. 1824–1831, 2007.

[4] H. Bateni and S. J. Olney, "Kinematic and Kinetic Variations of Below-Knee Amputee Gait," *JPO J. Prosthetics Orthot.*, vol. 14, no. 1, pp. 2–10, 2002.

[5] A. E. Ferris, J. M. Aldridge, C. A. Rábago, and J. M. Wilken, "Evaluation of a powered ankle-foot prosthetic system during walking," *Arch. Phys. Med. Rehabil.*, vol. 93, no. 11, pp. 1911–1918, 2012.

[6] D. J. Sanderson and P. E. Martin, "Lower extremity kinematic and kinetic adaptations in unilateral below-knee amputees during walking," *Gait Posture*, vol. 6, no. 2, pp. 126–136, 1997.

[7] A. H. Vrieling, H. G. van Keeken, T. Schoppen, E. Otten, J. P. K. Halbertsma, A. L. Hof, and K. Postema, "Gait initiation in lower limb amputees," *Gait Posture*, vol. 27, no. 3, pp. 423–430, Apr. 2008.

[8] N. P. Fey, A. K. Silverman, and R. R. Neptune, "The influence of increasing steady-state walking speed on muscle activity in below-knee amputees," *J. Electromyogr. Kinesiol.*, vol. 20, no. 1, pp. 155–161, 2010.

[9] D. A. Winter and S. E. Sienko, "Biomechanics of below-knee amputee gait," *J. Biomech.*, vol. 21, no. 5, pp. 361–367, Jan. 1988.

[10] R. R. Neptune, F. E. Zajac, and S. A. Kautz, "Muscle force redistributes segmental power for body progression during walking," *Gait Posture*, vol. 19, no. 2, pp. 194–205, 2004.

[11] A. R. Den Otter, A. C. H. Geurts, T. Mulder, and J. Duysens, "Speed related changes in muscle activity from normal to very slow walking speeds," *Gait Posture*, vol. 19, no. 3, pp. 270–278, Jun. 2004.

[12] J. Perry, L. A. Boyd, S. S. Rao, and S. J. Mulroy, "Prosthetic weight acceptance mechanics in transtibial amputees wearing the Single Axis, Seattle Lite, and Flex Foot," *IEEE Trans. Rehabil. Eng.*, vol. 5, no. 4, pp. 283–289, 1997.

[13] L. Nolan, A. Wit, K. Dudziñski, A. Lees, M. Lake, and M. Wychowañski, "Adjustments in gait symmetry with walking speed in trans-femoral and trans-tibial amputees," *Gait Posture*, vol. 17, no. 2, pp. 142–151, Apr. 2003.

[14] A. K. Silverman, N. P. Fey, A. Portillo, J. G. Walden, G. Bosker, and R. R. Neptune, "Compensatory mechanisms in below-knee amputee gait in response to increasing steady-state walking speeds," *Gait Posture*, vol. 28, no. 4, pp. 602–609, Nov. 2008.

[15] J. M. Czerniecki, “Rehabilitation in limb deficiency. 1. Gait and motion analysis,” *Arch. Phys. Med. Rehabil.*, vol. 77, no. 3, pp. S3–S8, Mar. 1996.
[16] J. J. Genin, G. J. Bastien, B. Franck, C. Detrembleur, and P. A. Willems, “Effect of speed on the energy cost of walking in unilateral traumatic lower limb amputees,” *Eur. J. Appl. Physiol.*, vol. 103, no. 6, pp. 655–663, Aug. 2008.
[17] D. W. Russ, K. Vandenborne, G. A. Walter, M. Elliott, and S. A. Binder-Macleod, “Effects of muscle activation on fatigue and metabolism in human skeletal muscle.,” *J. Appl. Physiol.*, vol. 92, no. 5, pp. 1978–86, 2002.
[18] J. Rubenson, H. T. Henry, P. M. Dimoulas, and R. L. Marsh, “The cost of running uphill: linking organismal and muscle energy use in guinea fowl (Numida meleagris).,” *J. Exp. Biol.*, vol. 209, no. Pt 13, pp. 2395–2408, 2006.
[19] E. S. Arch, S. J. Stanhope, and J. S. Higginson, “Passive-dynamic ankle-foot orthosis replicates soleus but not gastrocnemius muscle function during stance in gait: Insights for orthosis prescription.,” *Prosthet. Orthot. Int.*, vol. 40, no. 5, Oct. 2015.
[20] N. P. Fey, G. K. Klute, and R. R. Neptune, “Altering prosthetic foot stiffness influences foot and muscle function during below-knee amputee walking: A modeling and simulation analysis,” *J. Biomech.*, vol. 46, no. 4, pp. 637–644, 2013.
[21] J. D. Smith and P. E. Martin, “Effects of prosthetic mass distribution on metabolic costs and walking symmetry,” *J. Appl. Biomech.*, vol. 29, no. 3, pp. 317–328, 2013.
[22] S. J. Lin-Chan, D. H. Nielsen, H. J. Yack, M. J. Hsu, and D. G. Shurr, “The Effects of Added Prosthetic Mass on Physiologic Responses and Stride Frequency during Multiple Speeds of Walking in Persons with Transtibial Amputation,” *Arch. Phys. Med. Rehabil.*, vol. 84, no. 12, pp. 1865–1871, 2003.
[23] G. Chitragari, D. B. Mahler, B. J. Sumpio, P. A. Blume, and B. E. Sumpio, “Prosthetic options available for the diabetic lower limb amputee,” *Clinics in Podiatric Medicine and Surgery*, vol. 31, no. 1. pp. 174–185, 2014.
[24] H. M. Herr and A. M. Grabowski, “Bionic ankle-foot prosthesis normalizes walking gait for persons with leg amputation.,” *Proc. Biol. Sci.*, vol. 279, no. 1728, pp. 457–64, 2012.
[25] C. Mancinelli, B. L. Patritti, P. Tropea, R. M. Greenwald, R. Casler, H. Herr, and P. Bonato, “Comparing a passive-elastic and a powered prosthesis in transtibial amputees,” in *2011 Annual International Conference of the IEEE Engineering in Medicine and Biology Society*, 2011, pp. 8255–8258.
[26] A. H. Shultz, J. E. Mitchell, D. Truex, B. E. Lawson, E. Ledoux, and M. Goldfarb, “A walking controller for a powered ankle prosthesis,” *Conf. Proc. ... Annu. Int. Conf. IEEE Eng. Med. Biol. Soc. IEEE Eng. Med. Biol. Soc. Annu. Conf.*, vol. 2014, pp. 6203–6206, 2014.
[27] R. R. Neptune, S. A. Kautz, and F. E. Zajac, “Contributions of the individual ankle plantar flexors to support, forward progression and swing initiation during walking,” *J. Biomech.*, vol. 34, no. 11, pp. 1387–1398, 2001.
[28] R. Jacobs, M. F. Bobbert, and G. J. Van Ingen Schenau, “Mechanical output from individual muscles during explosive leg extensions: The role of biarticular muscles,” *J. Biomech.*, vol. 29, no. 4, pp. 513–523, Apr. 1996.
[29] J. P. Broker and R. J. Gregor, “Mechanical energy management in cycling: source relations and energy expenditure.,” *Medicine and science in sports and exercise*, vol. 26, no. 1. pp. 64–74, 1994.

[30] M. M. van der Krogt, S. L. Delp, and M. H. Schwartz, "How robust is human gait to muscle weakness?," *Gait Posture*, vol. 36, no. 1, pp. 113–119, 2012.
[31] P. Krishnaswamy, E. N. Brown, and H. M. Herr, "Human leg model predicts ankle muscle-tendon morphology, state, roles and energetics in walking," *PLoS Comput. Biol.*, vol. 7, no. 3, 2011.
[32] D. G. Thelen and F. C. Anderson, "Using computed muscle control to generate forward dynamic simulations of human walking from experimental data," *J. Biomech.*, vol. 39, no. 6, pp. 1107–1115, 2006.
[33] S. H. Collins, M. B. Wiggin, and G. S. Sawicki, "Reducing the energy cost of human walking using an unpowered exoskeleton," *Nature*, vol. 522, Apr. 2015.
[34] S. L. Delp, F. C. Anderson, A. S. Arnold, P. Loan, A. Habib, C. T. John, E. Guendelman, and D. G. Thelen, "OpenSim: Open source to create and analyze dynamic simulations of movement," *IEEE Trans. Biomed. Eng.*, vol. 54, no. 11, pp. 1940–1950, 2007.
[35] S. J. Mattes, P. E. Martin, and T. D. Royer, "Walking symmetry and energy cost in persons with unilateral transtibial amputations: Matching prosthetic and intact limb inertial properties," *Arch. Phys. Med. Rehabil.*, vol. 81, no. 5, pp. 561–568, 2000.
[36] A. K. LaPre, B. R. Umberger, and F. Sup, "Simulation of a powered ankle prosthesis with dynamic joint alignment," *Conf. Proc. ... Annu. Int. Conf. IEEE Eng. Med. Biol. Soc. IEEE Eng. Med. Biol. Soc. Annu. Conf.*, vol. 2014, pp. 1618–1621, 2014.
[37] S. M. Rigney, A. Simmons, and L. Kark, "A prosthesis-specific multi-link segment model of lower-limb amputee sprinting," *J. Biomech.*, vol. 49, no. 14, pp. 3185–3193, 2016.
[38] J. L. Hicks, T. K. Uchida, A. Seth, A. Rajagopal, and S. Delp, "Is my model good enough? Best practices for verification and validation of musculoskeletal models and simulations of human movement," *J. Biomech. Eng.*, vol. 137, no. February, p. 20905, 2015.
[39] K. Endo, E. Swart, and H. Herr, "An artificial gastrocnemius for a transtibial prosthesis," *Proc. 31st Annu. Int. Conf. IEEE Eng. Med. Biol. Soc. Eng. Futur. Biomed. EMBC 2009*, pp. 5034–5037, 2009.
[40] H. M. Herr, "VARIABLE-MECHANICAL-IMPEDANCE ARTIFICIAL LEGS," 14/804542, 2015.
[41] R. Unal, R. Carloni, S. M. Behrens, E. E. G. Hekman, S. Stramigioli, and H. F. J. M. Koopman, "Towards a fully passive transfemoral prosthesis for normal walking," *Proc. IEEE RAS EMBS Int. Conf. Biomed. Robot. Biomechatronics*, pp. 1949–1954, 2012.
[42] R. Unal, F. Klijnstra, S. M. Behrens, E. E. G. Hekman, S. Stramigioli, H. F. J. M. Koopman, and R. Carloni, "The control of recycling energy strorage capacity for WalkMECHadapt," *Proc. - IEEE Int. Work. Robot Hum. Interact. Commun.*, vol. 2014–Octob, no. October, pp. 720–725, 2014.
[43] A. K. Silverman and R. R. Neptune, "Muscle and prosthesis contributions to amputee walking mechanics: A modeling study," *J. Biomech.*, vol. 45, no. 13, pp. 2271–2278, 2012.
[44] J. D. Smith, A. E. Ferris, G. D. Heise, R. N. Hinrichs, and P. E. Martin, "Oscillation and reaction board techniques for estimating inertial properties of a below-knee prosthesis.," *J. Vis. Exp.*, no. 87, pp. 1–16, May 2014.
[45] A. Rajagopal, C. L. Dembia, M. S. DeMers, D. D. Delp, J. L. Hicks, and S. L. Delp, "Full-Body Musculoskeletal Model for Muscle-Driven Simulation of Human Gait," *IEEE*

Trans. Biomed. Eng., vol. 63, no. 10, pp. 2068–2079, 2016.
[46] J. Perry, J. M. Burnfield, and L. M. Cabico, *Gait analysis : normal and pathological function*. SLACK, 2010.
[47] C. Pew, "Design and Testing of a Variable Stiffness Transverse Plane Adaptor for Use in a Lower Limb Prosthesis," 2014.
[48] W. L. Childers and S. Siebert, "Marker-based method to measure movement between the residual limb and a transtibial prosthetic socket.," *Prosthet. Orthot. Int.*, vol. 40, no. 6, pp. 720–728, Dec. 2016.
[49] R. D. Wedge, A. K. Lapre, F. Sup, and B. R. Umberger, "EFFECTS OF WALKING SPEED ON THE STUMP-SOCKET INTERFACE IN TRANSTIBIAL AMPUTEES," pp. 2–3.
[50] H. Gholizadeh, N. A. Abu Osman, A. Eshraghi, S. Ali, and N. A. Razak, "Transtibial prosthesis suspension systems: Systematic review of literature," *Clinical Biomechanics*, vol. 29, no. 1. Elsevier Ltd, pp. 87–97, 2014.
[51] K. H. Yeates and G. Klute, "A Coronally-Clutching Ankle to Improve Amputee Balance on Coronally-Uneven and Unpredictable Terrain," University of Washington, 2016.
[52] A. Fridman, I. Ona, and E. Isakov, "The influence of prosthetic foot alignment on trans-tibial amputee gait.," *Prosthet. Orthot. Int.*, vol. 27, pp. 17–22, Jun. 2003.
[53] J. D. Smith, "Effects of Prosthesis Inertia on the Mechanics and Energetics of Amputee Locomotion," 2008.
[54] L. Nolan, "Lower limb strength in sports-active transtibial amputees.," *Prosthet. Orthot. Int.*, vol. 33, no. 3, pp. 230–241, 2009.
[55] E. Isakov, H. Burger, M. Gregorič, and C. Marinček, "Isokinetic and isometric strength of the thigh muscles in below-knee amputees," *Clin. Biomech.*, vol. 11, no. 4, pp. 233–235, 1996.
[56] D. K. Ryser, R. P. Erickson, and T. Cahalan, "Isometric and isokinetic hip abductor strength in persons with above-knee amputations," *Arch. Phys. Med. Rehabil.*, vol. 69, no. 10, pp. 840–845, 1988.
[57] M. Rosenberg, K. Chastain, and K. Steele, "MUSCLE STRENGTH IMPACTS PREDICTIONS OF MUSCLE DEMAND WITH SIMULATED ORTHOSES," *NWBS 2017 Abstr.*, vol. 1, 2017.
[58] A. J. Meyer, I. Eskinazi, J. N. Jackson, A. V Rao, C. Patten, and B. J. Fregly, "Muscle Synergies Facilitate Computational Prediction of Subject-specific Walking Motions," *Front. Bioeng. Biotechnol.*, vol. 4, p. 77, 2016.
[59] M. Sartori, J. W. Fernandez, L. Modenese, C. P. Carty, L. A. Barber, K. Oberhofer, J. Zhang, G. G. Handsfield, N. S. Stott, T. F. Besier, D. Farina, and D. G. Lloyd, "Toward modeling locomotion using electromyography-informed 3D models: application to cerebral palsy," *Wiley Interdiscip. Rev. Syst. Biol. Med.*, vol. 9, no. 2, p. e1368, Mar. 2017.
[60] J. Yong and J. Dunne, "Webinar: Tips and Tricks for Data Collection, Scaling and Inverse Kinematics in OpenSim," 2017. [Online]. Available: http://opensim.stanford.edu/support/event_details.html?id=179. [Accessed: 27-Apr-2017].
[61] T. Hothorn, F. Bretz, and P. Westfall, "Simultaneous Inference in General Parametric Models," *Biometrical J.*, vol. 50, no. 3, pp. 346–363, Jun. 2008.
[62] R. C. Team, "R: A language and environment for statistical computing." R Foundation for Statistical Computing, Vienna, Austria, 2014.

[63] D. M. Bates, M. Machler, B. M. Bolker, and S. C. Walker, “Fitting Linear Mixed-Effects Models using lme4,” *J. Stat. Softw.*, vol. 67, no. 1, 2014.
[64] B. R. UMBERGER, K. G. M. GERRITSEN, and P. E. MARTIN, “A Model of Human Muscle Energy Expenditure,” *Comput. Methods Biomech. Biomed. Engin.*, vol. 6, no. 2, pp. 99–111, May 2003.
[65] B. R. Umberger, “Stance and swing phase costs in human walking.,” *J. R. Soc. Interface*, vol. 7, no. 50, pp. 1329–40, Sep. 2010.
[66] T. K. Uchida, J. L. Hicks, C. L. Dembia, S. L. Delp, J. Lännergren, and J. Rosen, “Stretching Your Energetic Budget: How Tendon Compliance Affects the Metabolic Cost of Running,” *PLoS One*, vol. 11, no. 3, p. e0150378, Mar. 2016.
[67] B. Silver-Thorn, T. Current, and B. Kuhse, “Preliminary investigation of residual limb plantarflexion and dorsiflexion muscle activity during treadmill walking for trans-tibial amputees.,” *Prosthet. Orthot. Int.*, vol. 36, no. 4, pp. 435–42, 2012.
[68] P. Malcolm, W. Derave, S. Galle, D. De Clercq, and S. Daugherty, “A Simple Exoskeleton That Assists Plantarflexion Can Reduce the Metabolic Cost of Human Walking,” *PLoS One*, vol. 8, no. 2, p. e56137, Feb. 2013.

APPENDIX A: MODEL MASS PROPERTIES CALCULATIONS

```
clear all; close all; clc;

%Parallel axis Theorem: I_knee = I_com +m*d^2

%Intact I_com values (xx,yy,zz)
I_com_tib = [0.0504 0.0051 0.0511];
I_com_tal = [.001 .001 .001];
I_com_calc = [.0014 .0039 .0041];
I_com_toes = [.0001 .0002 .0001];

%GenericAmputee_l values (xx,yy,zz)
I_com_res = [.0063 .002936 .0063875]
I_com_sp = [.00763 .00189 .00770]; %From solidworks
I_com_foot = [.00384 .00347 .00057]; % From Solidworks

%Mass values for each segment
m_tib = 3.7075;
m_tal = 0.1;
m_calc = 1.25;
m_toes = .2166;
m_res = 0.5*m_tib; %Lit C
m_sp_SW = 0.59476; % From SolidWorks,
m_foot_SW = 0.35; % From SolidWorks, use as ratio

m_tot_h = m_tib+m_tal+m_calc + m_toes;
m_tot_a = 0.65*m_tot_h; % Lit D
m_prosth = m_tot_a - m_res; % = m_sp + m_foot
m_sp = (m_sp_SW/(m_sp_SW+m_foot_SW))*m_prosth;
m_foot = (m_foot_SW/(m_sp_SW+m_foot_SW))*m_prosth;

%COM Locations in local ref frames
com_tib1 = [0 -.1867 0]; % Knee = origin
com_tal1 = [-.01 -.4 0]; %knee = origin
com_calc1 = [.1 .03 0]; %subtalar = origin
com_toes1 = [.0346 .006 .0175]; % mtp = origin

%Joint Locations in Global reference frame
knee = [0 0 0];
ankle = [-.01 -.4 0];
subtalar = [-.04877 -.04195 -.00792]+ ankle;
mtp = [.1788 -.002 -.00108]+subtalar;
```

```
figure(1),
plot3(knee(3),knee(1), knee(2),'kx','linewidth',3), hold on
plot3(ankle(3),ankle(1),ankle(2), 'bx','linewidth',3)
plot3(subtalar(3),subtalar(1),subtalar(2), 'rx','linewidth',3)
plot3(mtp(3),mtp(1), mtp(2),'mx','linewidth',3)
xlabel('Z'),ylabel('X'),zlabel('Y')
title('intact limb COM and Joints')
%%
%COM locations wrt knee joint center (x,y,z)
%From .OSIM file
com_tib = [0 -.1867 0]; %NOT residual
com_tal = [-.01 -.4 0];
com_calc = com_calc1 + subtalar; %[0.05213 -.44195 0];
com_toes = com_toes1 + mtp; %[.16463 -.46795 -.0085];

plot3(com_tib(3),com_tib(1), com_tib(2),'ko','linewidth',3), hold on
plot3(com_tal(3),com_tal(1),com_tal(2), 'bo','linewidth',3)
plot3(com_calc(3),com_calc(1),com_calc(2), 'ro','linewidth',3)
plot3(com_toes(3),com_toes(1), com_toes(2),'mo','linewidth',3)

%From SW, literature and osim translations
interface = [0 -.2 0]; % knee = origin
ankle_amp = [0 -0.2 0] + interface;
com_res = [0 -0.1 0]; %Lit B
com_sp = [0 .06909 0]+ interface;
com_foot = [.07468 -.03354 .00197] + ankle_amp;

figure(2),
plot3(knee(3),knee(1), knee(2),'kx','linewidth',3), hold on
plot3(interface(3),interface(1),interface(2), 'bx','linewidth',3)
plot3(ankle_amp(3),ankle_amp(1),ankle_amp(2), 'rx','linewidth',3)
xlabel('Z'),ylabel('X'),zlabel('Y')
plot3(com_res(3),com_res(1), com_res(2),'ko','linewidth',3), hold on
plot3(com_sp(3),com_sp(1),com_sp(2), 'bo','linewidth',3)
plot3(com_foot(3),com_foot(1),com_foot(2), 'ro','linewidth',3)
title('Amputee CoM and Joints')
ylim([0 .4])

%calculate distances for each segment
d_tib = sqrt(sum(com_tib.^2));
d_tal = sqrt(sum(com_tal.^2));
d_calc = sqrt(sum(com_calc.^2));
d_toes = sqrt(sum(com_toes.^2));
d_res = sqrt(sum(com_res.^2));
d_sp = sqrt(sum(com_sp.^2));
d_foot = sqrt(sum(com_foot.^2));
```

```
%Calculate I_knee for intact limb
I_knee_tib = I_com_tib +m_tib*(d_tib^2);
I_knee_tal = I_com_tal +m_tal*(d_tal^2);
I_knee_calc = I_com_calc +m_calc*(d_calc^2);
I_knee_toes = I_com_toes +m_toes*(d_toes^2);

I_knee_intact = I_knee_tib+I_knee_tal+I_knee_calc+I_knee_toes

%Calculate I_knee for residual/prosth
I_knee_res = I_com_res+ m_res*(d_res^2);
I_knee_sp = I_com_sp+ m_sp*(d_sp^2);
I_knee_foot = I_com_foot+ m_foot*(d_foot^2);

I_knee_amputee = I_knee_res+I_knee_sp+I_knee_foot

j = I_knee_amputee./I_knee_intact

%Check with Lit A and Lit E calcs

%% Calculate with Socket and Pylon being separate
m_pylo = m_sp*(.10821/(.10821+.4865)) %Number ratio from SW
m_sock = m_sp*(.4865/(.10821+.4865))
com_pylo = [0 -.05117 0] %from SW
com_sock = [0 .0958 0]

I_com_sock = [.0069 .0018 .0070]*(m_sock/.4865) %From SW
I_com_pylo = [.00072 .00006 .00072]*(m_pylo/.10821) %From SW
```

APPENDIX B: BP FITTING PROTOCOL

Summary

This protocol is designed to custom fit the Biarticular Prosthesis to an individual amputee (or healthy subject on stilts)

Fitting Setup (before subject arrives)

1.1. Subject Number: _____
1.2. Weight: _____ lbs
1.3. Height: __ ft ___ in
1.4. Affected leg Left / Right
1.5. Subject shoe size _____ M / W US
1.6. Assemble BP enough to demo to subject
    1.6.1. Remove load cell to prevent damage
    1.6.2. Tape wires out of way
    1.6.3. Select correct Venture foot side / size M 9-11 = 26 cm; M 11+ = 27 cm
    1.6.4. Replace foot bumpers per College Park "Venture Gait Match"
        1.6.4.1. Front/Ankle: 0–120 = soft; 121–220 = med; 221-250 = firm
        1.6.4.2. Rear: 0–120 = soft; 121–160 = med; 161-200 = firm; 201–250 = XF
    1.6.5. Turn ankle adjuster in 2 turns from initial bumper contact
    1.6.6. Install foot sock and shell
    1.6.7. Install pylon suited to height
    1.6.8. Install iPecs
    1.6.9. Pick uprights suited to height
    1.6.10. Install correct thigh cuff per Allard "COMBO Brochure"
    1.6.11. Install correct knee strap per Allard "COMBO Brochure"
1.7. Clean lab and prepare a chair
1.8. Gather supplies
    1.8.1. Dry erase markers
    1.8.2. Soft tape measure
    1.8.3. Anthropometer
    1.8.4. Sony still camera (charge battery, verify space available on SD card)
    1.8.5. 3mm, 4mm, 6mm, 3/16" allen keys, big flat screwdriver, Philips screwdriver, 7mm wrench
    1.8.6. Blue loctite
1.9. Turn on treadmill
1.10. Print consents (verify revisions): BP, Registry, Repository, HIPA's, demographics

Fitting Procedure

1.11. Consent subject
1.12. If subject's shoes are inappropriate, give them to a pair of David's sneakers
1.13. Subject to don spandex shorts
    1.13.1. Find appropriately sized shorts for subject (from file cabinet)
    1.13.2. Tell subject it's a good time to use the restroom
    1.13.3. Notify people in wet lab

1.13.4. Close door to wet lab and to gait lab
1.14. Subject weight _____ lbs
1.15. Remove subject's shoes
1.16. Photograph affected leg hip to floor from all 4 sides
1.17. Affected leg measurements
1.17.1. With / Without shoe
1.17.2. Tibial plateau to ground _____ in
1.17.3. Thigh circumference 8" above mid-patella _____ in
1.17.4. Knee width (widest part) _____ in
1.17.5. Top of proximal pyramid adapter to ground _____ in
1.17.6. Test fit thigh cuff (verify correct side and size)
1.17.6.1. Push thigh cuff as high as is comfortable
1.17.6.2. Top of thigh cuff to ground _____ in
1.18. If possible, install BP on subject's socket
1.18.1. When disassembling pyramids, loosen only 2 screws so the other 2 maintain the alignment (mark the 2 screw positions)
1.18.2. When disassembling components of subject's prescribed prosthesis, use a marker to indicate orientation and/or position (sharpie can be used and removed from metal parts with acetone)
1.18.3. Adjust pylon length
1.18.4. Check knee joint height / lower upright length
1.18.5. Check thigh cuff fit
1.18.6. Check thigh cuff height / upper upright length
1.18.7. Check clearance of clutch to thigh
1.18.8. Check knee strap size / adjust
1.19. Return subject's prosthesis to original configuration
1.19.1. Apply Loctite to loosened fasteners
1.19.2. Torque all fasteners (10 N-m for clamps, 15 N-m for pyramids)
1.20. Have subject walk on treadmill with their prescribed prosthesis to acclimate to the treadmill
1.21. Turn off treadmill

APPENDIX C: EMG PLACEMENT PROTOCOL

EMG Data Collection Sheet Date: _____ Subject ID: _____ Residual Limb Side: _____

Placement Order		Channel 1 Residual Limb	Channel 2 Intact Limb	Ground (relative to electrode placement)	Test Maneuver	Electrode Placement	Image
1	Soleus (medial)	☐ 8	☐ 16	Proximal out of socket (symmetrical)	Plantarflex foot (knee flexed @90 deg, sitting)	Distal and anterior to gastroc	
2	Medial Gastrocnemius	☐ 7 (in-socket)	☐ 15	Proximal out of socket (symmetrical)	Plantarflex foot (knee extended→ supine easier)	1 handbreath below popliteal crease, medial side	
3	Biceps Femoris Long	☐ 3	☐ 11	Distal (long side parallel to electrodes)	Flex knee from <90 deg) (prone)	Midpoint between fibular head and ischial tuberosity. Or use popliteal crease to top of thigh, slightly more lateral side	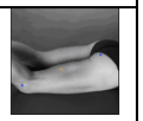
4	Tibialis Anterior	☐ 6 (in-socket)	☐ 14	Proximal out of socket (symmetrical)	Dorsiflex foot (supine/sitting)	4 fingerbreadths below tibial tuberosity and one fingerbreadth lateral to tibial crest	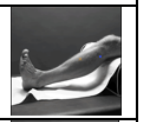
5	Rectus Femoris	☐ 4 (in-socket)	☐ 12	Distal	Extend knee w/out rot thigh (sitting)	Midpoint between superior patella and ASIS	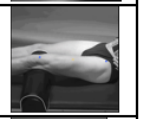
6	Vastus Medialis	☐ 5	☐ 13	Proximal	Extend knee w/out rot thigh (sitting)	Medial anterior to superior patella. Only about 2 fingerbreadths.	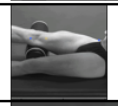
7	Gluteus Maximus	☐ 1	☐ 9	Proximal (under waistband)	Lift leg with knee flexed (prone)	Between GT and sacrum, or midway between waist and lower border (fibers angle down towards GT)	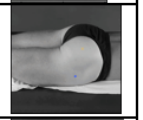
8	Gluteus Medius	☐ 2	☐ 10	Medial	Abduct thigh (sidelying)	1" distal to midpoint of iliac crest (find ASIS and follow ridge up)	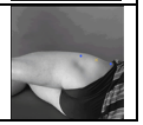

*Electrode #8 (residual SOL) is unused.

APPENDIX D: BP STUDY MARKER SET

Plug-in Gait Markers	Additional Markers

Upper Body

Head Markers

LFHD	Left front head	Located approximately over the left temple
RFHD	Right front head	Located approximately over the right temple
LBHD	Left back head	Placed on the back of the head, roughly in a horizontal plane of the front head markers
RFHD	Right back head	Placed on the back of the head, roughly in a horizontal plane of the front head markers

The markers over the temples define the origin, and the scale of the head. The rear markers define its orientation. If they cannot be placed level with the front markers, and the head is level in the static trial, tick the "Head Level" check box under options on “Run static model” in the pipeline when processing the static trial. Many users buy a headband and permanently attach markers to it.

Torso Markers

C7	7th cervical vertebra	Spinous process of the 7th cervical vertebrae
T10	10th thoracic vertebra	Spinous Process of the 10th thoracic vertebrae. Follow bottom of rib cage to spine
CLAV	Clavicle	Jugular Notch where the clavicles meet the sternum
STRN	Sternum	Xiphoid process of the Sternum
RBAK	Right Back	Placed in the middle of the right scapula. This marker has no symmetrical marker on the left side. This asymmetry helps the autolabeling routine determine right from left on the subject.

C7, T10, CLAV, STRN define the sagittal plane, hence their lateral positioning is most important.

Arm Markers

LSHO	Left shoulder marker	Placed on the Acromio-clavicular joint

LUA 1-4	Left upper arm cluster	Cluster of 4 markers rigidly attached to each other, placed laterally on the upper arm between the elbow and shoulder markers. See Figure 4 for 1-4 naming convention
LELB	Left elbow (lateral)	Placed on lateral elbow with LELM to approximate the elbow joint axis.
LELM	Left elbow (medial)	Placed on the medial epicondyle of the humerus.
LWRA	Left wrist marker A	Left wrist joint line, thumb side
LWRB	Left wrist marker B	Left wrist joint line, pinkie side
LFIN	Left fingers	Actually placed on the dorsum of the hand just below the head of the second metacarpal

All of these markers are also placed on the right side of the body, indicated with RSHO, RUA1-4, RELB, RELM, RWRA, RWRB, and RFIN.

Lower Body

Pelvis Markers

LASI	Left ASIS	Placed directly over the left anterior superior iliac spine
RASI	Right ASIS	Placed directly over the right anterior superior iliac spine
LPSI	Left PSIS	Placed directly over the left posterior superior iliac spine
RPSI	Right PSIS	Placed directly over the right posterior superior iliac spine

The LASI/RASI markers may need to be placed medially to the ASIS to get the marker to the correct position due to the curvature of the abdomen. In some patients, especially those who are obese, the markers either can't be placed exactly anterior to the ASIS, or are invisible in this position to cameras. In these cases, move each marker laterally by an equal amount, along the ASIS-ASIS axis. The true inter-ASIS Distance must then be recorded and entered on the subject parameters form. These markers, together with the LPSI and RPSI markers, define the pelvic axes.

Leg Markers

Markers that begin with an 'L' are also repeated on the right side of the body, and denoted with an 'R'.

LKNE	Left knee	Placed on the lateral epicondyle of the left knee (*) Placed on the lateral side of the knee joint hinge for the BP device.

LKNM	Left knee (medial)	Placed on the medial epicondyle of the left knee for prescribed prostheses. Placed on the medial side of the knee joint hinge for the BP device.
LTHI	Left thigh wand marker	Place the marker over the lower lateral 1/3 surface of the thigh, just below the swing of the hand, although the height is not critical. (**)
LTH 1-4	Left thigh marker cluster	Cluster of 4 markers rigidly attached to each other, placed laterally on the thigh. These are often placed on the BP thigh cuff. See Figure 4 for 1-4 naming convention.
LTIB	Left tibial wand marker	Similar to the thigh markers, these are placed over the lower 1/3 of the shank to determine the alignment of the ankle flexion axis (***)
LSK 1-4	Left shank marker cluster	Cluster of 4 markers rigidly attached to each other, placed laterally on the shank. See Figure 4 for 1-4 naming convention.
LANK	Left ankle	Placed on the lateral malleolus along an imaginary line that passes through the transmalleolar axis. These positions are mirrored on the amputated side for prescribed prostheses. BP ankle markers are place along the known joint line.
LANM	Left ankle (medial)	Placed on the medial malleolus along an imaginary line that passes through the transmalleolar axis. These positions are mirrored on the amputated side for prescribed prostheses. BP ankle markers are place along the known joint line.
LHF	Left fibular head	Placed at the head of the fibula, located just distal to the knee joint line
LTT	Left tibial tuberosity	Placed at the TT, bony landmark on the anterior of the tibia. On the amputated side, may have to be placed on the socket in the same relative position of the TT.
PYLO	Pylon parker	Placed laterally on the proximal end of the pylon. Used to define the residual and pylon lengths individually.

* To locate the "precise" point for the knee marker placement, passively flex and extend the knee a little while watching the skin surface on the lateral aspect of the knee joint. Identify where knee joint axis passes through the lateral side of the knee by finding the lateral skin surface that comes closest to remaining fixed in the thigh. This landmark should also be the point about which the lower leg appears to rotate. Mark this point with a pen. With an adult patient standing, this pen mark should be about 1.5 cm above the joint line, mid-way between the front and back of the joint. Attach the marker at this point.

**The thigh markers are used to calculate the knee flexion axis location and orientation. The antero-posterior placement of the marker is critical for correct alignment of the knee flexion axis. Try to keep the thigh marker off the belly of the muscle, but place the thigh marker at least two marker diameters proximal of the knee marker. Adjust the position of the marker so that it is aligned in the plane that contains the hip and knee joint centers and

the knee flexion/extension axis. There is also another method that uses a mirror to align this marker, allowing the operator to better judge the positioning.

***The tibial marker should lie in the plane that contains the knee and ankle joint centers and the ankle flexion/extension axis. In a normal subject the ankle joint axis, between the medial and lateral malleoli, is externally rotated by between 5 and 15 degrees with respect to the knee flexion axis. The placements of the shank markers should reflect this.

Foot markers

LHEE	Left heel	Placed over the second metatarsal head, on the mid-foot side of the equinus break between fore-foot and mid-foot Placed on the calcaneus at the same height above the **floor surface** as the toe marker
LTOE	Left 'toe'	Placed over the second metatarsal head, on the mid-foot side of the equinus break between fore-foot and mid-foot.
LMTP	Left MTP joint	Placed laterally on the 5th metatarsophalangeal joint (little toe side).
LMTM	Left MTP, medial	Placed medially on the 1st metatarsophalangeal joint (big toe side).

For the prosthetic foot, these markers should be placed to match the intact foot as best as possible. In particular, the HEE and TOE marker placement is significant for appropriate scaling of the foot and to determine the foot external rotation angle.

BP-Specific Markers

CLUL	Lateral clutch	Placed on the lateral side of the proximal end of the clutch-spring mechanism, where the string inserts the spool. Used to define the spring line of action and point of force application.
CLUM	Medial clutch	Placed on the medial side of the proximal end of the clutch-spring mechanism, where the string inserts the spool. Used to define the spring line of action and point of force application.
LoadCell	Spring Loadcell	Placed at the distal attachment of the spring. Used to determine the spring line of action and point of force application.

APPENDIX E: MARKER RECREATION CODE

```
function [trj, distErr] = recreateMarker(mk1, mk2, mk3, KnownPos)

% Function to use 3 known markers (rigidly attached) to solve for a 4th marker trajectory.
Created by Andrea Willson 3/30/2017.

% mk1, mk2 and mk3 are 3 known marker trajectories of size(n,3)
% mk1 is the traj. about which the coord sys will be generated (origin)
% if desired, mk3 can be a calculated joint center (such as AJC determined by averaging
RANK and RANM markers)

%Output (global) reference frame is the same as input(x-y-z), so would work with vicon
files or transformed opensim .TRCs

% trj is recreated marker trajectory, distErr is the average of the SDs ofthe distances
between the 3 known markers
%inputs: 3 known marker trajectories dimensions from a dynamic trial = (length(time),3)
cols are x-y-z in VICON coords,
...and one 4x3 vector of all known and 4th marker position (ie from static trial), in VICON
coords

%create normal length vectors to represent new coords in STATIC trial
x_globalS = (KnownPos(2,:) - KnownPos(1,:))/norm(KnownPos(2,:) - KnownPos(1,:));
y_globalSi = (KnownPos(3,:) - KnownPos(1,:))/norm(KnownPos(3,:) - KnownPos(1,:));
%use two pairs to define a plane
z_globalS = cross(x_globalS,y_globalSi)/norm(cross(x_globalS,y_globalSi));
y_globalS = cross(z_globalS, x_globalS)/norm(cross(z_globalS,x_globalS)); %ensures that all
3 axes are ~perpendicular

%create Rotational matrix to convert from Global ref frame to local frame,
...mk1 = origin
R_glob2loc = [x_globalS; y_globalS; z_globalS];

%Make norm(R) == 1
% R_glob2loc = R_glob2loc./(norm(R_glob2loc));


%Calculate position of missing marker in global frame, wrt mk1
P_global = (KnownPos(4,:)-KnownPos(1,:)).';

% Calculate position of missing marker in local frame
P_local = R_glob2loc*P_global;
P2_loc = R_glob2loc*((KnownPos(2,:)-KnownPos(1,:)).');
```

```
P3_loc = R_glob2loc*((KnownPos(3,:)-KnownPos(1,:)).');

%% Apply to Dynamic data
n = length(mk1(:,1)); %number of samples
%create normal length vectors to represent new coords in DYNAMIC trial
for j = 1:n
   x_globalD(j,:) = (mk2(j,:) - mk1(j,:))/norm(mk2(j,:) - mk1(j,:));
   y_globalDi(j,:) = (mk3(j,:) - mk1(j,:))/norm(mk3(j,:) - mk1(j,:));
   z_globalD(j,:) =
cross(x_globalD(j,:),y_globalDi(j,:))/norm(cross(x_globalD(j,:),y_globalDi(j,:)));
   y_globalD(j,:) =
cross(z_globalD(j,:),x_globalD(j,:))/norm(cross(z_globalD(j,:),x_globalD(j,:)));
end

R_loc2glob = zeros(3,3,n);
P_globalD = zeros(n,3);
for j = 1:n
   %Create R_loc2glob
   R_loc2glob(:,:,j) = [x_globalD(j,:); y_globalD(j,:); z_globalD(j,:)].'; %transpose bc it's
loc2glob
   P_globalD(j,:) = (R_loc2glob(:,:,j)*P_local).' + mk1(j,:);
   Rnorm(j)= norm(R_loc2glob(:,:,j));
end

%Calculate 'non-rigidity error' = known marker dist changes over time
for j = 1:n
   dist1(j,1) = norm(mk1(j,:)-mk2(j,:));
   dist2(j,1) = norm(mk2(j,:)-mk3(j,:));
   dist3(j,1) = norm(mk3(j,:)-mk1(j,:));
end
Dist = [dist1 dist2 dist3];
figure
plot(dist1,'linewidth',2), hold on
plot(dist2,'linewidth',2)
plot(dist3,'linewidth',2)

AvgDist = mean(Dist); % in mm
SD_Dist = std(Dist); %in mm

%outputs:
distErr = SD_Dist;
trj = P_globalD;

return
```

APPENDIX F: OPENSIM SCALING SETTINGS

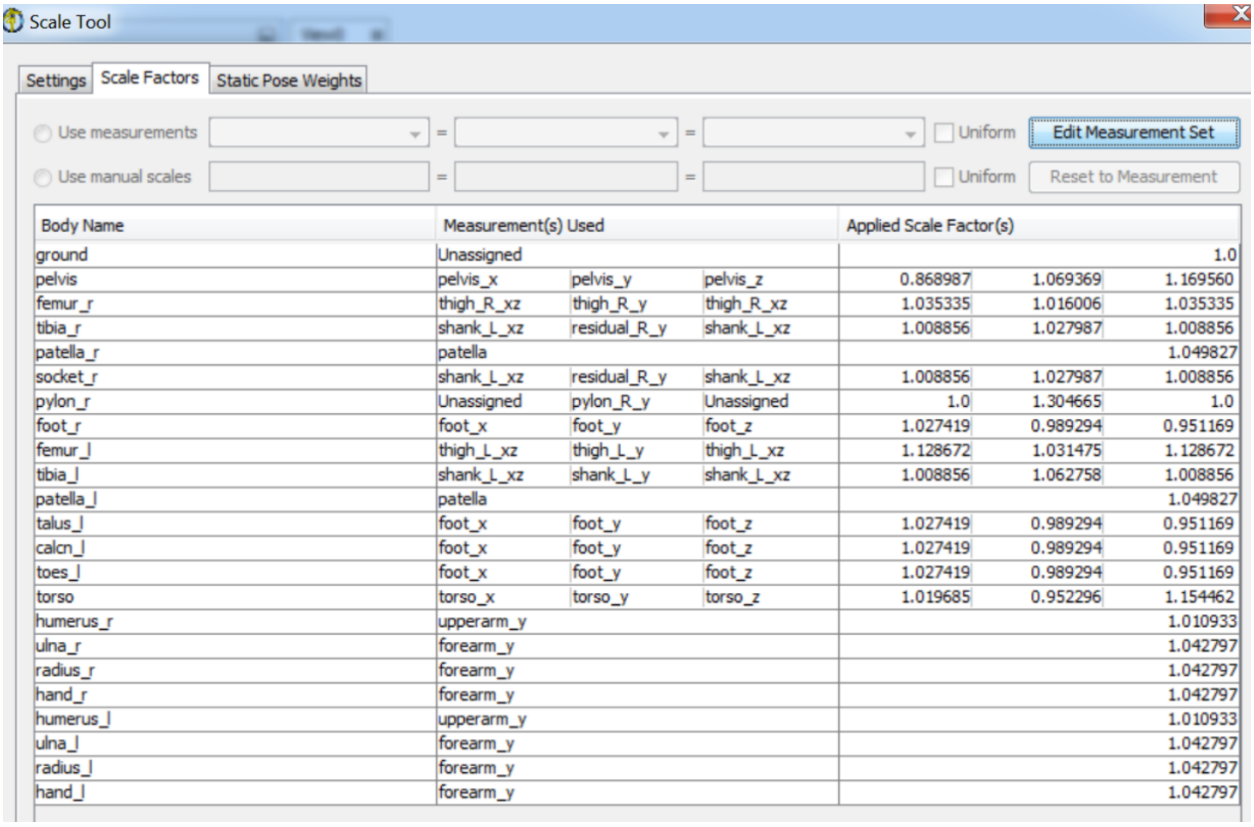

Scale Tool

Settings | Scale Factors | Static Pose Weights

Use measurements = = Uniform Edit Measurement Set

Use manual scales = = Uniform Reset to Measurement

Body Name	Measurement(s) Used			Applied Scale Factor(s)		
ground	Unassigned					1.0
pelvis	pelvis_x	pelvis_y	pelvis_z	0.868987	1.069369	1.169560
femur_r	thigh_R_xz	thigh_R_y	thigh_R_xz	1.035335	1.016006	1.035335
tibia_r	shank_L_xz	residual_R_y	shank_L_xz	1.008856	1.027987	1.008856
patella_r	patella					1.049827
socket_r	shank_L_xz	residual_R_y	shank_L_xz	1.008856	1.027987	1.008856
pylon_r	Unassigned	pylon_R_y	Unassigned	1.0	1.304665	1.0
foot_r	foot_x	foot_y	foot_z	1.027419	0.989294	0.951169
femur_l	thigh_L_xz	thigh_L_y	thigh_L_xz	1.128672	1.031475	1.128672
tibia_l	shank_L_xz	shank_L_y	shank_L_xz	1.008856	1.062758	1.008856
patella_l	patella					1.049827
talus_l	foot_x	foot_y	foot_z	1.027419	0.989294	0.951169
calcn_l	foot_x	foot_y	foot_z	1.027419	0.989294	0.951169
toes_l	foot_x	foot_y	foot_z	1.027419	0.989294	0.951169
torso	torso_x	torso_y	torso_z	1.019685	0.952296	1.154462
humerus_r	upperarm_y					1.010933
ulna_r	forearm_y					1.042797
radius_r	forearm_y					1.042797
hand_r	forearm_y					1.042797
humerus_l	upperarm_y					1.010933
ulna_l	forearm_y					1.042797
radius_l	forearm_y					1.042797
hand_l	forearm_y					1.042797

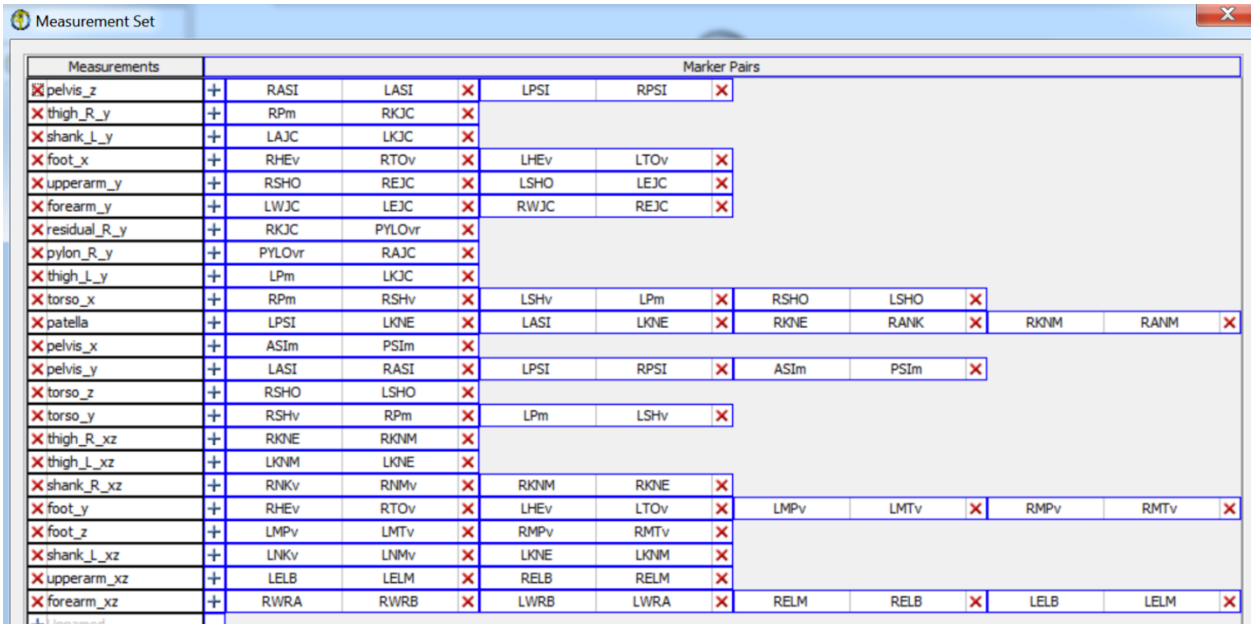

Measurement Set

Measurements	Marker Pairs								
pelvis_z	RASI	LASI	LPSI	RPSI					
thigh_R_y	RPm	RKJC							
shank_L_y	LAJC	LKJC							
foot_x	RHEv	RTOv	LHEv	LTOv					
upperarm_y	RSHO	REJC	LSHO	LEJC					
forearm_y	LWJC	LEJC	RWJC	REJC					
residual_R_y	RKJC	PYLOvr							
pylon_R_y	PYLOvr	RAJC							
thigh_L_y	LPm	LKJC							
torso_x	RPm	RSHv	LSHv	LPm	RSHO	LSHO			
patella	LPSI	LKNE	LASI	LKNE	RKNE	RANK	RKNM	RANM	
pelvis_x	ASIm	PSIm							
pelvis_y	LASI	RASI	LPSI	RPSI	ASIm	PSIm			
torso_z	RSHO	LSHO							
torso_y	RSHv	RPm	LPm	LSHv					
thigh_R_xz	RKNE	RKNM							
thigh_L_xz	LKNM	LKNE							
shank_R_xz	RNKv	RNMv	RKNM	RKNE					
foot_y	RHEv	RTOv	LHEv	LTOv	LMPv	LMTv	RMPv	RMTv	
foot_z	LMPv	LMTv	RMPv	RMTv					
shank_L_xz	LNKv	LNMv	LKNE	LKNM					
upperarm_xz	LELB	LELM	RELB	RELM					
forearm_xz	RWRA	RWRB	LWRB	LWRA	RELM	RELB	LELB	LELM	

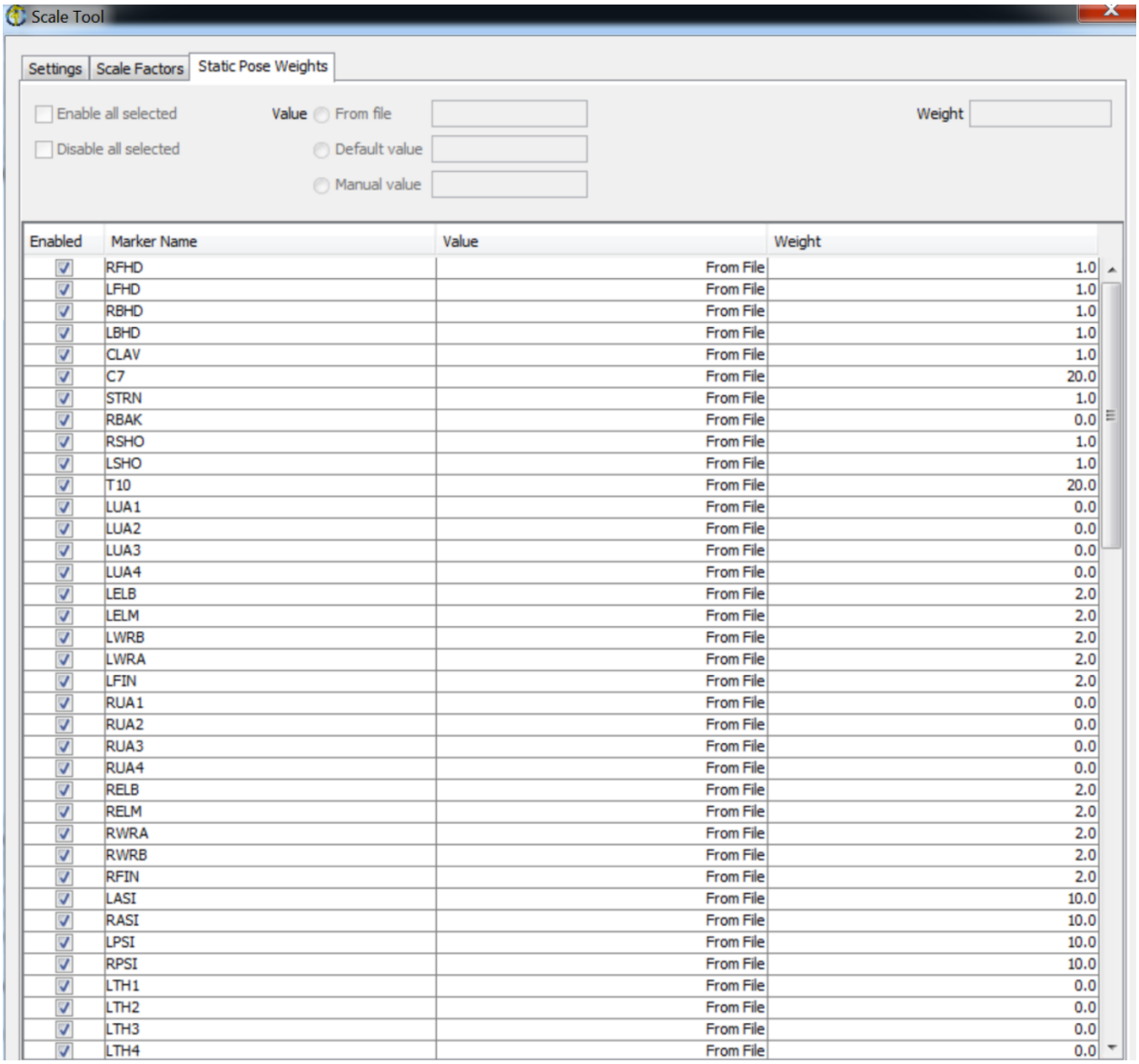

Enabled	Marker Name	Value	Weight
☑	RFHD	From File	1.0
☑	LFHD	From File	1.0
☑	RBHD	From File	1.0
☑	LBHD	From File	1.0
☑	CLAV	From File	1.0
☑	C7	From File	20.0
☑	STRN	From File	1.0
☑	RBAK	From File	0.0
☑	RSHO	From File	1.0
☑	LSHO	From File	1.0
☑	T10	From File	20.0
☑	LUA1	From File	0.0
☑	LUA2	From File	0.0
☑	LUA3	From File	0.0
☑	LUA4	From File	0.0
☑	LELB	From File	2.0
☑	LELM	From File	2.0
☑	LWRB	From File	2.0
☑	LWRA	From File	2.0
☑	LFIN	From File	2.0
☑	RUA1	From File	0.0
☑	RUA2	From File	0.0
☑	RUA3	From File	0.0
☑	RUA4	From File	0.0
☑	RELB	From File	2.0
☑	RELM	From File	2.0
☑	RWRA	From File	2.0
☑	RWRB	From File	2.0
☑	RFIN	From File	2.0
☑	LASI	From File	10.0
☑	RASI	From File	10.0
☑	LPSI	From File	10.0
☑	RPSI	From File	10.0
☑	LTH1	From File	0.0
☑	LTH2	From File	0.0
☑	LTH3	From File	0.0
☑	LTH4	From File	0.0

☑	LTHI	From File	0.0
☑	LKNE	From File	10.0
☑	LKNM	From File	10.0
☑	RTH1	From File	0.0
☑	RTH2	From File	0.0
☑	RTH3	From File	0.0
☑	RTH4	From File	0.0
☑	RTHI	From File	0.0
☑	RKNE	From File	10.0
☑	RKNM	From File	10.0
☑	LTT	From File	5.0
☑	LHF	From File	5.0
☑	LTIB	From File	0.0
☑	LSK1	From File	0.0
☑	LSK2	From File	0.0
☑	LSK3	From File	0.0
☑	LSK4	From File	0.0
☑	LANM	From File	10.0
☑	LANK	From File	10.0
☑	LHEE	From File	2.0
☑	LTOE	From File	4.0
☑	LMTM	From File	4.0
☑	LMTP	From File	4.0
☑	RTT	From File	5.0
☑	RHF	From File	5.0
☑	RTIB	From File	0.0
☑	RSK1	From File	0.0
☑	RSK2	From File	0.0
☑	RSK3	From File	0.0
☑	RSK4	From File	0.0
☑	RANK	From File	10.0
☑	RANM	From File	10.0
☑	RHEE	From File	2.0
☑	RTOE	From File	4.0
☑	RMTP	From File	4.0
☑	RMTM	From File	4.0
☑	PYLO	From File	5.0
☑	LKJC	From File	1.0
☑	RKJC	From File	1.0
☑	LHEv	From File	0.0
☑	RHEv	From File	0.0
☑	LTOv	From File	1.0
☑	RTOv	From File	1.0
☑	LMPv	From File	1.0
☑	RMPv	From File	1.0
☑	LMTv	From File	1.0
☑	RMTv	From File	1.0
☑	LNKv	From File	1.0
☑	RNKv	From File	1.0
☑	LNMv	From File	1.0
☑	RNMv	From File	1.0
☑	ASIm	From File	1.0
☑	PSIm	From File	1.0
☑	LPm	From File	1.0
☑	RPm	From File	1.0
☑	LAJC	From File	1.0
☑	RAJC	From File	1.0
☑	LWJC	From File	1.0
☑	RWJC	From File	1.0
☑	STRv	From File	1.0
☑	T10v	From File	1.0
☑	LSHv	From File	1.0
☑	RSHv	From File	1.0
☑	PYLOvr	From File	1.0
☑	REJC	From File	1.0
☑	LEJC	From File	1.0

APPENDIX G: OPENSIM INVERSE KINEMATICS SETTINGS

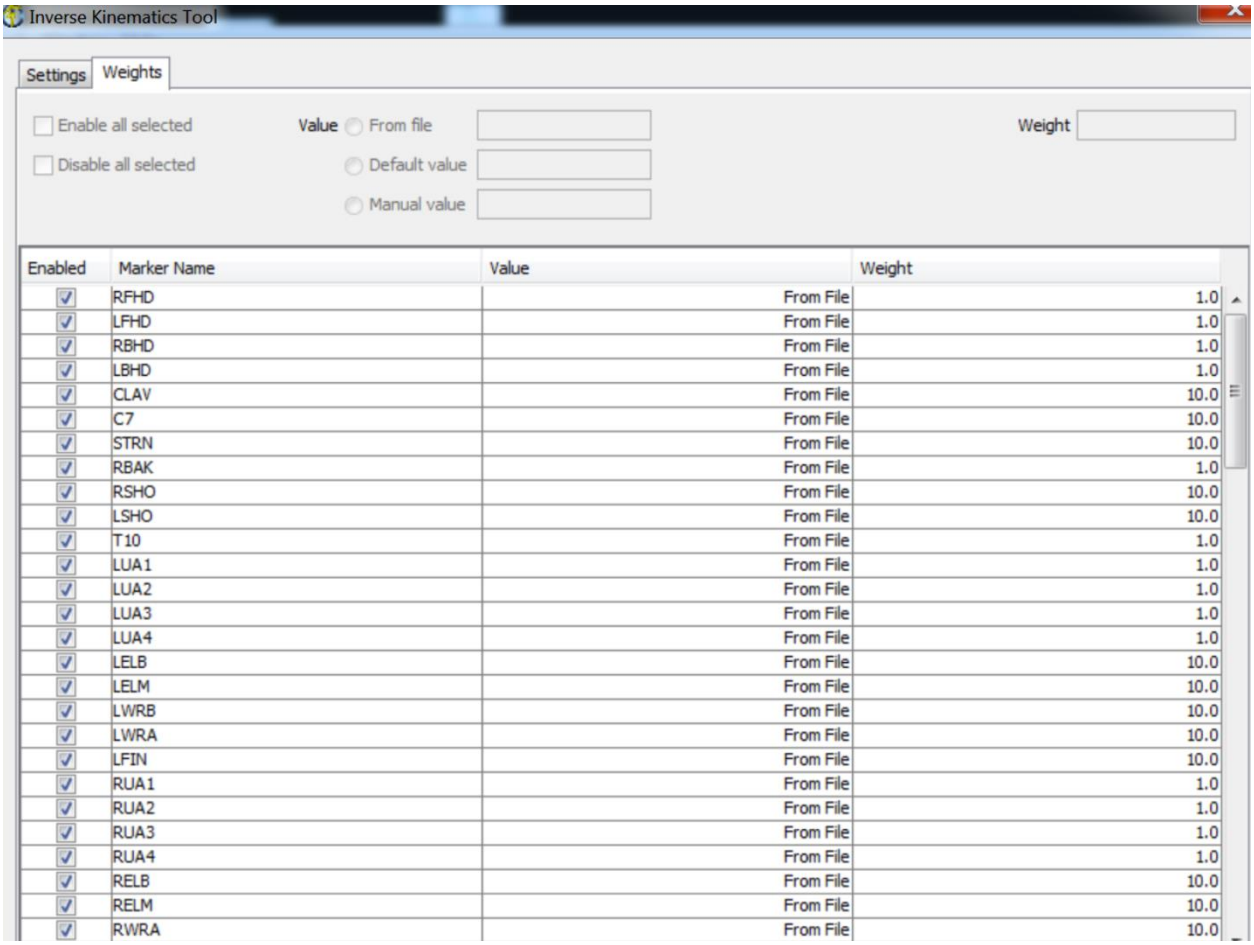

Enabled	Marker Name	Value	Weight
☑	RFHD	From File	1.0
☑	LFHD	From File	1.0
☑	RBHD	From File	1.0
☑	LBHD	From File	1.0
☑	CLAV	From File	10.0
☑	C7	From File	10.0
☑	STRN	From File	10.0
☑	RBAK	From File	1.0
☑	RSHO	From File	10.0
☑	LSHO	From File	10.0
☑	T10	From File	1.0
☑	LUA1	From File	1.0
☑	LUA2	From File	1.0
☑	LUA3	From File	1.0
☑	LUA4	From File	1.0
☑	LELB	From File	10.0
☑	LELM	From File	10.0
☑	LWRB	From File	10.0
☑	LWRA	From File	10.0
☑	LFIN	From File	10.0
☑	RUA1	From File	1.0
☑	RUA2	From File	1.0
☑	RUA3	From File	1.0
☑	RUA4	From File	1.0
☑	RELB	From File	10.0
☑	RELM	From File	10.0
☑	RWRA	From File	10.0

☑	RWRB	From File	10.0
☑	RFIN	From File	10.0
☑	LASI	From File	50.0
☑	RASI	From File	50.0
☑	LPSI	From File	50.0
☑	RPSI	From File	50.0
☑	LTH1	From File	1.0
☑	LTH2	From File	1.0
☑	LTH3	From File	1.0
☑	LTH4	From File	1.0
☑	LTHI	From File	1.0
☑	LKNE	From File	100.0
☑	LKNM	From File	100.0
☑	RTH1	From File	1.0
☑	RTH2	From File	1.0
☑	RTH3	From File	1.0
☑	RTH4	From File	1.0
☑	RTHI	From File	1.0
☑	RKNE	From File	100.0
☑	RKNM	From File	100.0
☑	LTT	From File	10.0
☑	LHF	From File	10.0
☑	LTIB	From File	1.0
☑	LSK1	From File	1.0
☑	LSK2	From File	1.0
☑	LSK3	From File	1.0
☑	LSK4	From File	1.0

☑	LANM	From File	100.0
☑	LANK	From File	100.0
☑	LHEE	From File	10.0
☑	LTOE	From File	10.0
☑	LMTM	From File	100.0
☑	LMTP	From File	100.0
☑	RTT	From File	10.0
☑	RHF	From File	10.0
☑	RTIB	From File	1.0
☑	RSK1	From File	1.0
☑	RSK2	From File	1.0
☑	RSK3	From File	1.0
☑	RSK4	From File	1.0
☑	RANK	From File	100.0
☑	RANM	From File	100.0
☑	RHEE	From File	10.0
☑	RTOE	From File	10.0
☑	RMTP	From File	100.0
☑	RMTM	From File	100.0

APPENDIX H: OPENSIM INVERSE DYNAMICS SETTINGS FILES

Setup.xml

```
<?xml version="1.0" encoding="UTF-8" ?>
<OpenSimDocument Version="30000">
	<InverseDynamicsTool name="BP_A_004_C3_01">
		<!--Directory used for writing results.-->

	<results_directory>C:\Users\CatoTheDellder\AndreaGoogleDrive\THESIS\BiarticularProsthesis\BP
_A_004\Simulations\BP\IDResults</results_directory>
		<!--Directory for input files-->
		<input_directory />
		<!--Name of the .osim file used to construct a model.-->

	<model_file>C:\Users\CatoTheDellder\AndreaGoogleDrive\THESIS\BiarticularProsthesis\BP_A_004
\Simulations\BP\GenericAmputee_scale2_BP_BP_A_004.osim</model_file>
		<time_range> 0.0083333 10</time_range>
		<forces_to_exclude> Muscles</forces_to_exclude>
	<external_loads_file>C:\Users\CatoTheDellder\AndreaGoogleDrive\THESIS\BiarticularProsthesis\B
P_A_004\Simulations\BP\ExternalForces\Spring\BP_A_004_C3_01_external_loads_S.xml</external_loads_fil
e>
	<coordinates_file>C:\Users\CatoTheDellder\AndreaGoogleDrive\THESIS\BiarticularProsthesis\BP_
A_004\Simulations\BP\IKResults\transformed_BP_A_004_C3_01_ik.mot</coordinates_file>
	<lowpass_cutoff_frequency_for_coordinates>6</lowpass_cutoff_frequency_for_coordinates>
	<output_gen_force_file>BP_A_004_C3_01_id_S.sto</output_gen_force_file>
		<joints_to_report_body_forces />
	<output_body_forces_file>body_forces_at_joints.sto</output_body_forces_file>
	</InverseDynamicsTool>
</OpenSimDocument>
```

ExternalLoads.xml (with spring forces applied)

```
<?xml version="1.0" encoding="UTF-8" ?>
<OpenSimDocument Version="30000">
	<ExternalLoads name="Ex2">
		<objects>
			<ExternalForce name="right">
				<isDisabled>false</isDisabled>
				<!--Name of the body the force is applied to.-->
				<applied_to_body>foot_r</applied_to_body>
	<force_expressed_in_body>ground</force_expressed_in_body>
	<point_expressed_in_body>ground</point_expressed_in_body>
				<force_identifier>ground_force_v</force_identifier>
				<point_identifier>ground_force_p</point_identifier>
				<torque_identifier>ground_torque_</torque_identifier>
				<data_source_name></data_source_name>
			</ExternalForce>
			<ExternalForce name="left">
	<isDisabled>false</isDisabled>
				<!--Name of the body the force is applied to.-->
				<applied_to_body>calcn_l</applied_to_body>
			<force_expressed_in_body>ground</force_expressed_in_body>
	<point_expressed_in_body>ground</point_expressed_in_body>
```

```
                        <force_identifier>1_ground_force_v</force_identifier>
                        <point_identifier>1_ground_force_p</point_identifier>
        <torque_identifier>1_ground_torque_</torque_identifier>
                        <data_source_name></data_source_name>
                    </ExternalForce>
                    <ExternalForce name="Prox">
                        <isDisabled>false</isDisabled>
                        <!--Name of the body the force is applied to.-->
                        <applied_to_body>femur_r</applied_to_body>
        <force_expressed_in_body>ground</force_expressed_in_body>
        <point_expressed_in_body>ground</point_expressed_in_body>
                        <force_identifier>2_ground_force_v</force_identifier>
                        <point_identifier>2_ground_force_p</point_identifier>
        <torque_identifier>2_ground_torque_</torque_identifier>
                    </ExternalForce>
                    <ExternalForce name="dist">
                        <isDisabled>false</isDisabled>
                        <!--Name of the body the force is applied to.-->
                        <applied_to_body>foot_r</applied_to_body>
        <force_expressed_in_body>ground</force_expressed_in_body>
        <point_expressed_in_body>ground</point_expressed_in_body>
                        <force_identifier>3_ground_force_v</force_identifier>
                        <point_identifier>3_ground_force_p</point_identifier>
        <torque_identifier>3_ground_torque_</torque_identifier>
                    </ExternalForce>
                </objects>
                <groups />
                <datafile>C:\Users\Administrator.UWIT-
C2MM7U3RDT\GoogleDrive\THESIS\BiarticularProsthesis\BP_A_005\Simulations\BP\ExternalForces\Spri
ng\BP_A_005_C3_01_grf_S.mot</datafile>
        <external_loads_model_kinematics_file>C:\Users\Administrator.UWIT-
C2MM7U3RDT\GoogleDrive\THESIS\BiarticularProsthesis\BP_A_005\Simulations\BP\IKResults\transform
ed_BP_A_005_C3_01_ik.mot</external_loads_model_kinematics_file>
        <lowpass_cutoff_frequency_for_load_kinematics>6</lowpass_cutoff_frequency_for_load_kinematics>
        </ExternalLoads>
</OpenSimDocument>
```

APPENDIX I: OPENSIM STATIC OPTIMIZATION SETTINGS FILE

```
<?xml version="1.0" encoding="utf-8"?><!--Generated from Matlab OSIM Model Tree v1.0-->
<OpenSimDocument Version="30000">
  <AnalyzeTool name="BP_A_005_C3_01">
    <model_file>C:\Users\CatoTheDellder\AndreaGoogleDrive\THESIS\BiarticularProsthesis\BP_A_005\Simulations\BP\GenericAmputee_scale2_BP_BP_A_005.osim</model_file>
    <replace_force_set>false</replace_force_set>
    <force_set_files>C:\Users\CatoTheDellder\AndreaGoogleDrive\THESIS\BiarticularProsthesis\BP_A_005\Simulations\BP\SOSetup\gait2354_StaticOpt_Actuators_amputeeR.xml</force_set_files>
    <results_directory>C:\Users\CatoTheDellder\AndreaGoogleDrive\THESIS\BiarticularProsthesis\BP_A_005\Simulations\BP\SOResults\</results_directory>
    <output_precision>8</output_precision>
    <initial_time>0.0083333</initial_time>
    <final_time>10</final_time>
    <solve_for_equilibrium_for_auxiliary_states>false</solve_for_equilibrium_for_auxiliary_states>
    <maximum_number_of_integrator_steps>20000</maximum_number_of_integrator_steps>
    <maximum_integrator_step_size>1</maximum_integrator_step_size>
    <minimum_integrator_step_size>1e-08</minimum_integrator_step_size>
    <integrator_error_tolerance>1e-05</integrator_error_tolerance>
    <AnalysisSet name="Analyses">
      <objects>
        <StaticOptimization name="StaticOptimization">
          <on>true</on>
          <start_time>0.0083333</start_time>
          <end_time>10</end_time>
          <step_interval>1</step_interval>
          <in_degrees>true</in_degrees>
          <use_model_force_set>true</use_model_force_set>
          <activation_exponent>2</activation_exponent>
          <use_muscle_physiology>true</use_muscle_physiology>
          <optimizer_convergence_criterion>0.0001</optimizer_convergence_criterion>
          <optimizer_max_iterations>100</optimizer_max_iterations>
        </StaticOptimization>
      </objects>
      <groups/>
    </AnalysisSet>
    <ControllerSet name="Controllers">
      <objects/>
      <groups/>
    </ControllerSet>
    <external_loads_file>C:\Users\CatoTheDellder\AndreaGoogleDrive\THESIS\BiarticularProsthesis\BP_A_005\Simulations\BP\ExternalForces\Spring\BP_A_005_C3_01_external_loads_S.xml</external_loads_file>
    <states_file/>
    <coordinates_file>C:\Users\CatoTheDellder\AndreaGoogleDrive\THESIS\BiarticularProsthesis\BP_A_005\Simulations\BP\IKResults\transformed_BP_A_005_C3_01_ik.mot</coordinates_file>
    <speeds_file/>
    <lowpass_cutoff_frequency_for_coordinates>6</lowpass_cutoff_frequency_for_coordinates>
  </AnalyzeTool>
</OpenSimDocument>
```

APPENDIX J: MODEL VALIDATION COMPARISION FOR ADDITIONAL SUBJECTS

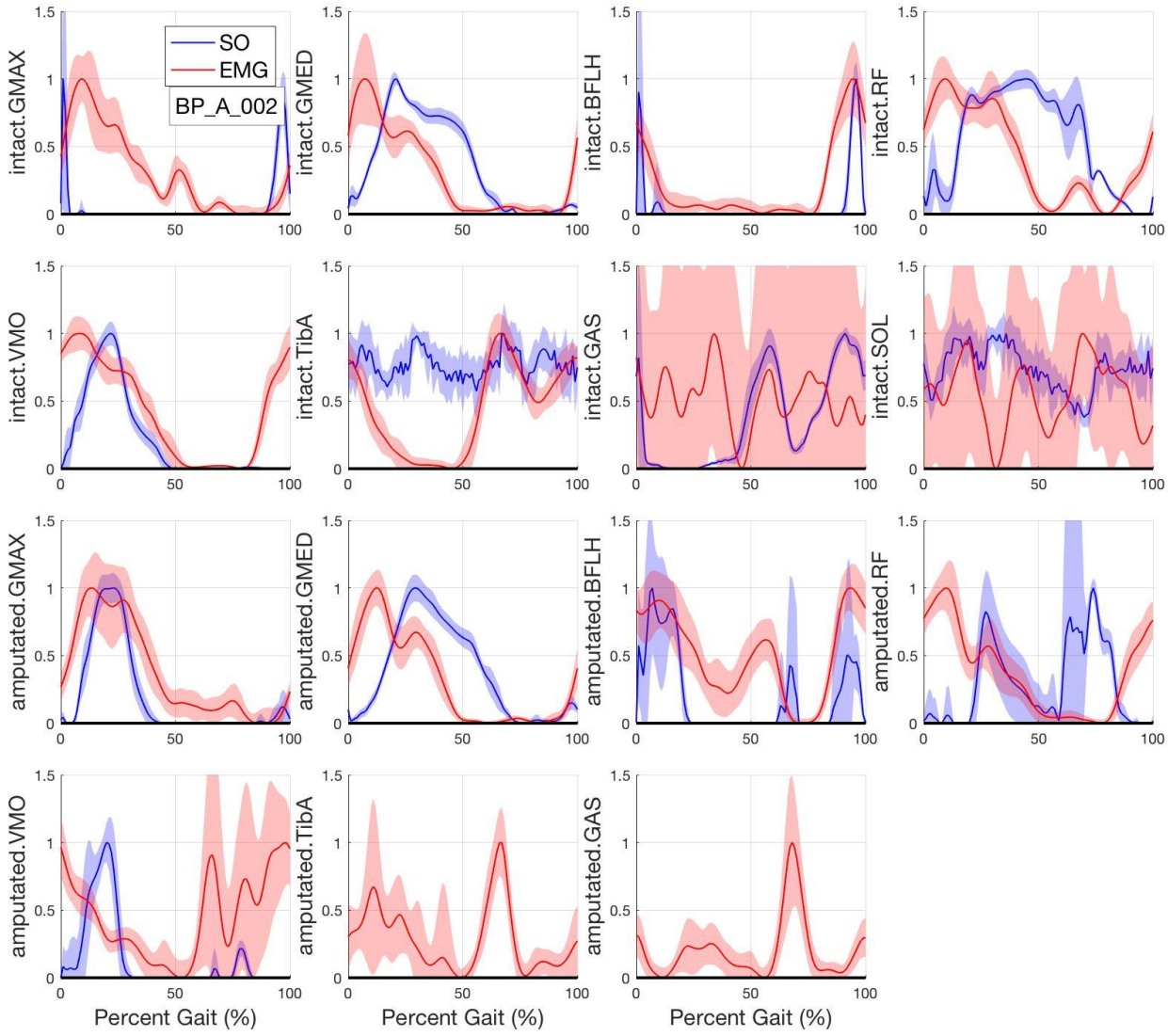

Figure J-1. Static Optimization (SO) and EMG qualitative comparison for Subject 2. Amputated TA and GAS were measured experimentally, but were not included in the OpenSim model and have no SO results. Amputated SOL was not measured in EMG or simulated in SO.

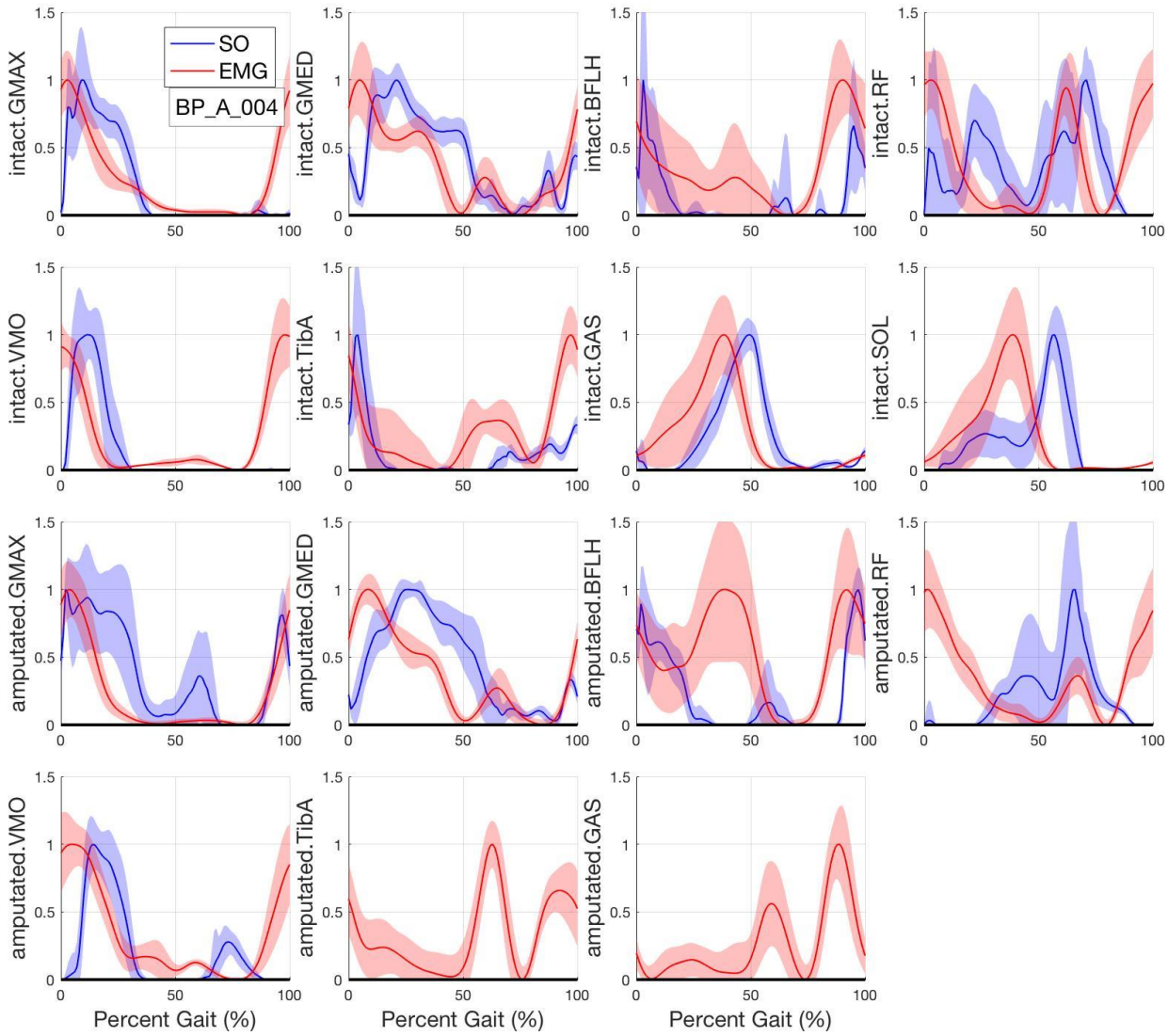

Figure J-2. Static Optimization (SO) and EMG qualitative comparison for Subject 4. Amputated TA and GAS were measured experimentally, but were not included in the OpenSim model and have no SO results. Amputated SOL was not measured in EMG or simulated in SO.

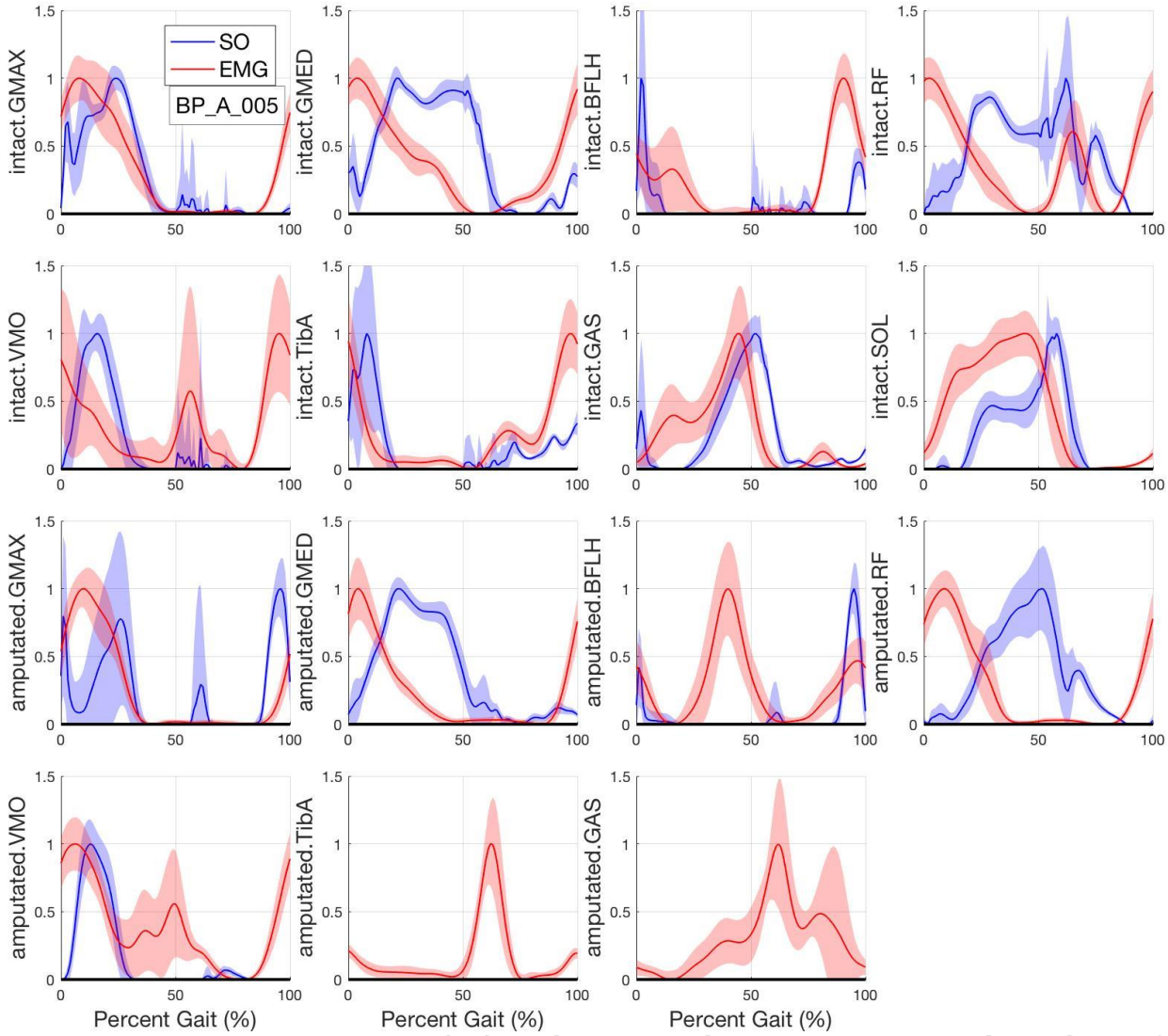

Figure J-3. Static Optimization (SO) and EMG qualitative comparison for Subject 5. Amputated TA and GAS were measured experimentally, but were not included in the OpenSim model and have no SO results. Amputated SOL was not measured in EMG or simulated in SO.

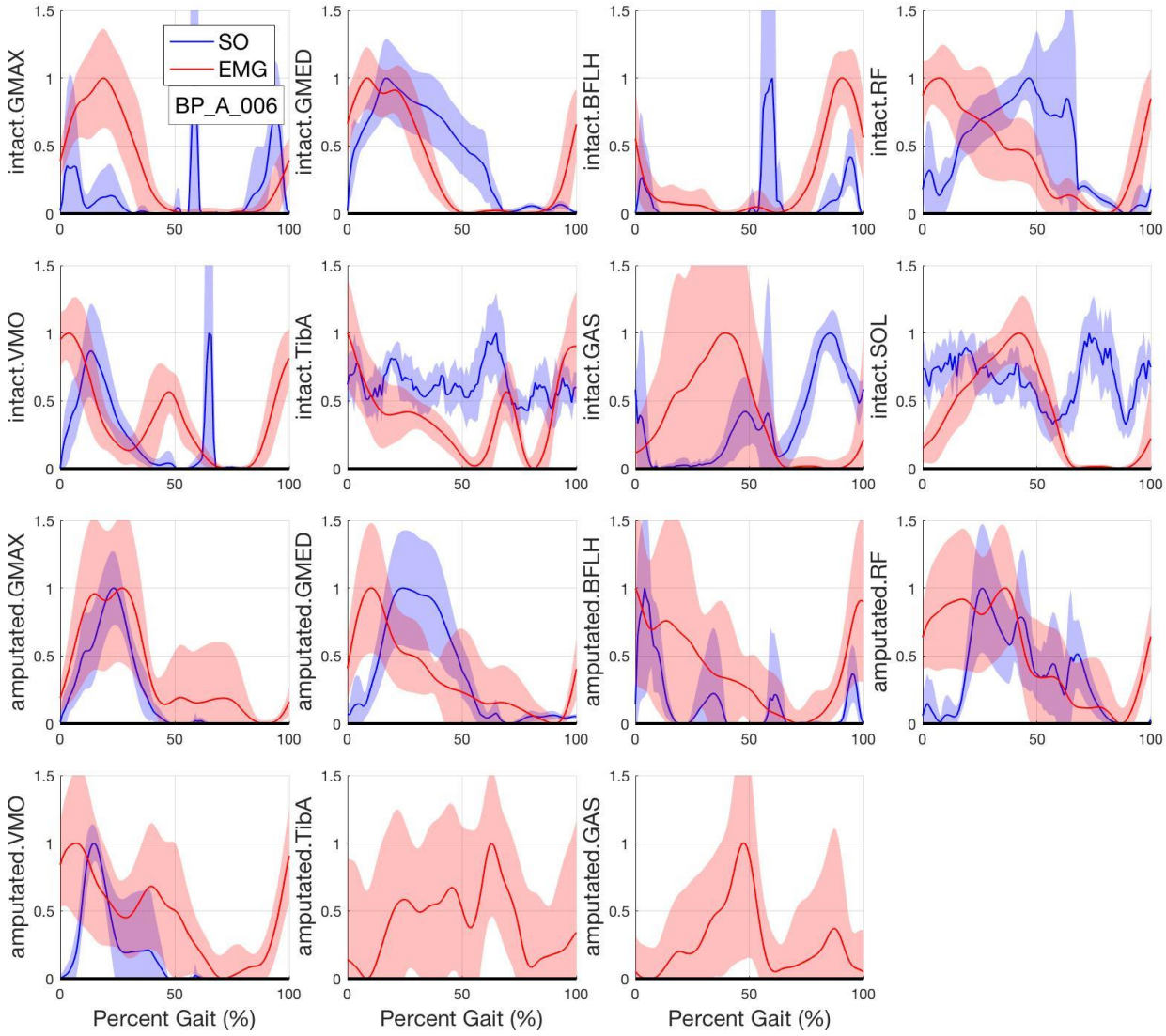

Figure J-4. Static Optimization (SO) and EMG qualitative comparison for Subject 6. Amputated TA and GAS were measured experimentally, but were not included in the OpenSim model and have no SO results. Amputated SOL was not measured in EMG or simulated in SO.

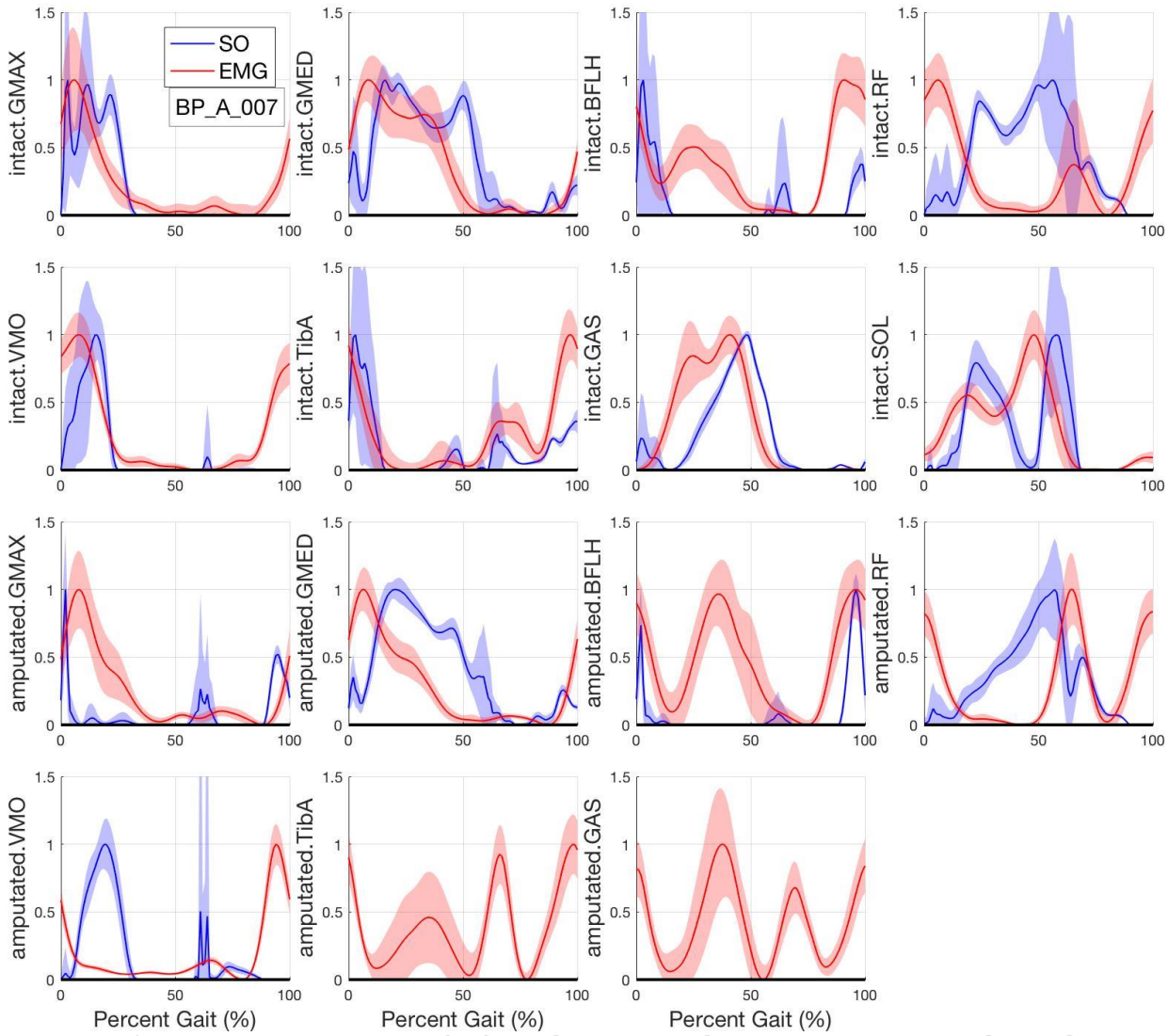

Figure J-5. Static Optimization (SO) and EMG qualitative comparison for Subject 7. Amputated TA and GAS were measured experimentally, but were not included in the OpenSim model and have no SO results. Amputated SOL was not measured in EMG or simulated in SO.

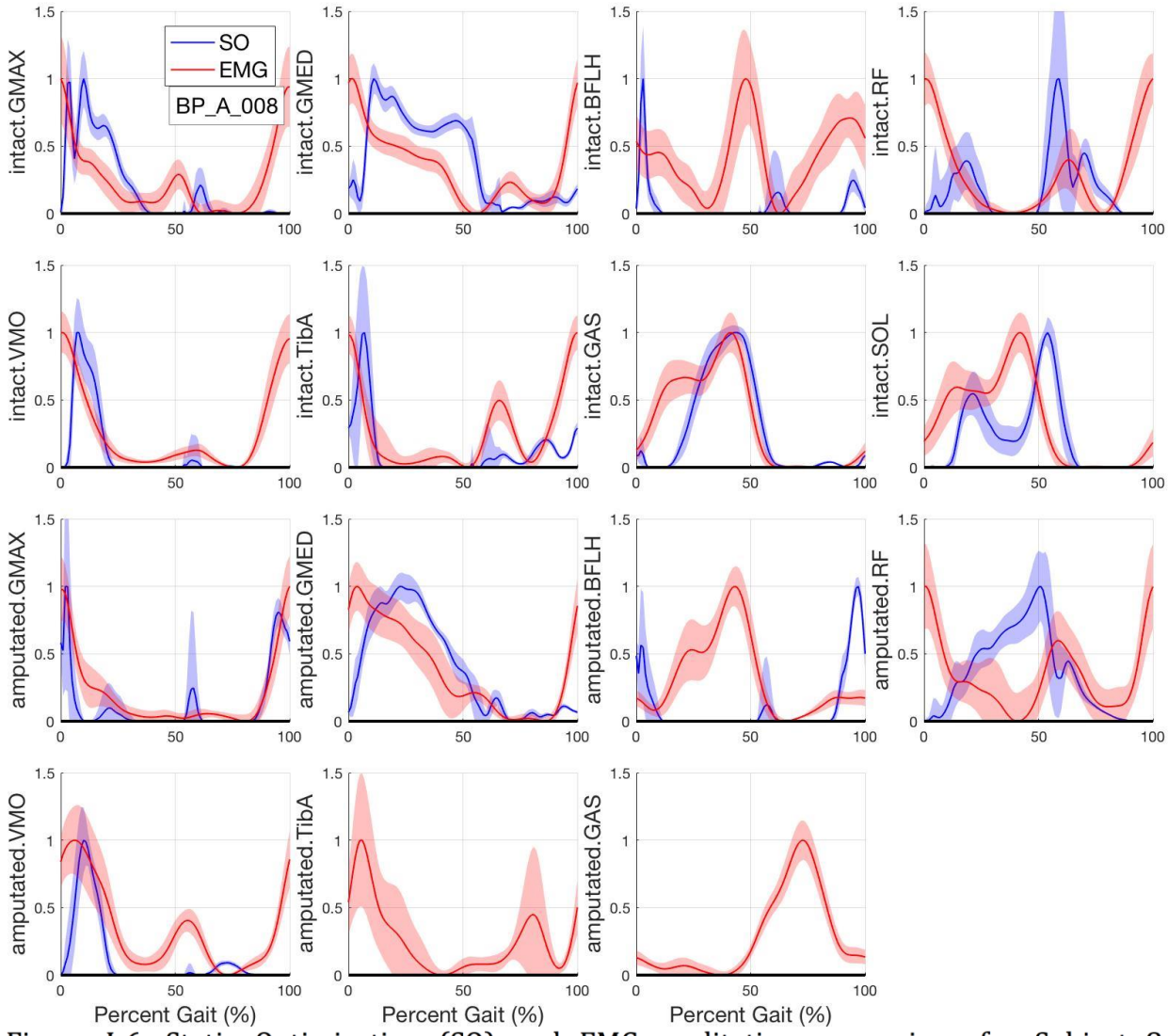

Figure J-6. Static Optimization (SO) and EMG qualitative comparison for Subject 8. Amputated TA and GAS were measured experimentally, but were not included in the OpenSim model and have no SO results. Amputated SOL was not measured in EMG or simulated in SO.